# QUANTIFYING DYNAMICS AND VARIABILITY IN NEURAL SYSTEMS

A Dissertation
Presented to
The Academic Faculty

By

Sharon Elizabeth Norman

In Partial Fulfillment
Of the Requirements for the Degree
Doctor of Philosophy in Bioengineering

Georgia Institute of Technology

December 2014

**QUANTIFYING DYNAMICS AND VARIABILITY IN NEURAL SYSTEMS**

Approved by:

Dr. Robert Butera
School of Electrical and Computer Engineering
*Georgia Institute of Technology*

Dr. Carmen Canavier
Department of Cell Biology and Anatomy
*Louisiana State University*

Dr. Garrett Stanley
Department of Biomedical Engineering
*Georgia Institute of Technology*

Dr. Robert Clewley
Neuroscience Institute
*Georgia State University*

Dr. Astrid Prinz
Department of Biology
*Emory University*

Date Approved: August 20, 2014

## ACKNOWLEDGEMENTS

No one finishes any large, multi-year accomplishment alone. The Laboratory for Neuroengineering has been a great place to work while I've been at Tech; thanks to all the Neurolabbies for making it an inviting and creative environment. Thanks to my advisor Rob Butera, who provided the right balance of advice, suggestions, and freedom to let me hone my scientific abilities. My committee members have also been especially supportive. Thanks to Carmen Canavier for all of your excellent advice, especially the suggestions on papers we're writing and papers we should be reading. Thanks to Astrid Prinz for your constructive suggestions and your willingness to share your expertise and your lab. Thanks to Garrett Stanley for your critiques and compliments, and for forcing me to think bigger and broaden my scope. Thanks to Rob Clewley for all your comments, particularly the ones that articulate and make clear dynamical mechanisms. Discussions with Roberta Berry were especially entertaining and made the policy paper and policy chapter infinitely better. Former Butera lab members Laveeta Joseph , Natalia Toporikova, and Risa Lin were instrumental to my success regarding experimental preparations, computational models, and RTXI/dynamic clamp, respectively. Current lab members Vineet Tiruvadi and Yogi Patel have been helpful with discussions about synchrony and RTXI code. Thanks to Wafa Soofi for listening to me talk over and over about PRCs. Maxine McClain and Clare Gollnick were always willing to talk science, or get a beer, or do both. Thank you to my family and my in-laws; your support during the last several years has helped me tremendously. Finally, thank you to my husband James Norman,

for everything you do. My time in graduate school has been funded by a National Science Foundation IGERT Fellowship, a National Science Foundation Graduate Research Fellowship, and a National Institutes of Health grant, R01-NS054281.

**TABLE OF CONTENTS**

## LIST OF TABLES

## LIST OF FIGURES

## LIST OF SYMBOLS AND ABBREVIATIONS

| | |
|---|---|
| AR | autoregressive |
| ARIMA | autoregressive integrated moving average |
| CDF | cumulative distribution function |
| CPG | central pattern generator |
| CV | coefficient of variation |
| EEG | electroencephalogram |
| ISI | interspike interval |
| MA | moving average |
| NIS | neural interface systems |
| PDF | probability distribution function |
| PRC | phase resetting curve |
| R | raw vector length |
| r | normalized vector length |
| STG | stomatogastric ganglion |
| ts | stimulus time interval |
| tr | recovery time interval |

## SUMMARY

The brain is a complex system and orchestrates a number of functions crucial to organism survival. Synchronized neural activity, in which the firing of neurons is coordinated in time, is an observed phenomenon in many of these functions; the conditions that promote synchrony and the dynamics of synchronized activity are active areas of investigation because they are incompletely understood. In addition, variability is intrinsic to biological systems, but the effect of neuron spike time variability on synchronization dynamics is a much less studied question.

To understand how small neural circuits synchronize, we employ a hybrid circuit model composed of one biological and one computational neuron; the logic is that conditions for and dynamics of synchronization in small systems can inform how synchronization occurs in large circuits. Prior hybrid circuit experiments revealed that irregularity in biological neuron spike timing could change synchronization or phase-locking in the circuit, sometimes resulting in repeated transitions between phase-locking, where the phase offset between neuron spikes is conserved, and phase-slipping, where the phase offset between neuron spikes is changing every cycle because one neuron is spiking faster than the other. In addition, a computational model of two interacting neurons could not replicate these transitions when a white noise Gaussian random process was used to represent interspike interval, but an interspike interval process with history and a Gaussian component could. I show that interspike interval can be represented as an autoregressive integrated moving average process, where ISI

is dependent on past history and a stochastic component with history. I suggest, using integrate and fire model simulations, that stochastic activity in adaptation channels could be responsible for the history dependence observed in this system. This evidence of stochastic, non-white noise in neural systems suggests that our understanding of network dynamics could be enhanced by including more complex, but relevant, forms of noise.

To predict or explain synchronization dynamics in two-neuron circuits (such as the hybrid circuit), a map can be constructed. The phase resetting curve (PRC), which describes how an oscillator responds to input given at a particular time during the oscillation cycle, is measured for both components. These curves can be used to form a map; intersections on this map correspond to stable or unstable phase relationships between the oscillators. There are three cases where the map cannot yield a clear prediction: 1) If the PRC cannot be measured, perhaps because the oscillators are not separable; 2) If the PRC is too noisy to determine intersections; or 3) If one or both oscillators has variable periods, in which case the PRC represents oscillator activity at one point in time but may not represent it at a future time. I show that cycle-by-cycle dynamics of the coupled system can be used to infer what the underlying dynamic map looks like, even if it cannot be measured. Using this method, stable fixed points can be distinguished from attractors that result from the ghost of a fixed point. In addition, networks with similar phase histograms but different underlying dynamics can be resolved, and the movement of stable fixed points while one neuron's period is changing is observable. The time-series vector method is a

valuable tool for distinguishing dynamics, and can be adapted for use in larger populations and non-reciprocal circuits.

Finally, we discuss larger implications of neuroscience research, specifically the use of neural interfaces for national security. Neural interfaces for human enhancement in a national security context raise a number of unique ethical and policy concerns not common to dual use research of concern or traditional human subjects research. Guidelines about which technologies should be developed are lacking. We discuss a two-step framework with 1) an initial screen to prioritize technologies that should be reviewed immediately, and 2) a comprehensive ethical review regarding concerns for the enhanced individual, operational norms, and multi-use applications in the case of transfer to civilian contexts.

# CHAPTER 1: INTRODUCTION

## 1.1 Synchronization

Vertebrate and invertebrate animals are capable of simple and complex tasks. The brain is instrumental for both. In biological systems, we attribute meaning to repeatable patterns of activity, neural or otherwise. The presence of synchronous cellular populations, where all components are active at approximately the same time, can have obvious functional significance; the coordinated firing activity of respiratory system neurons in the brainstem (Funk & Greer, 2013; Koshiya & Smith, 1999) or pacemaking cardiac myocytes of the heart (Bleeker, Mackaay, Masson-Pevet, Bouman, & Becker, 1980) function in such a manner. In addition, oscillations of similar frequency in spatially distinct areas of the brain are interpreted to have significance for cognitive-level function (Siegel, Donner, & Engel, 2012). At the small circuit level, coordinated neural activity is the backbone of central pattern generating circuits. Central pattern generators (CPGs) are robust and maintain crucial functions in invertebrate systems (Selverston, 2010); they are present in vertebrate systems as well (Hagglund et al., 2013). Large neural populations and small neural circuits are made up of individual neurons, which have their own patterns of spike activity. Variability of these individual components likely affects function of the network as a whole, but precisely how remains incompletely understood.

### 1.1.1 Synchrony in health and disease

Synchronization of neural populations, and in particular the presence of gamma rhythms, is hypothesized to underlie a number of cognitive functions (Colgin & Moser, 2010). This type of synchronized activity is especially implicated in memory (Jürgen Fell et al., 2001; Jutras & Buffalo, 2010).

The dysfunction of synchrony can manifest in a number of disorders (Uhlhaas & Singer, 2006, 2012). In schizophrenia, patients show less across-brain synchronization at gamma frequencies than control subjects when performing visual completion tasks (Grützner et al., 2013; Spencer et al., 2003). The epileptic brain appears to show disconnected activity between brain regions but too much synchrony within brain regions (Dominguez et al., 2005). Parkinsonian tremor is associated with synchronized activity in the subthalamic nucleus (Cagnan, Kuhn, & Brown, 2014). These observations suggest that synchronization has a role to play in both the healthy and afflicted brain.

### 1.1.2 Levels of synchrony

Synchronization of neural activity is defined differently at different scales, and the tools used to describe and visualize synchrony are also scale-dependent. Population- or brain-level activity is measured using neuroimaging techniques such as functional magnetic resonance imaging (fMRI) or electrical techniques such as electroencephalogram (EEG). At the whole-brain level, synchrony can refer to the spectral power of a given frequency in a specific region, or it can mean coherence between two distinct regions, in which case it reflects the

presence of a common frequency band between those two regions (Cohen & Gulbinaite, 2014).

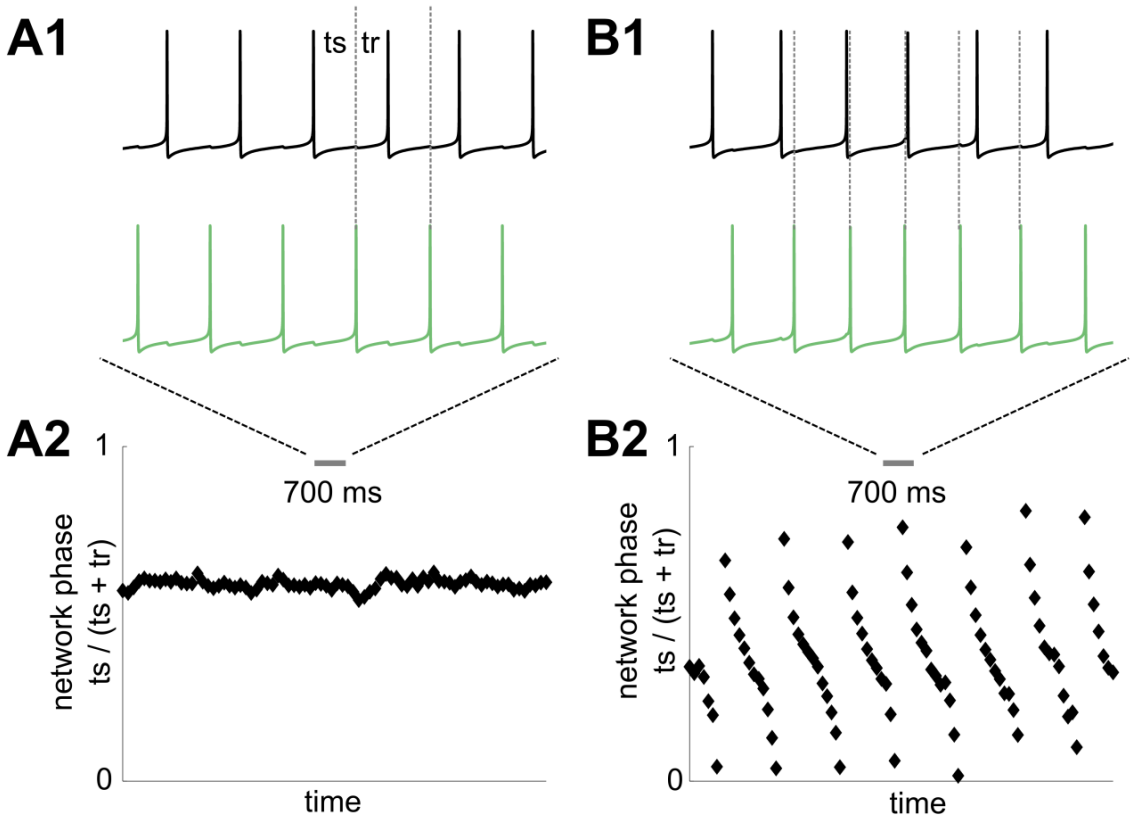


**Figure 1: Network activity patterns in a simulated two-neuron circuit.** Note this this figure appears again later in Chapter 2 as Figure 3. (A1) the green neuron spikes at the same stimulus time interval ts and has a consistent recovery time interval tr during the black neuron interspike interval. (A2) network phase in the phase-locked system is consistent over time; each point plots the network phase during one reference neuron interspike interval. (B1) the green neuron spikes at a slightly different ts in every black neuron interspike interval. (B2) The phase slipping system has a different network phase every cycle.

At the small circuit level, spike patterns are defined by temporal and phasic relationships between specific components (Figure 1 A1, B1). We define network phase as the time when one component is active during the circuit's network cycle (Figure 1 A2, B2). One neuron is taken to be the reference (in Figure 1, this is the black neuron) and defines the network period. Phase-locking implies that a consistent phasic relationship is maintained between two oscillators (or two populations of oscillators) (Figure 1, A2); synchrony is a special case of phase-locking where the temporal offset between the oscillating components is zero, such that they are active at the same time.

Phase-slipping, in which a preferred phase can emerge but the relationship is not stable, is another pattern apparent in two-cell networks (described in the next section and in Figure 1 B2). Synchronization in this case is transient and interspersed with phase slips. It occurs when one neuron is spiking at a faster frequency than the other; when they are coupled, the network phase is continuously changing, because the phase at which the faster neuron spikes during the slower neuron's period changes every cycle.

### 1.1.3 The hybrid circuit: a synchrony test bed

While the importance of synchrony in neural systems is acknowledged, the conditions that can create synchronous or phase-locked activity are still an active area of academic interest. We can explore the conditions and dynamics of synchrony in a small neural network and apply those findings to explain dynamics in much larger networks. We use the dynamic clamp (Prinz, Abbott, &

Marder, 2004; Sharp, O'Neil, Abbott, & Marder, 1993) to couple two neurons, one biological and one computational, to each other in real time, as shown in Figure 2.

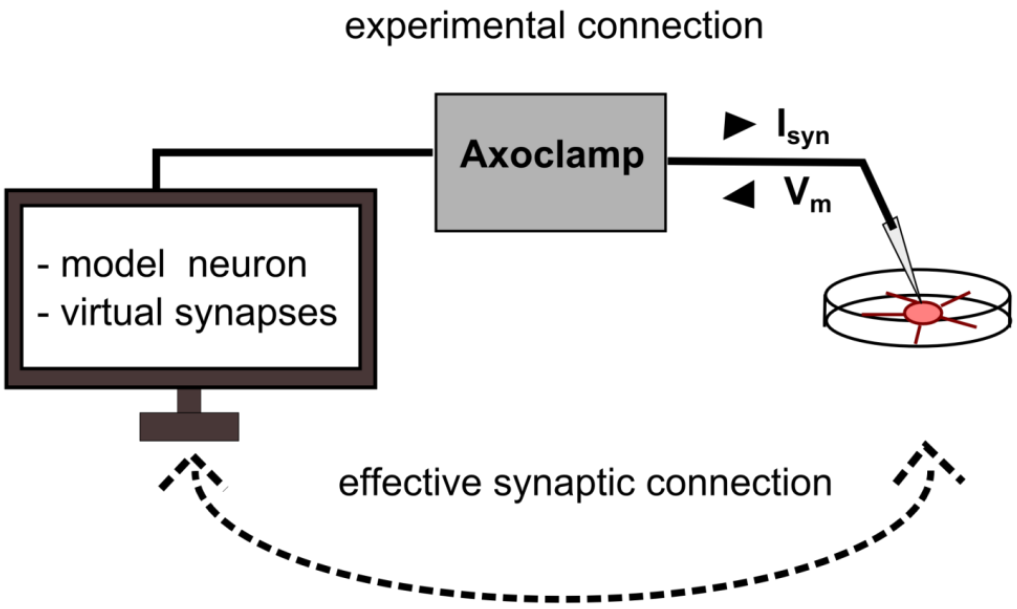


**Figure 2: Hybrid circuit diagram**. One biological and one computational neuron are reciprocally connected using the dynamic clamp.

The study of two-cell circuits can inform how larger circuits are put together and produce their dynamics. Two-cell circuits may also play an important role in shaping the network activity of those larger circuits. In recent work by Gollo and colleagues, reciprocally connected network components could influence network activity and, more specifically, could make synchronous activity possible in the presence of noise and conduction delays (Gollo, Mirasso, Sporns, & Breakspear, 2014). This conclusion held regardless of whether the modeled network components were individual neurons, neural populations, or neural mass models. Reciprocal connections present in more complex configurations may have profound effects on network dynamics.

Networks of neurons in mammalian systems involve more neurons with more connections than networks in invertebrate systems. While such systems may have their own unique organizing principles, understanding small circuits will likely inform how large circuits work. The properties that allow small central pattern generating circuits to maintain a stable rhythm may also exist in more complex pattern generators.

### 1.2 Phase resetting theory

Phase resetting theory examines how oscillators respond to inputs and allows us to make predictions about the types of activity that result after perturbation or in the presence of coupling to other oscillators (Glass & Mackey, 1988; Schulthesis, Prinz, & Butera, 2012; Winfree, 2001). The tools and assumptions when using phase resetting theory depend on the type of coupling present in a system: weak or

pulsatile. In the weak coupling case, the perturbations are not large enough to significantly distort the oscillator's limit cycle (Schwemmer & Lewis, 2012). In pulsatile coupling, there is no restriction on the size of the perturbation, so long as the oscillator returns to its limit cycle quickly (Canavier & Achuthan, 2010). This work is based on a pulsatile coupling assumption

The phase resetting curve (PRC) describes how an oscillator responds to inputs given at specific times during the oscillator cycle (Glass & Mackey, 1988; Winfree, 2001). It can be used to predict of two neurons will synchronize in a circuit. For neurons, the PRC describes the cellular response to input. One can make predictions about how inputs affect a cell, and can extend those predictions to how regular, periodic input from anther oscillator may affect a cell.

The PRC can be used to generate a dynamic map for synchrony prediction. This map involves plotting PRCs from two different oscillators against one another (Thounaojam, Cui, Norman, Butera, & Canavier, 2014). Intersections on this dynamic map correspond to fixed points of the coupled system. Stable fixed points are those where the stimulus interval ts of one oscillator and the recovery interval tr of the other neuron are equal, and vice versa. This phase relationship remains stable over time. In contrast, if there are no intersections, the system will continue to iterate between the curves, never reaching a stable phase relationship.

Two fundamental assumptions underlie the construction of the PRC-based map. First, neurons are assumed to be approximately regular oscillators. Second, the

PRC must be measurable. The PRC-based map represents a snapshot of cellular phase resetting properties in time. If a neuron changes the spike frequency or sensitivity to input, the PRC-based map will be outdated and may not yield accurate predictions. The map is also not useful if PRCs cannot be measured. This can happen if oscillators cannot be separated. If the PRC can be measured but it noisy, synchrony prediction may still be difficult.

### 1.3 Variability

Specific forms of neural activity, such as synchronization and phase-locking, seem to be important for neural function. However, patterns of activity are not always regular and often exhibit some form of variability. For example, central pattern generators may not keep a perfectly regular network frequency (Soofi, Archila, & Prinz, 2012; Lamont S. Tang et al., 2010), or a phase-locked network can show variability in the network phase over time (Thounaojam et al., 2014).

Variability in the timing of network activity can arise in a number of places, as can variability in individual neuron spike timing. Invertebrate systems are known to be sensitive to temperature and network frequency will speed up when preparations are warmed (Katz, 2004; L. S. Tang, Taylor, Rinberg, & Marder, 2012; Lamont S. Tang et al., 2010). Despite the warming, stable network activity persists, though at a higher frequency (L. S. Tang et al., 2012; Lamont S. Tang et al., 2010); the STG network only ceases to function when its pacemaker "crashes" at temperatures outside the physiological range (Rinberg, Taylor, & Marder, 2013). At the connection level, synaptic transmission involves sequences of probabilistic

events, such as vesicle release and neurotransmitter binding. Each of these probabilistic events contributes to variability in postsynaptic response. Absent synapses, a population of stochastic ion channels can elicit irregular firing in otherwise silent simulated neurons (Chow & White, 1996). The addition of white noise to an integrate and fire model creates an interspike interval (ISI) histogram with a long right tail (Gerstein & Mandelbrot, 1964); the addition of colored noise creates an ISI series with correlational structure, where sequential ISIs are correlated and show history (Lindner, 2004).

Variability at the single cell level can manifest as variability in population output. Recently we provided evidence, in a two-cell circuit, that changes in the biological neuron spiking frequency can cause changes in the phase-locked activity of a coupled hybrid circuit (Thounaojam et al., 2014). In the STG, changes in the frequency of the entire network do not result in a loss of phase locking (Soofi et al., 2012; L. S. Tang et al., 2012) – the system is robust against such changes. Variability of individual neural components can, but does not have to, affect variability of the network output.

Dynamical analysis of neural systems often does not incorporate noise. From noiseless simulations, we know that general networks coupled all-to-all with strong pulsatile coupling will synchronize (Mirollo & Strogatz, 1990). Likewise, two-neuron circuits with different intrinsic frequencies and different coupling strengths can show several different forms of near-synchronous activity (Maran & Canavier, 2008). Synchronization is also possible in networks with variable

topology, such as random or small-world connectivity (Shao, Tsao, & Butera, 2006; Watts & Strogatz, 1998). But what happens when we incorporate noise into such analysis? And how noisy are neurons?

Noise is added at different levels to neural simulations. At the level of an individual neuron, Gaussian white noise (Gerstein & Mandelbrot, 1964) or colored noise (Chacron, Longtin, & Maler, 2001; Lindner, 2004; Middleton, Chacron, Lindner, & Longtin, 2003) are added as current inputs to increase the variability of, or simulate noisy input to, the isolated neuron. In networks with excitatory and inhibitory components, noise added as Poisson inputs disrupts synchronization if sufficiently strong (Börgers & Kopell, 2005). In two-cell circuits where both neurons are represented as OU processes, their activity upon coupling can actually become more regular (Ly & Ermentrout, 2010). Noise can be advantageous for systems; stochastic resonance, in which a small, normally undetectable signal is made more detectable in the presence of noise (McDonnell & Abbott, 2009), is the classic example. It is known that noise affects network activity; describing and incorporating biologically-relevant noise is therefore important.

### 1.4 Earlier experiments motivating this work

Recently published work from the Canavier and Butera labs has shown that neural variability can strongly influence network activity patterns (Thounaojam et al., 2014). Experiments involved hybrid circuits of one biological neuron coupled to one computational neuron. When coupled together, some of the hybrid circuits maintained a stable phase-locked relationship, but some transitioned

between phase locking and phase slipping. The biological neuron supplies most of the noise present in this system, so the variability had to be attributable to the biological neuron.

Simulations of two coupled neurons were conducted to determine what type of noise could replicate the transitions between phase locking and phase slipping. Gaussian noise added to the period or PRC of one neuron were insufficient to replicate transitions between slipping and locking. Representing the period of the neuron as an OU process, with a dependence on past values of ISI and a stochastic component, did capture transition activity.

The goals for the work presented here arose naturally from the unanswered questions of the work above. History and randomness seem important, but what is the best representation for neuron spike time variability? How does variability look over long periods of time? How can we capture underlying network dynamics in the presence of neuron variability that continuously changes the dynamic map?

### 1.5 Project preview

A short description of each project and the main findings.

Project 1: Network activity in neural circuits is determined by system dynamics. System dynamics can be predicted using maps based on the phase resetting curve (PRC), but this approach assumes that neuron interspike interval is

constant and that the PRC is measurable. The time series of a coupled system can be used to predict the location and presence of stable fixed points and attractors resulting from the ghost of a fixed point. This method extends the concept of the PRC-based map to cases where noise, nonstationarity, or immesurability preclude the use of the map.

Project 2: Intrinsic neuron spike time variability can change observed network activity (Thounaojam et al., 2014). On average, an ARIMA (0, 1, 1) model can describe interspike interval over time and capture correlational features of ISI and delta ISI. These correlations can be replicated in an integrate-and-fire model with two different noise processes, representing fast current fluctuations and stochastic activity in a finite population of adaptation current channels (Schwalger, Fisch, Benda, & Lindner, 2010). Sequential ISIs are not independent and can be represented as a type of random walk; white noise and noisy adaptation currents are a plausible biophysical mechanism for this representation.

Project 3: National security applications of neuroscience are currently under development, but guidance is lacking about which types of technologies should be developed, particularly from ethical and policy standpoints. We propose a framework to evaluate feasibility and current scientific state for various technologies  Which technologies should be developed, from strategic, realistic, and ethical points of view, is not clear. We propose a framework that incorporates the current state of scientific knowledge, engineering feasibility,

and potential strategic impact as an initial screen to prioritize technologies for further ethical review. Our comprehensive ethical review assesses concerns for the enhanced individual, operational implications, and multi-use applications.

# CHAPTER 2: DYNAMIC CHANGES OF COUPLED SYSTEM SOLUTION TOPOLOGY REVEALED THROUGH TIME SERIES ANALYSIS

## 2.1 Introduction

Synchronized activity is present in many biological systems. Coordinated, phase-locked cellular activity plays a role in the reliable function of mechanisms crucial for survival of invertebrates and vertebrates. Cardiac myocytes act in a coordinated manner to orchestrate pumping of the heart, beginning with near synchronization of the cells in the intrinsically pacing sinoatrial node (Boyett, Honjo, & Kodama, 2000). In mammals, respiration involves the coordinated activity of neurons in the brainstem (Koshiya & Smith, 1999). Synchronization within and between brain regions is interpreted to play a role in cognitive level function (Juergen Fell & Axmacher, 2011; Jutras & Buffalo, 2010).

Despite the critical role synchronization plays in biological systems, the mechanisms by which these systems obtain persistent synchronized activity and the dynamics of this activity are incompletely understood. We use a hybrid circuit consisting of one biological neuron, one model neuron, and two reciprocal model synapses connecting them to explore conditions that establish synchrony or phase-locking and the dynamics of this activity. Earlier experiments in hybrid circuits have shown that transitions between phase-locked network activity and phase slipping network activity can occur when no user-defined parameters of the circuit are changed, indicating that the biological component alone is responsible for these changes (Thounaojam et al., 2014).

As discussed in Chapter 1, the phase resetting curve (PRC) is a tool that describes how oscillators respond to input given at various times during the oscillator cycle (Glass & Mackey, 1988; Winfree, 2001). PRCs can vary depending on how they are measured and what assumptions are placed on the type of coupling between oscillators; weak (reviewed in (Schwemmer & Lewis, 2012)) and pulsatile (reviewed in (Canavier & Achuthan, 2010)) are two forms of coupling. In this document, we generally adhere to the pulsatile coupling assumption. The PRC can be used to predict if synchronization between two neurons will occur by constructing a map using PRCs measured from both neurons (Sieling, Canavier, & Prinz, 2009). Stable fixed points on this map correspond to stable, phase-locked activity in a neural circuit, while regions where the curves are close together but nonintersecting are indicative of system activity that can remain relatively locked over time but experiences some phase slips. Because fixed points and PRC-based curves of a network can be observed on the map, it is an excellent tool for predicting and explaining dynamics behind why specific patterns of network activity exist.

The PRC-based map is useful for explaining and predicting system dynamics, but there are cases where it does not work. PRCs measured in experimental preparations can be noisy, making the detection of intersections on a map difficult. If the PRC from each neuron cannot be measured in isolation, the map itself cannot be constructed. Most fundamentally, one of the underlying assumptions to the map is that neuron frequency and sensitivity to input remain constant over time, meaning the PRC remains constant over time. Neuron

properties, in particular interspike interval, do not remain constant over time, however (see Chapter 3). A way to identify underlying system dynamics, in the absence of the PRC or in the presence of noise and variability, that shape network activity would be a useful contribution to the field.

We present a method based on the time series of a coupled system that can resolve dynamical changes in hybrid circuits over time. This technique is not for synchrony prediction per se but can provide evidence for the existence of stable fixed points or ghost attractors, particularly in the presence of noise. The method is an extension of maps based on the PRC, but measurement of the PRC is not required. The method can be extended to systems with non-reciprocal connections and likely can be adapted to work with populations of neurons.

## 2.2 Methods

### 2.2.1 Electrophysiology

*Aplysia californica* were ordered from the National Resource Facility for Aplysia (Miami, FL) and housed in saltwater tanks until used. Animals were anesthetized using an injection of 50% volume per body weight of 330 mM MgCl2 solution (Jhala, Tamvacakis, & Katz, 2011). The abdominal ganglion was removed and pinned out in a Sylgard-lined dish. High $Mg^{2+}$ low $Ca^{2+}$ solution was perfused through the dish during experiments. High $Mg^{2+}$ low $Ca^{2+}$ consists of, in mM, 330 NaCl, 10 KCl, 90 MgCl2, 20 MgSO4, 2 CaCl2, and 10 HEPES (Nowotny, Zhigulin, Selverston, Abarbanel, & Rabinovich, 2003). The purpose of this recording solution is to silence synaptic transmission and effectively isolate cells in the

ganglion (Nowotny et al., 2003). Temperature of the perfused culture was maintained using a Peltier device and proportional-integrative-derivative controller.

Electrodes for these experiments had resistances of approximately 6-15 MΩs. Thin-walled glass capillaries (0.75 mm inner diameter, 1 mm outer diameter, with filament) were pulled on a Sutter P-97 puller and filled with 3 M potassium acetate. Silver wires chlorided in bleach served as reference and pipette electrodes. Voltage and current were measured and applied using an Axoclamp 2B amplifier (Axon Instruments). Data were sampled at 10 kHz via a data acquisition card (National Instruments).

### 2.2.2 Experimental hybrid circuits

Hybrid circuits were formed by connecting a biological and model neuron in real time with inhibitory synapses. The model neuron is a conductance-based Wang Buzsaki model (Wang & Buzsaki, 1996). Reciprocal inhibitory alpha-shaped conductances were implemented in Real Time eXperiment Interface (RTXI, www.rtxi.org) (Lin, Bettencourt, White, Christini, & Butera, 2010). Equations describing the inhibitory synapses were:

$$I = g_{syn} * \left(V_m - E_{syn}\right)$$

$$g_{syn} = g_{max} * \frac{e}{\tau} * \alpha$$

$$\frac{d\alpha}{dt} = -\frac{\alpha}{\tau} + y$$

$$\frac{dy}{dt} = -\frac{y}{\tau}$$

$y = y + 1$ when a presynaptic spike occurs

Tau for the synapses was set to 10 ms for experimental hybrid circuits.

Activity in hybrid circuits can be characterized by network phase over time, which is defined in Figure 3. The biological neuron is defined as the reference neuron; the time between the reference neuron spike and the model neuron spike is the stimulus time interval ts, and the time between the model neuron spike and the next reference neuron spike is the recovery time interval tr (Figure 3 A1). In a phase-locked network like the one presented in Figure 3 A1, ts and tr are consistent over time from cycle to cycle. This means the network phase of a phase-locked system, shown in Figure 3 A2, is also consistent over time. Network phase of the coupled system is defined as

$$network\ phase = \frac{ts}{ts + tr}$$

Each dot in Figure 3 A2 and B2 represents the network phase calculated for one reference neuron interspike interval (ISI). Two observed forms of network activity are phase locking (Figure 3 A1 and A2) and phase slipping (Figure 3 B1 and B2).

In contrast to phase locking, where the phase offset and network phase between reference neuron spikes and other neuron spikes remains approximately constant over time, phase slipping occurs if one neuron is spiking faster than the other, such that ts and tr change every cycle (Figure 3 B1), which then changes the network phase every cycle (Figure 3 B2).

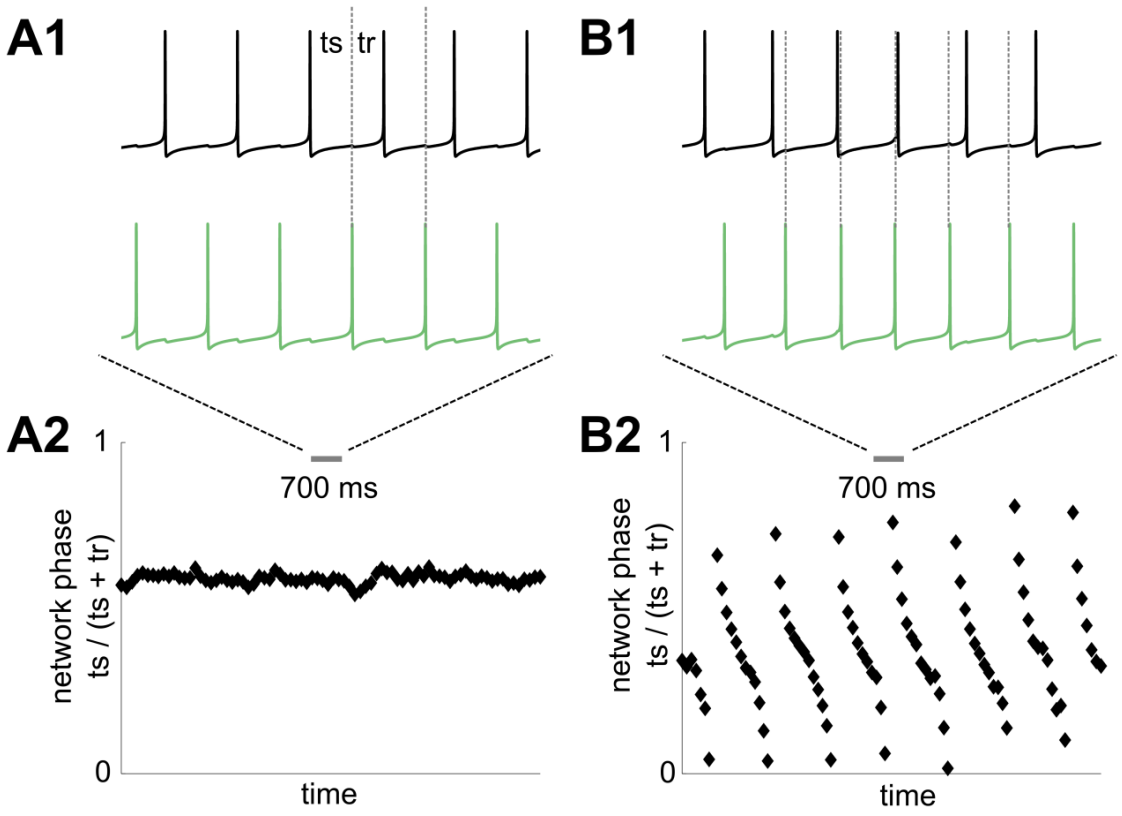


**Figure 3: Definition of network phase.** (A1) the time between a reference neuron spike (black) and the green neuron spike is the coupled system stimulus time interval ts; the recovery time interval tr is the time between the green spike and the next reference neuron spike. (A2) network phase is defined as ts / (ts + tr), which is approximately constant In the phase-locked case. Each point in this plot represents one network phase calculation per reference neuron interspike interval. (B1) in the phase slipping case, the green neuron spikes faster than the black neuron and ts and tr change every cycle. (B2) during phase slipping, the network phase changes from cycle to cycle, though a "preferred" phase can still be seen. Data for this figure is from a simulated hybrid circuit of two Wang-Buzsaki model neurons with parameters: [Neuron 1: $I_{app}$ = 0.212 nA, gsyn21 = 40 uS; Neuron 2, left: $I_{app}$ = 0.222 nA, gsyn12 = 50: Neuron 2, right: $I_{app}$ = 0.222, gsyn 12 = 100 uS].

### 2.2.3 Simulated hybrid circuits

Hybrid circuits were simulated in XPPAUT using two Wang-Buzsaki conductance-based models (Wang & Buzsaki, 1996) and the synaptic equations described previously. The synaptic time constant tau was set to 1 ms in these simulations to ensure that the synaptic waveform did not occupy a significant portion of the 80-110 ms interspike interval of the simulated neurons. One neuron, intended to model the biological neuron, has added Gaussian current noise; other parameters for this neuron do not change. The parameters for this neuron are $I_{app}$ = 0.212 nA and $g_{syn21}$ = 40 uS; these values produce an interspike interval (ISI) of approximately 100 ms and a maximum phase resetting of 0.2 (phase resetting is explained in the next section). Parameters for the second neuron of the simulated hybrid circuit are varied over a range of intrinsic spiking frequencies and coupling strengths; this range of parameters is chosen such that it still promotes 1:1 phase-locking between the two neurons of the simulated hybrid circuit.

### 2.2.4 Phase resetting curves

Phase resetting curves (PRCs) describe how perturbations given at some point during an oscillator's cycle change the oscillator period (Glass & Mackey, 1988; Winfree, 2001). The PRC presented here is measured by supplying inhibitory perturbations, similar to what would occur in the coupled hybrid circuit, at various times during the neuron's ISI (Figure 4A). In the experimental hybrid circuit, PRC perturbations are supplied to the biological neuron and the model neuron using custom modules in RTXI. The time from the last spike to the

perturbation is the stimulus time interval ts, the time from the perturbation to the next spike is the recovery time interval tr, the perturbed interval is P1, the interval after the perturbed interval is P2, and the unperturbed interval, taken to be the average of the five periods before perturbation, is P0 (Figure 4B). The phase resetting curve plots phase reset against stimulus phase, which are defined as

$$F1(\varphi) = \frac{(P1 - P0)}{P0}$$

and

$$\varphi = \frac{ts}{P0}$$

respectively (Figure 4B). Second order phase resetting is defined as

$$F2(\varphi) = \frac{(P2 - P0)}{P0}$$

where P2 is the interval after the perturbed interval. Second order phase resetting characterizes changes in neuron period from the perturbation that have not disappeared by the interval after perturbation. Second order phase resetting tends to be small in *Aplysia* neurons (Cui, Canavier, & Butera, 2009), but inclusion of second order phase resetting in analytical synchrony predictions increases the accuracy of the prediction (Oprisan, S.A., 2004).

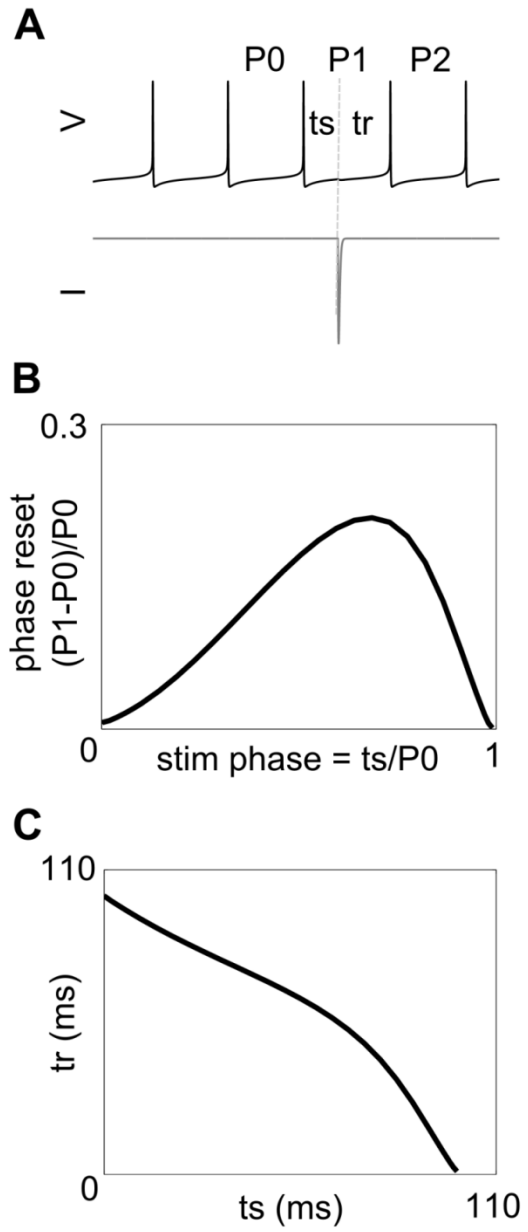


**Figure 4: Definition of phase resetting curves and ts-tr curves.** (A) voltage trace, top; current trace, bottom. Current perturbations are applied to the neuron to measure the phase resetting curve (PRC) at various stimulus time timervals (ts). The time from the perturbation to the next spike is the recovery time tr, the unperturbed interval is P0 (calculated as the average of five cycles prior to perturbation). (B) the PRC plots phase reset (P1 – P0) / P0 against stimulus phase ts / P0; both quantities are unitless. (C) the ts-tr curve plots stimulus time and recovery time against each other; the ts-tr curve captures similar information to the PRC, but retains time information. This simulated neuron has $I_{app}$ = 0.212 nA and gsyn = 40 uS.

The information from the PRCs can alternatively be presented on the stimulus interval-recovery interval plane. In this case, ts and tr are plotted on different axes and form the ts-tr curve (Figure 4C). White the PRC is unitless, the ts-tr curve retains temporal information. Ts-tr curves can be used to form a map to predict synchrony (discussed below); second order phase resetting can be included in these maps if steady-state activity is of interest. This approach is used in (Sieling et al., 2009), and the maps contained therein are called "equilibrium ts*-tr* plots." Second order phase resetting affects only the ts part of the ts-tr curve, as described in (Oprisan, S.A., 2004; Sieling et al., 2009):

$$ts' = P0 * \left(\varphi + F2(\varphi)\right)$$

$$tr' = P0 * \left(1 - \varphi + F1(\varphi)\right)$$

All ts-tr curves presented in this chapter have second order phase resetting incorporated.

### 2.2.5 Dynamic map for synchrony prediction

The measured PRCs can be used to create a dynamic map that predicts or explains synchronization in the circuit (Achuthan & Canavier, 2009; Thounaojam et al., 2014). The dynamic map plots the ts-tr curve from one neuron as x versus y and the ts-tr curve from the other neuron as y versus x (Figure 5, A1 and A2). Intersections of the ts-tr curves (Figure 5 A1) correspond to fixed points of the system, which can be stable or unstable. At a fixed point, the ts of one neuron

equals the tr from the other neuron and vice versa (Figure 5 B1); if this relationship persists even in the presence of small perturbations, the fixed point is stable and the system will show stable phase locking and a stable network phase. If there are no intersections on the dynamic map (Figure 5 A2), then the phasic relationship changes from cycle to cycle and the system shows phase slips. When the curves of the dynamic map are very close but do not intersect, a preferred phase can be observed; this preferred phase is the result of a "ghost" of a fixed point that does not exist but still has dynamic effects due to its proximity to a bifurcation (Izhikevich, 2010). During a phase slip or phase walkthrough, two spikes can occur during one reference period. In this case, the time interval between the reference spike and the first other spike is ts, and the time interval between the second spike and the next reference spike is defined as tr* (Figure 5 B2). Because ts and tr* are usually small, these points appear near the origin of the dynamic map.

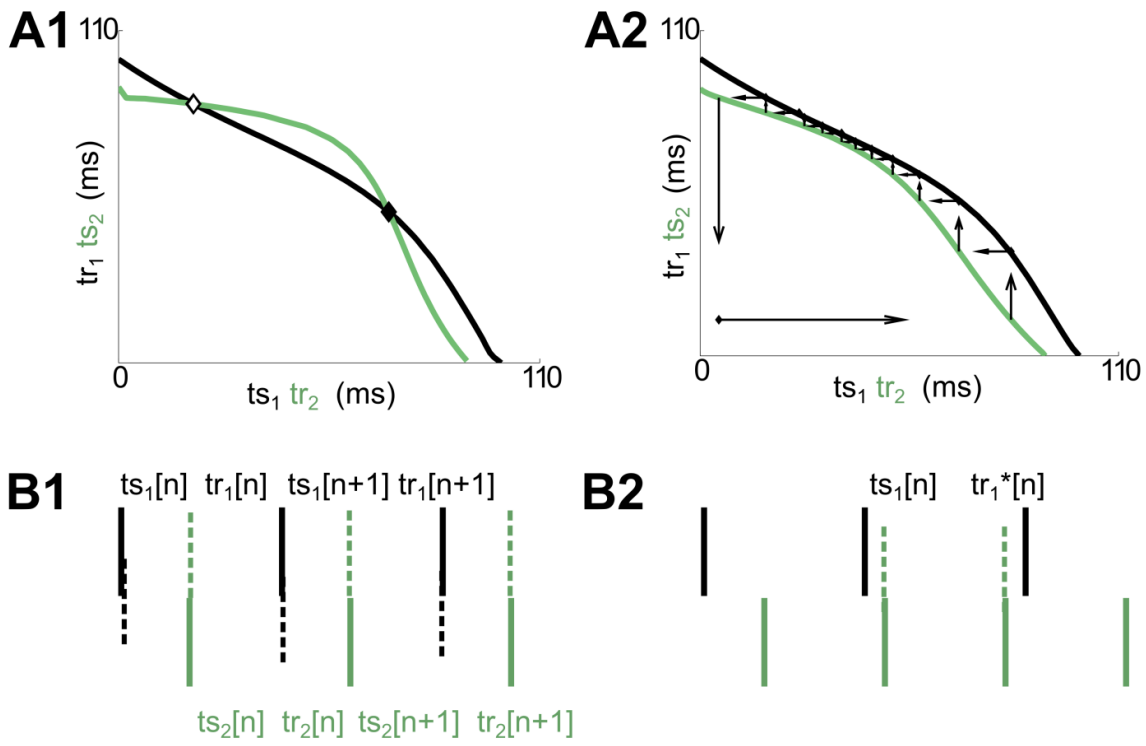


**Figure 5: The PRC-based map can be used to predict synchronization.** (A1) ts and tr of each neuron are plotted on alternative axes; intersections of these curves correspond to stable (solid diamond) and unstable (open diamond) fixed points. (A2) if the curves do not intersect, there are no fixed points and the system instead iterates between the curves, though regions where curves are close together correspond to network phases seen more often than others. (B1) Each line represents a spike of the green or black neuron. At a fixed point, the stimulus time interval of one neuron equals the recovery time interval of the other neuron and vice versa. (B2) when two spikes occur during the reference neuron cycle, the time between the reference spike and the next spike is ts, the time between the second green spike and the next reference spike is tr*, and this pair of points appears near the origin because ts and tr* are usually small. Data from simulated hybrid circuit.

### 2.2.6 Time series vector method

The PRC-based map (or "equilibrium ts*-tr* plot") presupposes that PRCs for both neurons can be measured and that they do not change over time, as well as that intersections on the map are resolvable. These conditions are not always met. An approach that can distinguish different dynamic cases in the presence of these shortcomings, in particular when dynamics can't be resolved by observing network phase alone, is needed.

The time series of a coupled system can be represented on the ts-tr plane, where ts and tr are the coupled system stimulus time interval and recovery time interval (as presented in Figure 3 A1 and B1). The distance and angle between sequential (ts, tr) pairs can be represented as vectors (Figure 6). The vertical and horizontal distances between sequential (ts, tr) pairs are defined as

$$\Delta ts\,[n] = ts\,[n+1] - ts\,[n]$$

$$\Delta tr\,[n] = tr\,[n+1] - tr\,[n]$$

The vector angle between sequential points is

$$angle = \tan^{-1}\frac{\Delta tr\,[n]}{\Delta ts\,[n]}$$

and the vector magnitude and normalized vector magnitude are

$$R[n] = \sqrt{\Delta ts[n]^2 + \Delta tr[n]^2}$$

$$r = \frac{R[n]}{ISI\ [n]}$$

$$ISI\ [n] = ts\ [n+1] + tr\ [n+1]$$

The raw vector magnitude is normalized by ISI to yield a number greater than zero but less than one; this normalization makes the vector magnitude unitless (as opposed to being in units of time), and facilitates comparison between cases with different interspike intervals.

Noise is necessary to effectively use the vector method. Perturbations move the system off a stable fixed point or away from the ghost of a fixed point (sometimes referred to here as a ghost attractor); the trajectories in response to these noisy perturbations, either toward the stable fixed point or near a ghost attractor, are what is analyzed to distinguish those dynamic cases. The necessity of noise makes this method ideal for experimental preparations, where noise is an intrinsic part of the system.

A flowchart illustrating how to use the vector method to distinguish stable fixed points from ghost attractors, based only on the coupled system time series, is presented in Figure 7.

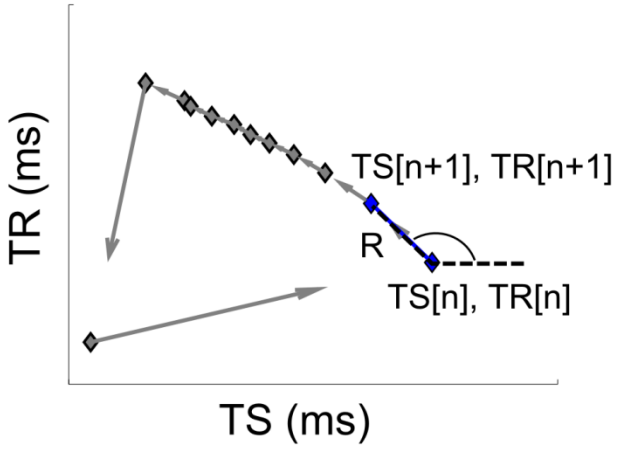


**Figure 6: Vectors can capture system movement around the ts-tr plane.** Vectors between sequential (ts, tr) pairs can be represented by a magnitude (distance) and an angle. The vector magnitude is normalized by the interspike interval to yield a number between 0 and 1. The vector magnitudes and angles quantify trajectories between sequential points around the map. Data from simulated hybrid circuit with $I_{app}$ = 0.212 nA, gsyn = 50 uS, and added current noise with standard deviation 0.1 nA.

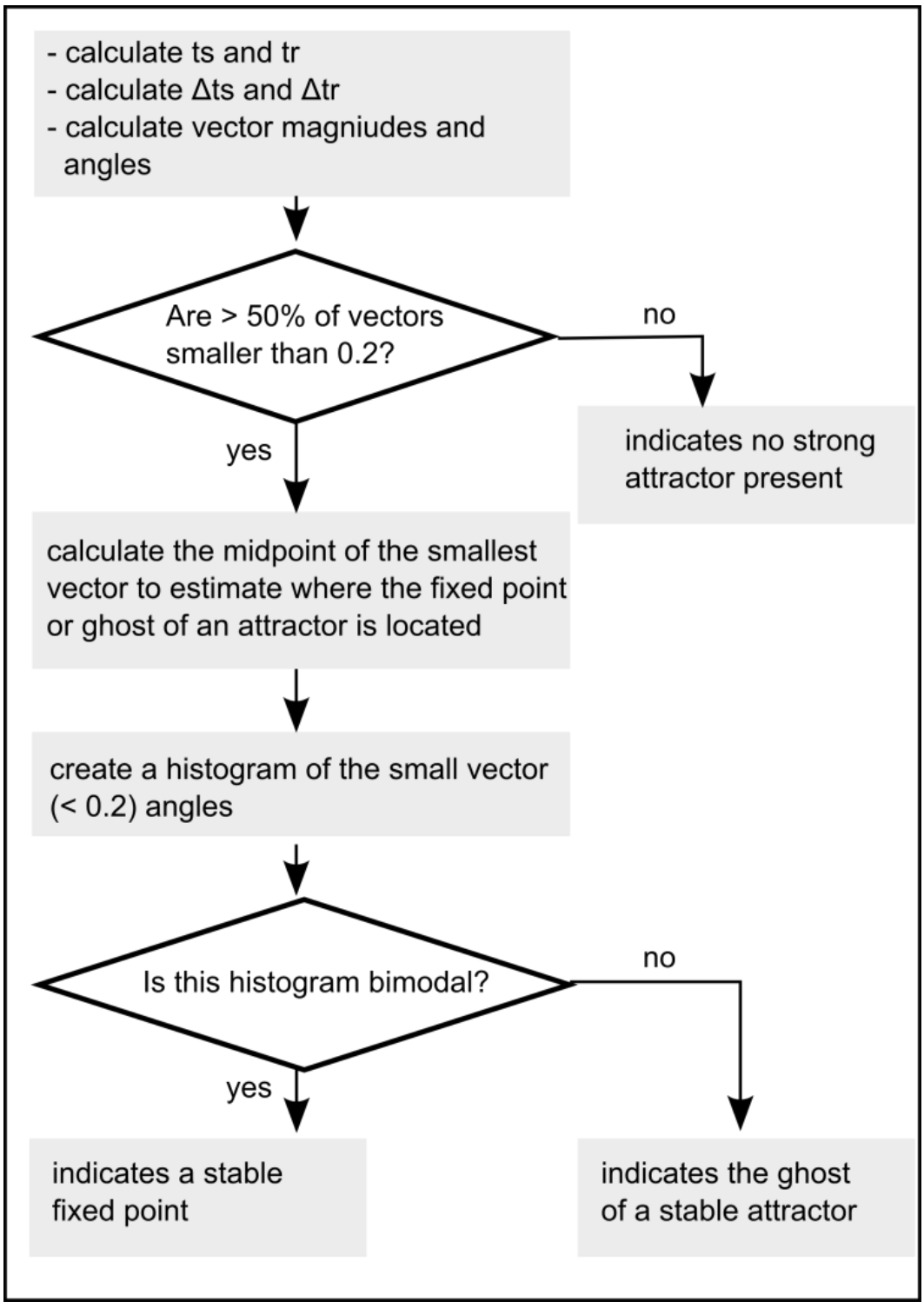


**Figure 7: Flowchart illustrating how to use the vector method.**

## 2.3 Results and Discussion

### 2.3.1 Phase slipping and phase-locking have distinct characteristics in the vector magnitude-angle space

Phase slipping and phase-locking can be distinguished using the time series vector method. Where systems spend the most time, the distance between sequential (ts, tr) points is small. Trajectories of sequential points are shown in Figure 8 A1 and A2, though to enhance clarity, the arrows shown do not fully connect the sequential points. In the phase-locked case (Figure 8 A1), all the arrows in the ts-tr plane are small, whereas in the phase slipping case (Figure 8 A2), arrows are small in the right half of the ts-tr space and large in the left half. Phase slips, which occur in the left half of this ts-tr space, have large vector magnitudes, but vectors near the ghost attractor have small vector magnitudes. In two dimensional histograms of the vector magnitude-angle space (Figure 8 B1 and B2), phase slips appear on the right side of the space, where vector magnitudes are closer to 1. Small vectors, near the left side of the vector magnitude-angle space, correspond to arrows near stable fixed points (Figure 8 B1) or ghost attractors (Figure 8 B2), where the system slows down and trajectories between sequential (ts,tr) pairs are small. The midpoint of the smallest vector that is not the result of two spikes during one reference interval, like the example in Figure 5 B2, is used to predict the location of a stable fixed point or ghost attractor on the ts-tr plane.

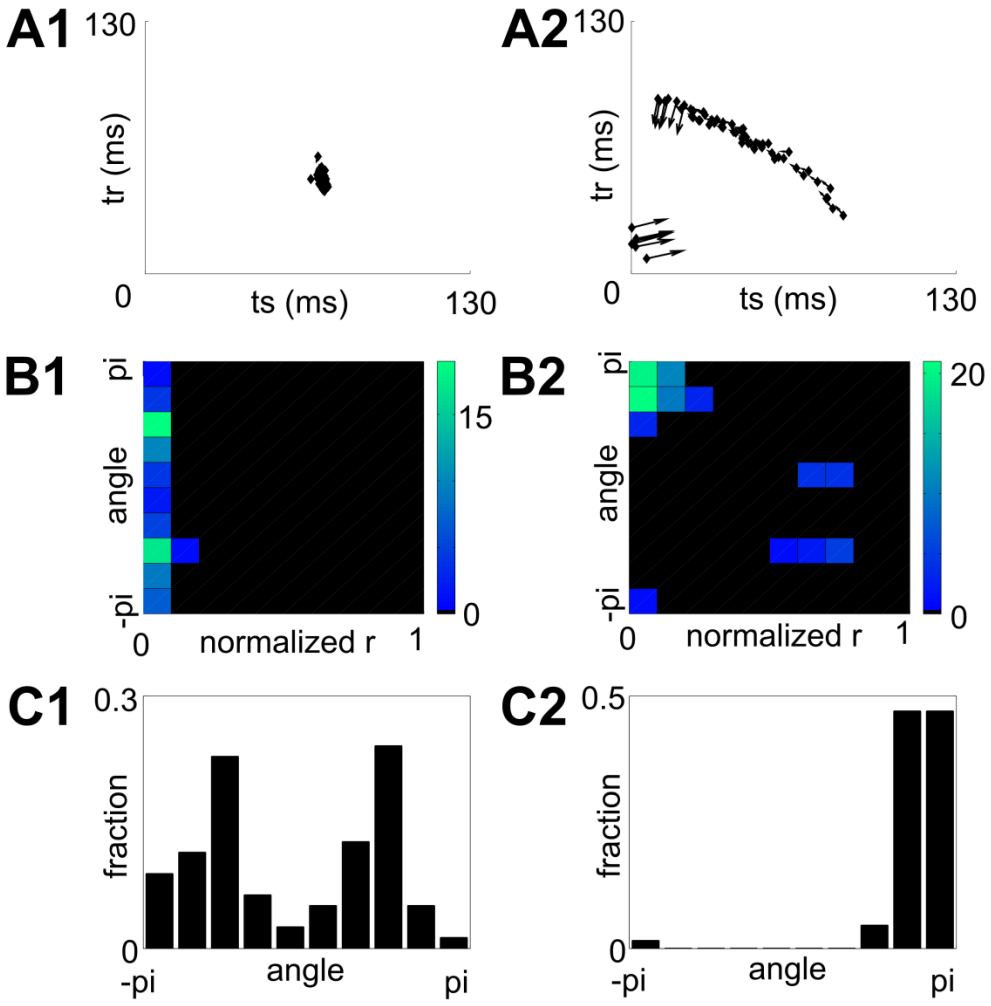


**Figure 8: The magnitude-angle vector space reveals system dynamics.** (A1) ts-tr trajectories in a phase-locked case with stable fixed point. (A2) ts-tr trajectories in a phase slipping case with a ghost attractor present. (B1) magnitude-angle vector space as a two dimensional histogram of normalized vector length and vector angle; colors within each square represent the number of vectors that have those characteristics. In the stable fixed point case, only small vectors are present. (B2) two dimensional magnitude-angle vector space in the ghost attractor case, where small and large vectors are present. (C1). Histogram of small-magnitude (<0.2) vector angles is bimodal in the stable fixed point case. (C2) histogram of small-magnitude (<0.2) vector angles is unimodal in the ghost attractor case. [Neuron 1: $I_{app}$ = 0.212 nA, gsyn21 = 40 uS; Neuron 2, left: $I_{app}$ = 0.222 nA, gsyn12 = 100: Neuron 2, right: $I_{app}$ = 0.222, gsyn 12 = 50 uS].

Examination of the vector angles where vector magnitudes are small can aid in distinguishing ghost attractors from stable fixed points. Small vectors are defined here as those with a magnitude less than 0.2. In the stable attractor case (Figure 8 C1), the small-magnitude vector angles are bimodal appearance. This occurs because when the system is shifted off the stable fixed point, it can be shifted off on either side of the stable fixed point, to one of the ts-tr curves. The trajectory of return can occur from either side of the stable fixed point, yielding small-magnitude vectors with a bimodal angle distribution but a wide range of angles represented. In contrast, in the ghost attractor case, the vectors progress in one direction (Figure 8 A2) and the angles of all these vectors are similar. Perturbations away from the ghost attractor will result in trajectories that only have one prominent direction, regardless of which side of this ghost attractor the system is perturbed to, making the small-magnitude vector angle histogram unimodal (Figure 8 C2).

The time series vector method can be used on experimental hybrid circuit data, shown in Figure 9. The computational neuron in the experimental hybrid circuit is noiseless; all noisy perturbations are supplied by the biological neuron. Cases that show obvious phase-locking (Figure 9 A1) or phase slipping (Figure 9 A2) are presented. Figure 9 A1 and A2 show network phase over time before, during, and after coupling; the grey bar represents when the system is coupled and synapses are on, while the shorter black bar represents one minute. Phase slips are present in both cases and appear as vectors with magnitude greater than 0.5 in Figure 9 B1 and B2. Examination of the low magnitude (less than 0.2) vector

angles reveals a bimodal distribution for the phase-locked case (Figure 9 C1) and a unimodal distribution for the phase slipping case (Figure 9 C2). PRCs measured for the model neuron (blue), biological neuron before coupling (solid circles) and biological neuron after coupling (hollow squares) are shown in Figure 9 D1 and D2. The coral-colored diamond in Figure 9 D1 and D2 represents the midpoint of the smallest magnitude vector, which should be near a stable fixed point or where the two ts-tr curves from each neuron are close, in the case of no ts-tr curve intersection. The neuron slows down after coupling in both cases, which shifts the PRC outward in Figures 9 D1 and D2. In Figure 9 D1, an intersection of the ts-tr curves is apparent before coupling but not after, while in Figure 9 D2, there is no intersection present, which explains the phase slipping network activity. The outlier point and the point with ts less than zero in Figure 9 D1 are artifacts of incorporating second order phase resetting into the ts-tr curve.

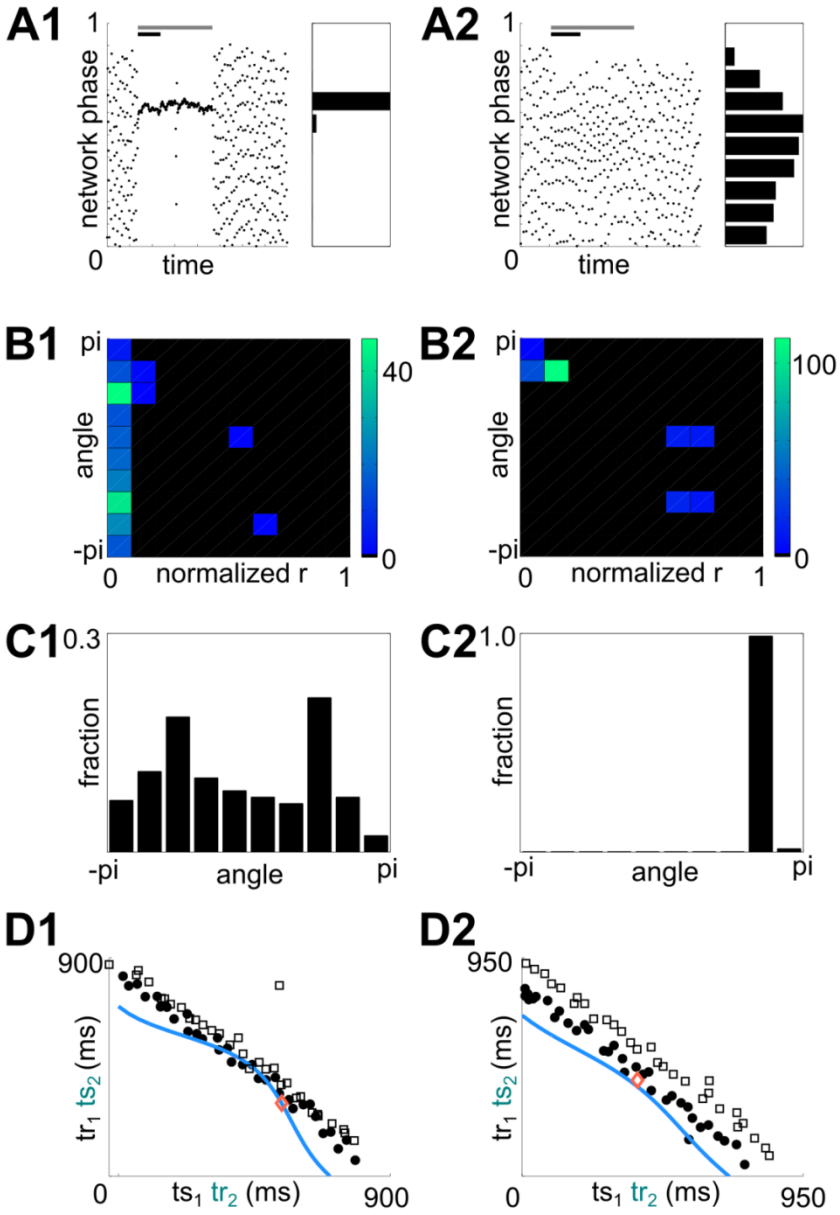


**Figure 9: Use of the method on experimental data: phase locking and phase slipping cases.** (A1) locked network phase. The system is coupled during the grey bar; black bar represents 1 minute. (A2) slipping network phase. (B1) two dimensional histogram of vector angle and magnitude; the phase-locked system has mostly small magnitude vectors. (B2) the phase slipping system has small and large magnitude vectors. (C1) the small-magnitude vector histogram is bimodal in the locked case. (C2) the small-magnitude vector histogram is unimodal in the slipping case. (D1) ts-tr curves of the model (blue) and biological neuron measured before (solid circles) and after (open squares) coupling. The coral diamond is the midpoint of the smallest vector, or predicted fixed point. (D2) same symbols as D1, but for the phase slipping case.

### 2.3.2 The presence and location of attractors can be determined by examining small vector characteristics

Simulations of the hybrid circuit were conducted using two Wang Buzsaki conductance-based model neurons (Wang & Buzsaki, 1996), reciprocally coupled using the inhibitory synapses already described. A noise current with Gaussian distribution, mean zero, and various standard deviations was added to only one of these models to simulate the biological neuron (neuron 1, black, Figure 10A). The parameters of neuron 2, the noiseless neuron, were varied such that a range of intrinsic frequencies and coupling strengths were represented. Noiseless ts-tr curves of both neurons are shown in Figure 10B (ts-tr curves for neuron 2 are blue, ts-tr curves for neuron 1 are black) and intersections of these curves are indicated with red dots. The x and y dimensions of Figure 10B represent a parameter space of neuron 2 characteristics; rows have identical ISI but different coupling strengths and therefore maximum phase resetting values, while columns have the same coupling strengths but different ISIs.

To evaluate the vector method, I compared stable fixed point locations predicted using the vector method against the fixed point locations predicted using noiseless tr-ts curve intersections. Figure 10C shows the separation between a stable fixed point predicted by the vector method and the nearest intersection of the noiseless ts-tr curves for various levels of added noise. The x and y dimensions represent the same neuron 2 parameter space as in Figure 10B. Error terms are only calculated for cases known to have stable fixed points, according to the ts-tr curves in Figure 10B. As the magnitude of the noise standard deviation

increases, so does the error between predicted fixed point location and nearest noiseless ts-tr curve intersection.

Another evaluation metric is to compare how well the vector method predicts stable fixed points as compared to another method used with experimental hybrid circuit data (Figure 11). The "ground truth" for whether stable fixed points are present or not is shown in Figure 11 A; this matrix has x and y dimensions that represent the parameter space of neuron 2 in the simulated hybrid circuit. This space is identical to the one presented in Figure 10B and 10C. Regions that contain a stable fixed point, as determined by intersections of the noiseless ts-tr curves in Figure 10B, are shaded blue, while regions without a stable fixed point are shaded black.

In circular statistics, $R^2$ is a measure of dispersion; it is the squared mean vector length R, which is the average length of N unit-length vectors, each representing a circular variable, that are added geometrically (Baschelet, 1981). Network phase is a circular variable, because a network phase of 0 and a network phase of 1 represent the same value. Systems with network phase $R^2$ values above 0.7 are considered to be strongly phase-locked (Sieling et al., 2009; Thounaojam et al., 2014); because strong phase locking is often the consequence of a stable fixed point, high $R^2$ implies a stable fixed point is present. Figure 11 B1 shows regions of neuron 2 parameter space in simulated hybrid circuits that have network phase $R^2$ values above 0.7 in white and regions with simulated hybrid circuit network phase $R^2$ below 0.7 as black. A noise current with Gaussian

distribution, mean zero, and standard deviation 2.5 is added to neuron 1 in all the stimulated hybrid circuits in this figure. Figure 11 C1 and D1 are shaded identically except that the noise current for neuron 1 has standard deviations of 0.9 and 0.5 instead.

Figure 11 B2 shows the vector method predictions of stable fixed points. According to the flowchart in Figure 7, only cases with a majority of small vectors show evidence of strong interaction between the two neurons of the simulated hybrid circuit. In the left panel of Figure 11 B2, regions that show simulated hybrid circuit activity where more than 50% of the vectors are smaller than 0.2 are shaded white, else they are shaded black. Of those regions shaded white in the left side of Figure 11 B2, the ones with small-magnitude angle histograms that are bimodal, as determined by eye, are shaded red in the right panel of Figure 11 B2. As explained previously, bimodal angle histograms for small-magnitude vectors are indicative of stable fixed points. Figure 11 C2 and D2 are shaded identically as Figure 11 B2, only the noise current added to neuron 1 of the simulated hybrid circuit has standard deviation 0.9 and 0.5 nA, respectively.

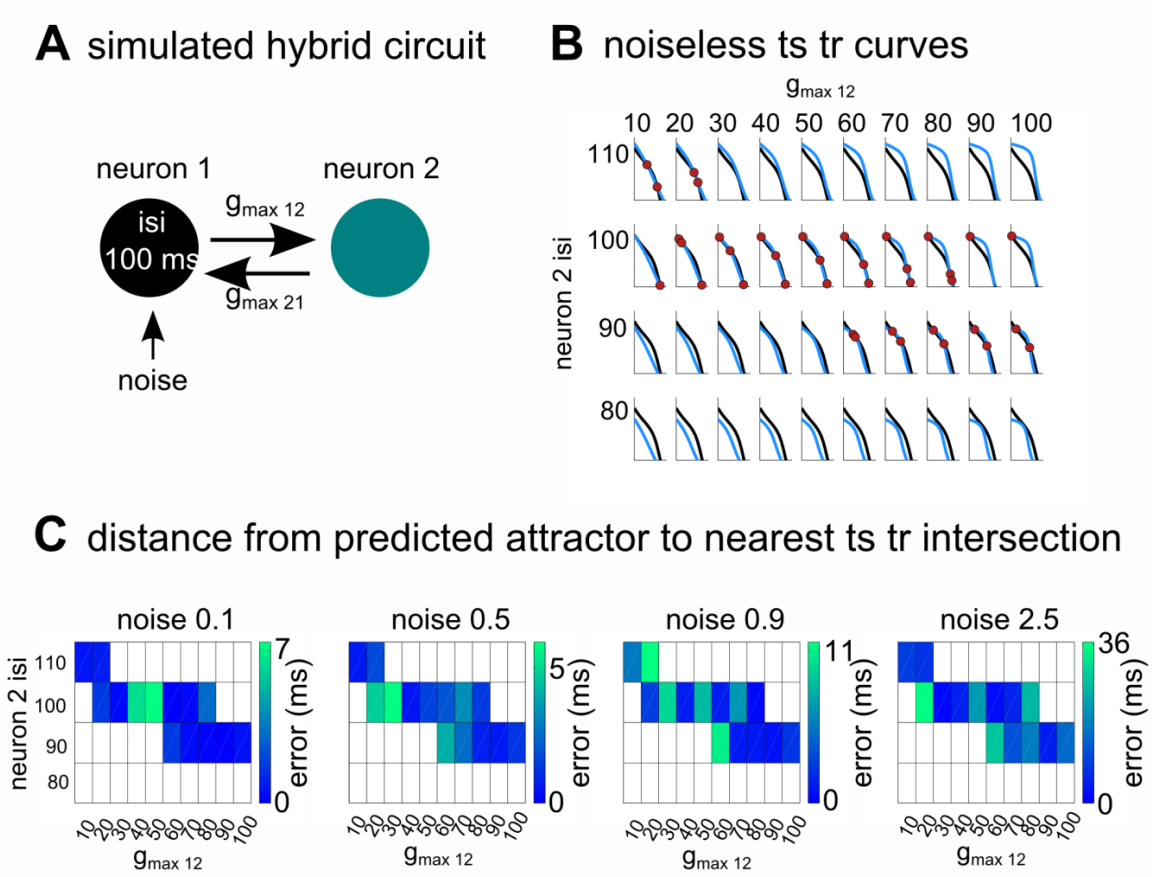


**Figure 10: Simulated hybrid circuit and use of the vector method over a parameter space.** (A) schematic of simulated hybrid circuit. (B) ts-tr curves from noiseless neuron simulations; neuron 1(black), neuron 2(blue) and intersections (red dots). (C) error between predicted stable fixed point and nearest intersection from panel B, for different levels of noise added to neuron 1.

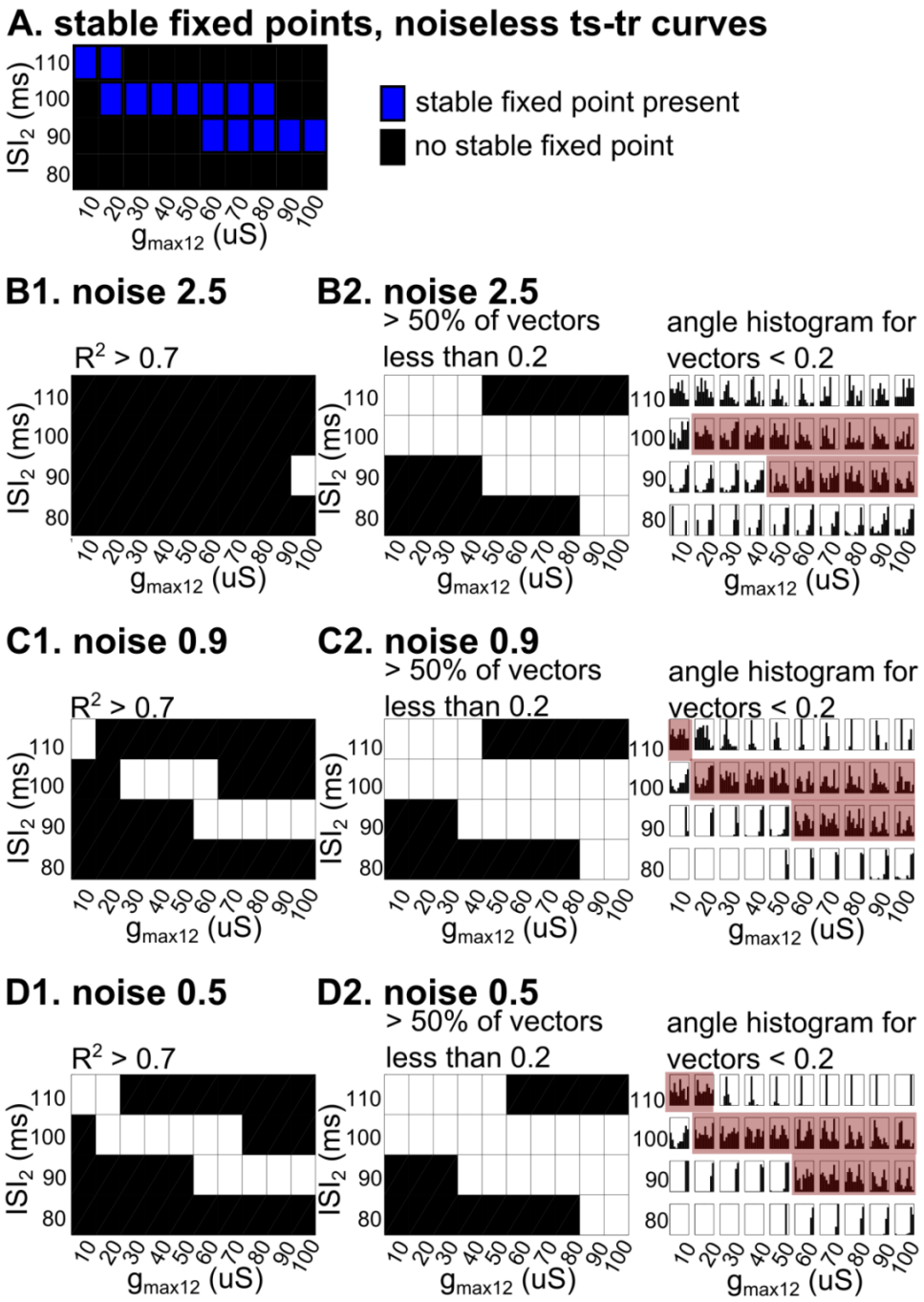


**Figure 11: Evaluation of stable fixed point identification: vector method and $R^2$.** (A) colors represent parameter space regions that contain (blue) and do not contain (black) stable fixed points, according to noiseless ts-tr curves shown in Figure 10B. (B1) simulated hybrid circuits with network phase R2 above (white) and below (black) 0.7. (B2) simulated hybrid circuits with more than 50% of vectors smaller than 0.2 (left) shown in white; of those, the angle histograms identified as bimodal are shaded red. Current noise added to simulated hybrid circuits with standard deviation 2.5 nA (B1, B2), 0.9 nA (C1, C2), 0.5 nA (D1, D2).

From Figure 11, it is apparent that the vector method is better than $R^2$ at detecting stable fixed points in noisy simulated hybrid circuits, though $R^2$ works perfectly in low noise conditions. To quantify the panels of Figure 11 formally, Table 1 shows number of false positives, true positives, false negatives, and true negatives per noise condition and per method. True positives are cases where a stable fixed point is predicted and one exists, false positives are cases where a stable fixed point is predicted but does not exist, true negatives are cases where a stable fixed point was not predicted and one does not exist, and false negatives are cases where a stable fixed point was not predicted but one is present. Out of the 40 regions presented in the matrix of Figure 11A, 14 contain stable fixed points and 26 do not.

The vector method is more accurate and sensitive than $R^2$ at identifying stable fixed points in 2 out of the 3 noise conditions surveyed here (Table 2). Accuracy is a measure of correctness and is defined as the number of identified true positives and true negatives over the sum of actual positives and negatives (Zhu, Zeng, & Wang, 2010). Sensitivity is defined as the number of identified true positives over the sum of identified true positives and false negatives (Zhu et al., 2010); it is an indication of how specific each method is when detecting stable fixed points.

**Table 1: Evaluation of the vector method and $R^2$ as a way to identify stable fixed points**

| | | R2 > 0.7 | vector method | | R2 > 0.7 | vector method |
|---|---|---|---|---|---|---|
| **noise 2.5** | correctly identified as stable fixed point | 1 | 12 | true positive rate | 7.1 % | 85.7 % |
| | incorrectly identified as stable fixed point | 0 | 3 | false positive rate | 0.0 % | 11.5 % |
| | correctly identified as not stable fixed point | 26 | 23 | true negative rate | 100.0 % | 88.5 % |
| | incorrectly identified as not stable fixed point | 13 | 2 | false negative rate | 92.9 % | 14.3 % |
| **noise 0.9** | correctly identified as stable fixed point | 10 | 13 | true positive rate | 71.4 % | 92.9 % |
| | incorrectly identified as stable fixed point | 0 | 2 | false positive rate | 0.0 % | 7.7 % |
| | correctly identified as not stable fixed point | 26 | 24 | true negative rate | 100.0 % | 92.3 % |
| | incorrectly identified as not stable fixed point | 4 | 1 | false negative rate | 28.6 % | 7.1 % |
| **noise 0.5** | correctly identified as stable fixed point | 13 | 14 | true positive rate | 92.9 % | 100.0 % |
| | incorrectly identified as stable fixed point | 0 | 2 | false positive rate | 0.0 % | 7.7 % |
| | correctly identified as not stable fixed point | 26 | 24 | true negative rate | 100.0 % | 92.3 % |
| | incorrectly identified as not stable fixed point | 1 | 0 | false negative rate | 7.1 % | 0.0 % |

**Table 2: Accuracy and sensitivity of each method for finding stable fixed points**

| noise level | | R2 > 0.7 | vector method |
|---|---|---|---|
| 2.5 | accuracy | 68 % | 88 % |
| | sensitivity | 7 % | 86 % |
| 0.9 | accuracy | 90 % | 93 % |
| | sensitivity | 71 % | 93 % |
| 0.5 | accuracy | 98 % | 95 % |
| | sensitivity | 93 % | 100 % |

### 2.3.3 The time series vector method can resolve cases of similar phase with different dynamics

If the PRC-based map cannot be constructed for a hybrid circuit and only the network phase over time is accessible, system dynamics can appear ambiguous, especially in the presence of noise (Figure 12 A1 and A2). Network phase traces for the stimulated hybrid circuits presented in Figure 12 A1 and 12A2 are similar over time and show episodes of phase locking and phase slipping. Examination of the magnitude-angle space and angle histograms (Figure 12 B1 and B2) can reveal the case with a stable fixed point (Figure 12 B1) from the case with a ghost attractor (Figure 12 B2). The small-magnitude vector angle histogram is bimodal in the stable fixed point case (Figure 12 C1) and unimodal for the ghost attractor case (Figure 12 C2). For comparison, the ts-tr curves from noiseless neuron simulations (neuron 1 black, neuron 2 blue), ts-tr intersections (if present, red circles), and predicted stable fixed point (Figure 12 D1) or predicted ghost attractor (Figure D2) in open squares are shown.

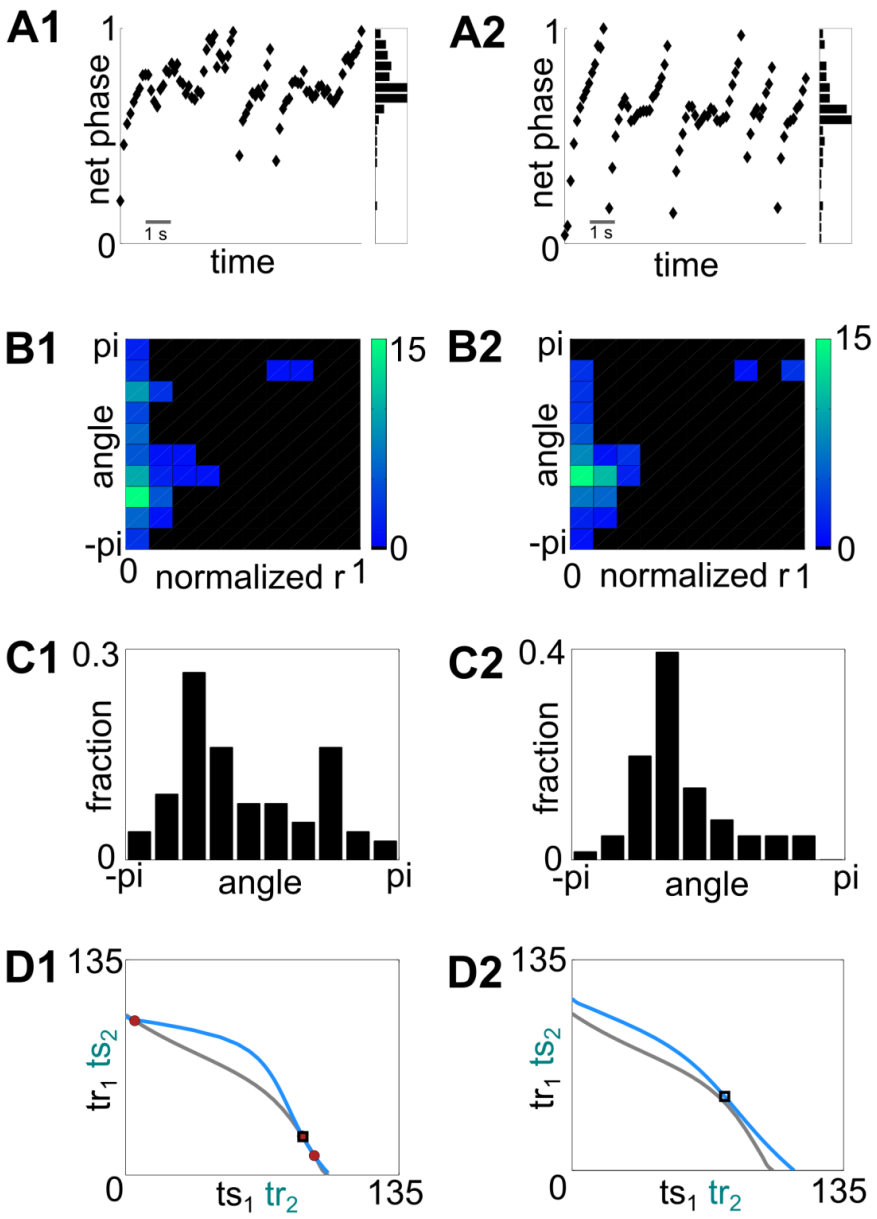


**Figure 12: Vector angles can distinguish cases with similar network phase but different underlying dynamics.** (A1) network phase over time, histogram shown to the right. Stable fixed point case. (A2). Network phase over time, ghost attractor case. (B1) vector magnitude-angle for stable fixed point case. (B2) vector magnitude-angle space for ghost attractor case. (C1) histogram of small-magnitude (<0.2) vector angles, stable fixed point. (C2) histogram of small-magnitude (<0.2) vector angles, ghost attractor. (D1) noiseless ts-tr curves for each simulated neuron (neuron 1 grey, neuron 2 blue); intersections shown in red, with predicted fixed point as an open black square directly over one intersection. (D2) same as D1, but no intersections exist. Data from simulated hybrid circuits with the following parameters: [Neuron 1: $I_{app}$ = 0.212 nA, gsyn21 = 40 uS; Neuron 2, left: $I_{app}$ = 0.212 nA, gsyn12 = 80: Neuron 2, right: $I_{app}$ = 0.204, gsyn 12 = 30 uS].

### 2.3.4 The time series vector method captures dynamic changes induced by noise

Noiseless ts-tr curves can reveal if a coupled system has fixed points in the noiseless case. The addition of noise can change observed system activity and system dynamics. Figure 13 shows two simulated hybrid circuits with identical parameters except the standard deviation of the current noise added to neuron 1. Network phase histograms are similar for the 0.9 (Figure 13 A1) and 2.5 (Figure 13 A2) nA noise cases. The vector magnitude-angle spaces of both cases show evidence of phase slipping and phase-locking, though there is a single peak of angles at small vectors for the 0.9 noise level (Figure 13 B1) and multiple angle peaks at small vector magnitudes for the 2.5 noise level (Figure 13 B2). This difference in small-magnitude vector angles is evidence in those histograms (Figure 13 C1 and C2). The addition of more noise induces a multimodal peak in the angle histogram; a bimodal distribution is a hallmark of stable fixed points (discussed previously), though there are three prominent peaks in Figure 13 C2.

The noise-induced stable fixed point dynamics can be explained using the ts-tr curves. Figure 13 D shows the noiseless ts-tr curves for neurons 1 and 2 of the simulated hybrid circuit as solid black and blue lines, respectively. Ts-tr curves for neurons with an intrinsic ISI 10 ms slower and 10 ms faster than the solid black ts-tr curve are shown as black dotted and dashed ts-tr curves, respectively. As is, the solid blue and black ts-tr curves do not intersect, so no stable fixed point is present. If neuron 1 were to speed up and possess a ts-tr curve equivalent to the black dashed trace, an intersection between this curve and the solid blue ts-tr

curve would be present. If instead neuron 1 were to slow down, the ts-tr curve would shift outward to where the dotted ts-tr curve is located, in which case this system would have no fixed point present. A shift in the intrinsic frequency or ISI of the noisy neuron in a simulated hybrid circuit, then, is sufficient to change the system dynamics of the circuit by creating or destroying a stable fixed point.

Current noise added to a simulated neuron makes the ISIs of that neuron irregular. Examples of a Wang-Buzsaki model neuron with added current noise that has a Gaussian distribution, zero mean, and various standard deviations is shown in Figure 14. Larger standard deviations of the noisy current result in more irregular ISIs, as can be seen in the ISI time traces (Figure 14, left), histograms (Figure 14, middle), and summary statistics (Figure 14, right). For current noise with mean zero and standard deviation 0.9 and 2.5, the mean ISI is approximately 100 ms but the ISI standard deviation is approximately 2 ms and 10 ms, respectively. This means that in the latter case, the neuron has a range of ISIs, including some 10 ms faster and 10 ms slower than in the noiseless case. As discussed in the preceeding paragraph, the ts-tr curves of neurons at one end of that range will form a stable fixed point with the ts-tr curve from the other neuron in the simulated hybrid circuit, resulting in system dynamics that have stable fixed point type characteristics.

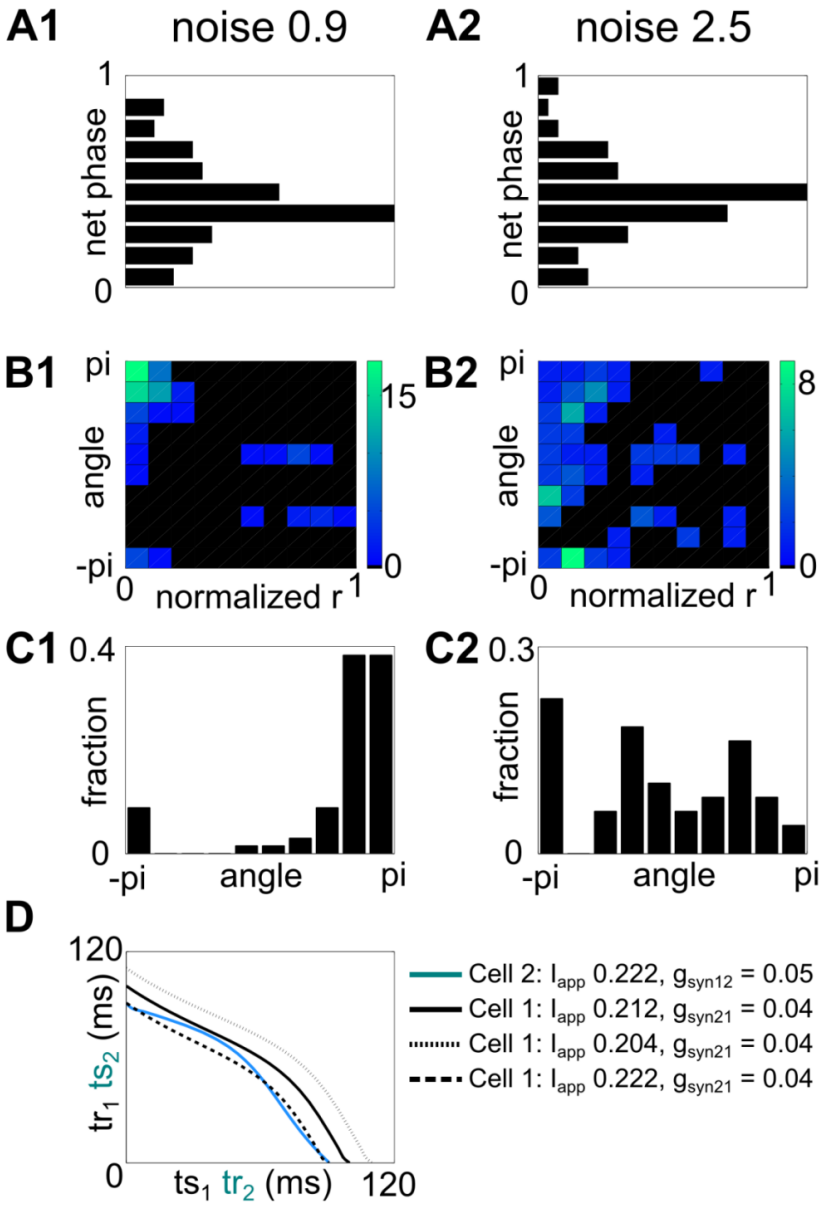


**Figure 13: The vector method can identify dynamic changes due to noise.** (A1)network phase of simulated hybrid circuit with added current noise (mean 0, standard deviation 0.9 nA). (A2) network phase for the same hybrid circuit with greater noise (standard deviation 2.5). (B1)angle-magnitude space for 0.9 noise condition and (B2) 2.5 noise condition. (C1) angle histograms of small-magnitude (<0.2) vectors suggest that the low noise case has a ghost attractor. (C2) angle histograms of small-magnitude vectors for the large noise condition suggest a stable fixed point. (D) noiseless ts tr curves. Solid black and blue curves represent noiseless ts-tr curves with parameters used for the simulated hybrid circuit. Dotted and dashed black lines represent ts-tr curves from simulated neurons with ISIs that are 10 ms higher and lower, respectively, than the solid black curve. Data from simulated hybrid circuits.

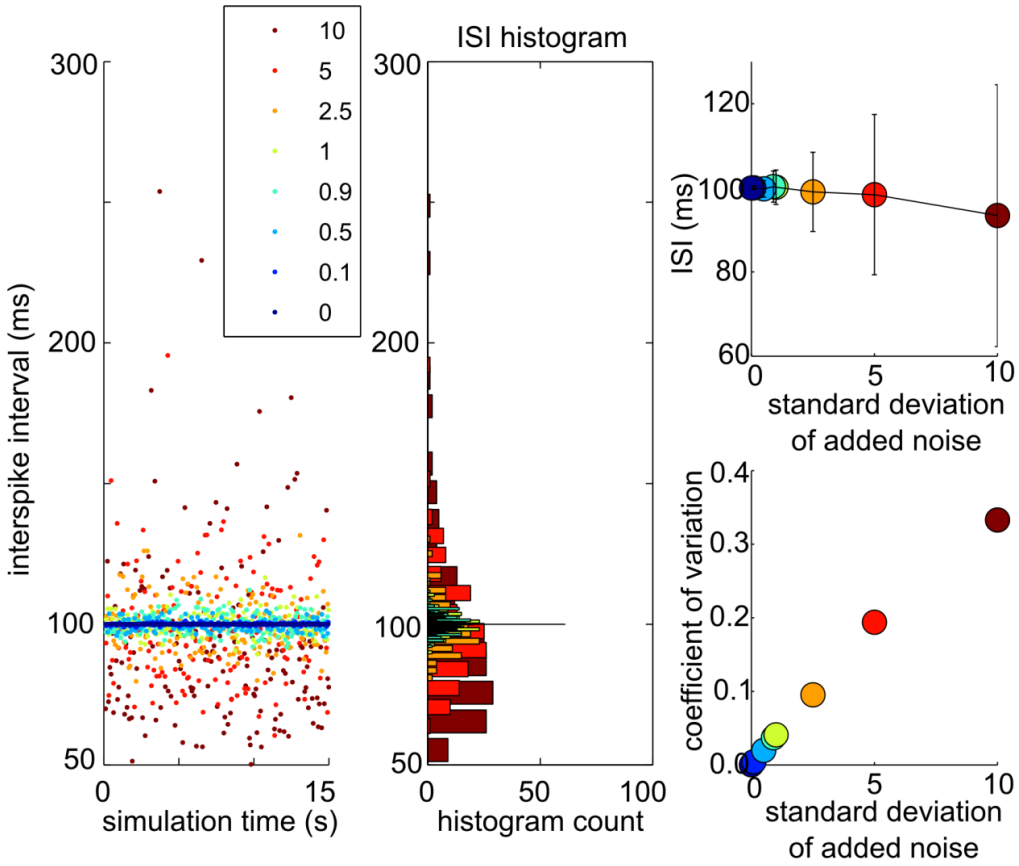


**Figure 14: Interspike interval of simulated Wang-Buzsaki neuron with various levels of current noise added.** Left, interspike interval (ISI) over 15 seconds of simulation time; mean zero Gaussian current noise is added to the neuron with standard deviation (nA) indicated in the legend. Middle, histogram of ISIs for various noise levels, again color coded as in legend. Right top, mean ISI and one ISI standard deviation as a function of standard deviation of added current noise. Right bottom, coefficient of variation of ISI as a function of current noise standard deviation. Applied current for this model simulation is 0.212 nA.

**Table 3: Mean ISI and ISI standard deviation of simulated neuron with noise.** Quantification of statistics in Figure 14, right panel.

| added current noise standard deviation (nA) | 0 | 0.1 | 0.5 | 0.9 | 1.0 | 2.5 | 5.0 | 10.0 |
|---|---|---|---|---|---|---|---|---|
| mean ISI (ms) | 100.0 | 100.0 | 99.7 | 100.3 | 100.1 | 99.1 | 98.4 | 93.4 |
| ISI standard deviation (ms) | 0.0 | 0.4 | 2.0 | 3.7 | 4.1 | 9.4 | 19.1 | 31.1 |
| coefficient of variation (CV), % | 0.0 | 0.4 % | 2.0 % | 3.7 % | 4.1 % | 9.5 % | 19.4 % | 33.3 % |

### 2.3.5 Changes in dynamics over time can be resolved using vector characteristics

A significant limitation of using the ts-tr maps is that the maps assume that phase resetting characteristics, which set the amount of curvature of the ts-tr curve, and intrinsic frequency, which determines the intercepts of the x and y axes of the map, remain consistent over time. Even if the synaptic coupling strength $g_{max}$ were kept constant, changes in intrinsic frequency can change the maximum phase resetting of the PRC, therefore changing the curvature of the ts tr curves. The vector method does not have these limitations.

Spiking neurons have variable interspike intervals (see Chapter 3). This intrinsic variability can change network phase over time. Figure 15A shows network phase of an experimental hybrid circuit over time. The grey bar represents the time the system was coupled, while the shorter colored bars represent 30 second segments in time. The system remains phase-locked for most of the coupling episode, though some phase slipping is present during the blue interval.

The midpoint of the shortest vector is the predicted location of a stable fixed point or ghost attractor. The location of this point moves around during the coupling episode. Figure 15B shows (ts, tr) pairs for each cycle during coupling (black diamonds) and the predicted stable fixed point or ghost attractor for each of the 30 second segments in the corresponding colored diamonds; the predicted attractor for the entire coupling episode is shown as a grey diamond.

Changes in the predicted stable fixed point or ghost attractor location mean that the timing relationship between the two neurons changed. The precise timing of neuron activity can be meaningful, such as the 20 ms offsets ideal for spike timing dependent plasticity (Bi & Poo, 1998). Changes in relative timing of the two neurons could also result in network phase changes, but this is not required.

The presence of a stable fixed point or ghost attractor present during the 30 second subsets can still be determined using the vector magnitude-angle space and the distribution shape of the small-magnitude vector angle histograms. In Figure 15 C1, the bimodal small-magnitude (<0.2) angle histogram implies that a stable fixed point exists during the yellow subset of Figure 15 A, which is also implied by the relatively steady phase locking observed in this subset in Figure 15 A. Figures 15 C2 and C4 show bimodal angle histograms which indicate a stable fixed point, in agreement with the phase-locked activity observed during the green and purple subsets of Figure 15 A, respectively. In Figure 15 C3, the unimodal histogram of angles for vectors with small magnitudes indicates that a ghost attractor, rather than a stable fixed point, is present, and the phase slipping seen during the blue subset of Figure 15 A supports this assessment.

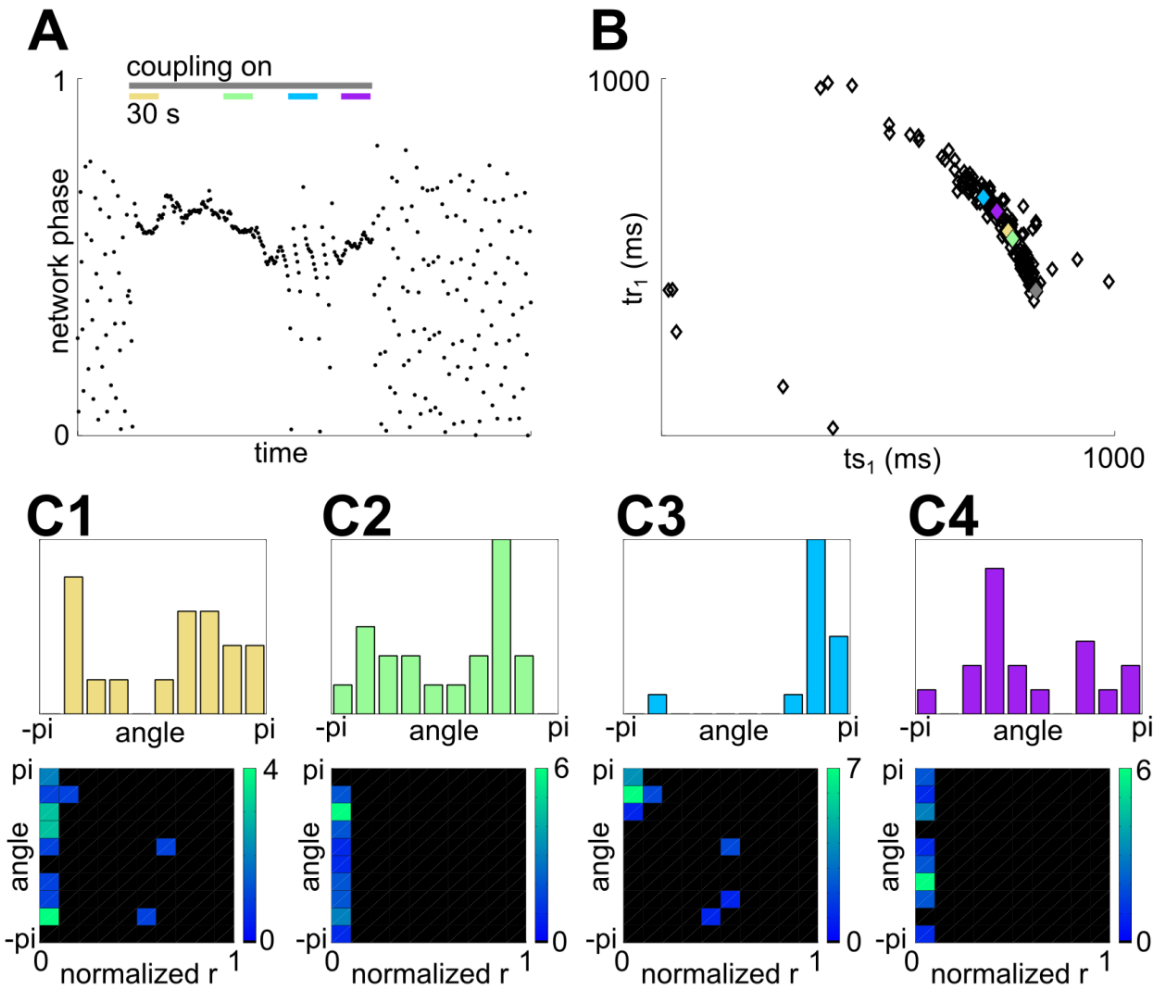


**Figure 15: Movement of attractors and transitions between types of activity can be captured using the vector method.** (A) network phase before, during, and after coupling (coupling on during grey bar). Colored subsets are 30 seconds long. (B)coupled system (ts,tr) pairs (black diamonds), and predicted stable fixed point or ghost attractor for each colored subset and the entire coupling episode (grey diamond). (C1) angle histogram of small-magnitude (<0.2) vectors (top) and angle-magnitude space (bottom) for the yellow subset. (C2) same as C1 for the green subset. (C3) same as C1 for the blue subset. (C4) same as C1 for the purple subset. Data from experimental hybrid circuits.

## 2.4 Conclusions

Neural systems show many types of activity. Phase-locked and synchronous activity are known to be important for function. These types of activity can be studied in a hybrid circuit preparation, where only the biological neuron imparts biologically-relevant noise into the system. A map based on measured PRCs can explain and predict these types of activity, but not if the PRCs can't be measured, are extremely noisy, or change over time.

The method presented here is based on constructing vectors from the coupled system time series and does not have the same limitations as the PRC-based map. Large magnitude vectors indicate phase slips while small vectors indicate strongly interacting systems that may have stable fixed points or ghost attractors. If the distribution of the small vector angles is bimodal, the system likely has a stable fixed point present; if the angle distribution is unimodal, this is a hallmark of a ghost attractor. If there are no small vectors present, the system is not interacting strongly, or at all.

The method provides a way to determine dynamics in small circuits, even when the PRC cannot be measured or is changing over time. Phase-locking and phase slipping network activity can be used as indicators of stable fixed points and ghost attractors, respectively, but network phase activity can show both slipping and locking features such that underlying dynamics are ambiguous. Cases with similar network phase over time and network phase histograms but different dynamics can be distinguished, even in the presence of noise, using the vector

method. In addition, noise-induced attractors not predicted by a noiseless PRC-based map can be detected using the time series vector method. Intrinsic frequency variability that shifts a stable fixed point or changes dynamics can also be resolved by the vector method.

The method is extendable to circuits without reciprocal connections. If constructing a PRC-based map of this case, the ts-tr curve of the driving neuron would be a flat diagonal line while the driven neuron ts-tr curve would have more curvature, depending on the strength of coupling. Characterization of vectors in terms of angles and magnitudes remains the same.

The dynamics of small circuits are relevant to larger networks. Recent work by Gollo and colleagues demonstrated that a network with a reciprocally coupled circuit within it could produce synchronous activity, even in the presence of noise (Gollo et al., 2014), so understanding how two-cell circuits synchronize is relevant to understanding larger networks. It is possible that the vector method presented here can also be used to characterize the dynamic interactions within a network and may provide clues to connections that are more and less critical for circuit function.

### 2.5 Statement of effort

Simulations and hybrid circuit experiments in Chapter 2 were performed by me. Contributions to develop the vector method were made by Rob Butera, Carmen Canavier, and myself.

# CHAPTER 3: STOCHASTICITY AND HISTORY ARE REQUIRED TO REPRESENT INTRINSIC SLOW VARIABILITY IN NEURON INTERSPIKE INTERVAL

## 3.1 Introduction

Biological systems show variability at many scales, and neurons are no exception. How neurons accomplish survival-level and cognitive-level functions is a central question of neuroscience. How variability at the single neuron level influences network function and what type of variability is present in neural systems are relevant to this larger question.

Phase-locked neural activity seems to be present in many neural functions. Synchronization is thought to play a role in memory (Juergen Fell & Axmacher, 2011; Jutras & Buffalo, 2010). Patients with schizophrenia and epilepsy have disrupted forms of synchronization (Uhlhaas & Singer, 2006). At the invertebrate level, central pattern generators (CPGs) rely on coordinated, phase-locked activity to achieve various functions (Marder & Calabrese, 1996); feeding and escaping are two such functions governed by CPGs (Selverston, 2010). Precisely how synchronization and phase-locking are achieved and persist in neural systems is still incompletely understood and remains an active area of study.

Previous studies indicate that biological variability can change network activity (Thounaojam et al., 2014). In a hybrid circuit model, we showed that when user-controlled parameters were held constant, the hybrid circuit could transition between phase-locked activity, where one neuron is active at approximately

the same phase of the reference neuron's cycle, and phase slipping activity, where one neuron spikes faster than the other and the relationship between the oscillators changes from cycle to cycle. In simulations of this system, Gaussian noise added to the phase resetting curve or the period of one of the neurons was not sufficient to instigate the transitions between locking and slipping that were observed in the experiments. However, by representing the biological neuron as an Ornstein-Uhlenbeck (OU)-type process (Uhlenbeck & Ornstein, 1930), with an explicit dependence on past history and a stochastic component, transitions from phase locking to phase slipping and back could be captured in simulation.

Prior work indicates that history and randomness are both important to mimic the dynamics of the hybrid circuit. Modelling the ISI of one neuron with an OU process can replicate experimentally observed transitions, but the ideal representation of neural variability over time remains unclear. The mechanism behind such variability is also unclear, as are the effects of this type of noise on larger networks. We conduced hours-long recordings of intrinsically active neurons in *Aplysia californica,* identified a discrete process model of ISI over time that captures features of the data, and identified a potential biophysical mechanism for the observed experimental features.

## 3.2 Methods

### 3.2.1 Electrophysiology

*Aplysia californica* were ordered from the National Resource for Aplysia (Miami, FL) and housed in saltwater tanks at room temperature until use. Animals were anesthetized with 330 mM MgCl2 solution, injected at approximately 50% volume per body weight (Jhala et al., 2011). The abdominal ganglion was removed and pinned into a Sylgard-lined 35 mm petri dish. The dish was filled with high $Mg^{2+}$ low $Ca^{2+}$ saline, containing (in mM): 330 NaCl, 10 KCl, 90 $MgCl_2$, 20 $MgSO_4$, 2 $CaCl_2$, and 10 HEPES (Nowotny et al., 2003). This saline reduces synaptic activity and isolates the neuron (Nowotny et al., 2003), though some inhibitory pulses were seen in a few voltage traces (see limitations section). The connective tissue around the ganglion was removed with fine scissors and forceps to allow access to individual neurons. Endogenously active neurons in the lower left quadrant of the abdominal ganglion (Frazier, Kandel, Kupfermann, Waziri, & Coggeshall, 1967) were targeted for recording, with the exception of data set 5, which was from the right half of the ganglion.

Preparations were perfused with high $Mg^{2+}$ low $Ca^{2+}$ saline during experiments. The petri dish and inlet tubing were placed on a Peltier device whose temperature was adjusted via a proportional integrative derivative (PID) controller. Temperature for PID controlled adjustments was measured using a resistive thermal device (RTD) in the dish, while saline temperature was also measured and recorded from using thermocouple and thermistor probes.

Thin-walled glass capillaries (0.75 mm inner diameter, 1.0 mm outer diameter) were pulled on a Sutter P-97 puller. Capillaries were filled with 3 M potassium acetate solution and a silver wire chlorided in bleach. Electrode resistance was approximately 6-15 MΩs. An Axoclamp 2B amplifier was used to measure voltage and supply currents for checking resistances. Data were sampled at 10 kHz via a National Instruments data acquisition card. Recording and stimulus commands were implemented using custom modules built on Real Time eXperiment Interface (RTXI, www.rtxi.org) (Lin et al., 2010).

### 3.2.2 Spike train analysis

At least the initial 20-30 minutes of each recording, when cell resistance was measured, was removed. Voltage transients measured as spikes and two very large outlier ISIs (set 8) were also removed. Spike times were determined by crossings of -20 mV thresholds(-35 mV for set 1, to accommodate lower spike heights). Interspike interval (ISI) is defined as the time between two sequential spike times. Delta ISI is the difference between two sequential ISIs. Data analysis was performed in MATLAB; autocorrelation and partial autocorrelation coefficients were calculated using the built-in autocorr() and parcorr() functions.

### 3.2.3 Autoregressive integrated moving average models

Autoregressive integrated moving average (ARIMA) models are flexible linear models that describe discrete processes (Box & Jenkins, 1970). The ARIMA (p, d, q) description represents a process with p autoregressive components, d orders of differencing, and q moving average components. Autoregressive

components are those with an explicit dependence on earlier values of the process. The integrative quantity represents the number of times the process had to be differenced to become stationary; ARIMA models are unique because the process itself does not have to be stationary, only stationary at some level of differencing. The moving average component represents a random white noise process with explicit dependence on some number of prior random white noise processes.

The general form for an ARIMA model, as presented in (Box & Jenkins, 1970), is

$$\phi(B)\nabla^d z_t = \theta_0 + \theta(B)a_t$$

Here, $\phi$ represent autoregressive coefficients, B represents the backspace shift operator, $\nabla$ is the difference operator, d is the order of differencing, z is the process, $\Theta_0$ is a constant, $\Theta$ are moving average coefficients, and a is a white noise process (Box & Jenkins, 1970). As an example, an ARIMA (1, 1, 1) process to describe ISI would be written

$$\Delta ISI\ [n] - \phi * \Delta\ ISI\ [n-1] = a[n] - \theta * a[n-1] + \theta_0$$

A number of heuristics are used to determine the proper orders of each of the components. The series is differenced until either the autocorrelation or partial autocorrelation (or both) of the differenced series drops off relatively quickly (Box & Jenkins, 1970). If the autocorrelation drops off quickly, this suggests a moving

average process of order equal to the number of nonzero lags; if instead the partial autocorrelation drops of quickly, this suggests an autoregressive process equal to the number of nonzero lags. If both drop off quickly, autoregressive and moving average components may be necessary to represent the sequence.

There can be some ambiguity in selecting a proper model, particularly with regard to the number of times the series needs differenced or the order of components. One way to compare models against one another is to compare the Akaike Information Criterion (AIC) (Ozaki, 1977). The AIC is a metric which rewards the fit of the model (log likelihood) while penalizing the number of parameters (coefficients) in the model. An ARIMA (p, d, q) model has p + q + 1 degrees of freedom, for the p autoregressive coefficients, q moving average coefficients, and one constant. Coefficients for models with $0^{th}$ or $1^{st}$ order components were estimated and AIC calculated using MATLAB functions.

ARIMA models with $0^{th}$ or $1^{st}$ order p, d, and q values were estimated because these models are conceptually simple and because correlational features of experimental data indicated an ARIMA (0, 1, 1) model might be sufficient to represent these data (see sections 3.3.1.3 and 3.3.2.1). In addition, some of these models are familiar and, as such, form a good basis for comparison; for example, an ARIMA(0, 1, 0) process represents a random walk in which the next value is equal to the prior value plus an independent, normally distributed random number. An ARIMA (0, 0, 1) model is itself an independent random process with a

normal distribution. The ARIMA(1, 0, 0) is equivalent to an OU process with zero mean and a scaled white noise term.

Residuals from estimated models should be evaluated to determine if models are performing well or not. Ideally, residuals should be uncorrelated. The Ljung-Box Q statistic is a measure of residual correlation (Ljung & Box, 1978). The null hypothesis of the Q statistic is that the residuals are uncorrelated; a rejection of the null hypothesis with $p < 0.05$ implies that residuals are correlated and that a different model with more parameters may better represent the data.

ARIMA model estimation and evaluation were done in MATLAB. Specific functions used include arima() to specify models, estimate() to estimate coefficients, infer() to infer residuals, aicbic() to calculate AIC, and lbqstat() to calculate the Ljung-Box Q statistic.

### 3.2.4 Integrate and fire model with adaptation

To explore how experimentally observed correlational features could be produced at a mechanistic level, we use the integrate and fire model presented in (Schwalger et al., 2010). The model, as presented in that paper, is defined by the following equations:

$$\dot{v} = \mu - \beta(w + \eta) + \sqrt{2D}\xi(t)$$

$$\dot{w} = (-w + w_{\infty})/\tau$$

$$\dot{\eta} = \left( -\eta + \sqrt{\frac{2\tau\sigma^2}{N_a}}\xi(t) \right) / \tau$$

The static driving current μ is set to 0.4 $V_{thresh}$/ms, such that the model continuously spikes. The white noise terms in the voltage equation and OU noise equation have mean zero and standard deviation $\sqrt{dt}$. The white noise component on right side of the first equation adds fast noise with intensity scaled by D, and the slower noise component with time constant tau represents an adaptation current with stochastic populations of channels. The adaptation current is scaled by β = 3 $V_{thresh}$/ms and is proportional to the fraction of open channels (w + η). The total number of stochastic channels is $N_a$. The activation variable w increases the number of open channels and is related to spiking; $w_\infty$ is set to 1 for one millisecond ($tau_{AP}$ = 1 ms) when a spike occurs. If the population of channels Na is very large or infinite, the contribution by the adaptation current β*w is deterministic. The Ornstein-Uhlenbeck process η introduces noise; σ and its scaling factor λ are described by

$$\langle \sigma^2 \rangle = r\tau_{AP} - (r\tau_{AP})^2$$

$$r = \frac{\lambda\mu}{V_{thresh}}$$

$$\lambda = \left(1 + \frac{\beta\tau_{AP}}{V_{thresh}}\right)^{-1}$$

This model was implemented in MATLAB using the forward Euler method, due to the presence of stochastic components. Step size was set to 1 μs and a total simulation time of 7000 ms was used to generate at least 500 ISIs. The first 100 ISIs were removed and the next 400 used to calculate autocorrelations and estimate ARIMA model parameters. Five simulations for each set of tested model parameters were run. Parameters $V_{thresh}$ = 1 and $V_{reset}$ = 0. Parameter ranges for D, tau, and $N_a$ were: D ($V_{thresh}^2$/ms) = [0, 0.000001, 0.00001, 0.0001, 0.001, 0.01, 0.1]; $N_a$ (channels) = [100, 1000, 10000, 100000, infinity]; tau (ms) = [1000 100000].

## 3.3 Results and Discussion

### 3.3.1 Characteristics of experimental data

3.3.1.1 Interspike interval is variable over time but delta ISI is more consistent

All data sets show variability in interspike interval (ISI) over time (Figure 16). Histograms (Figure 16, right) of ISI are irregular and are dependent on the time window observed (not shown). A shift in the mean or standard deviation of ISI over time can change spike time variability metrics such as the coefficient of variation (CV, ratio of ISI standard deviation to the mean ISI).

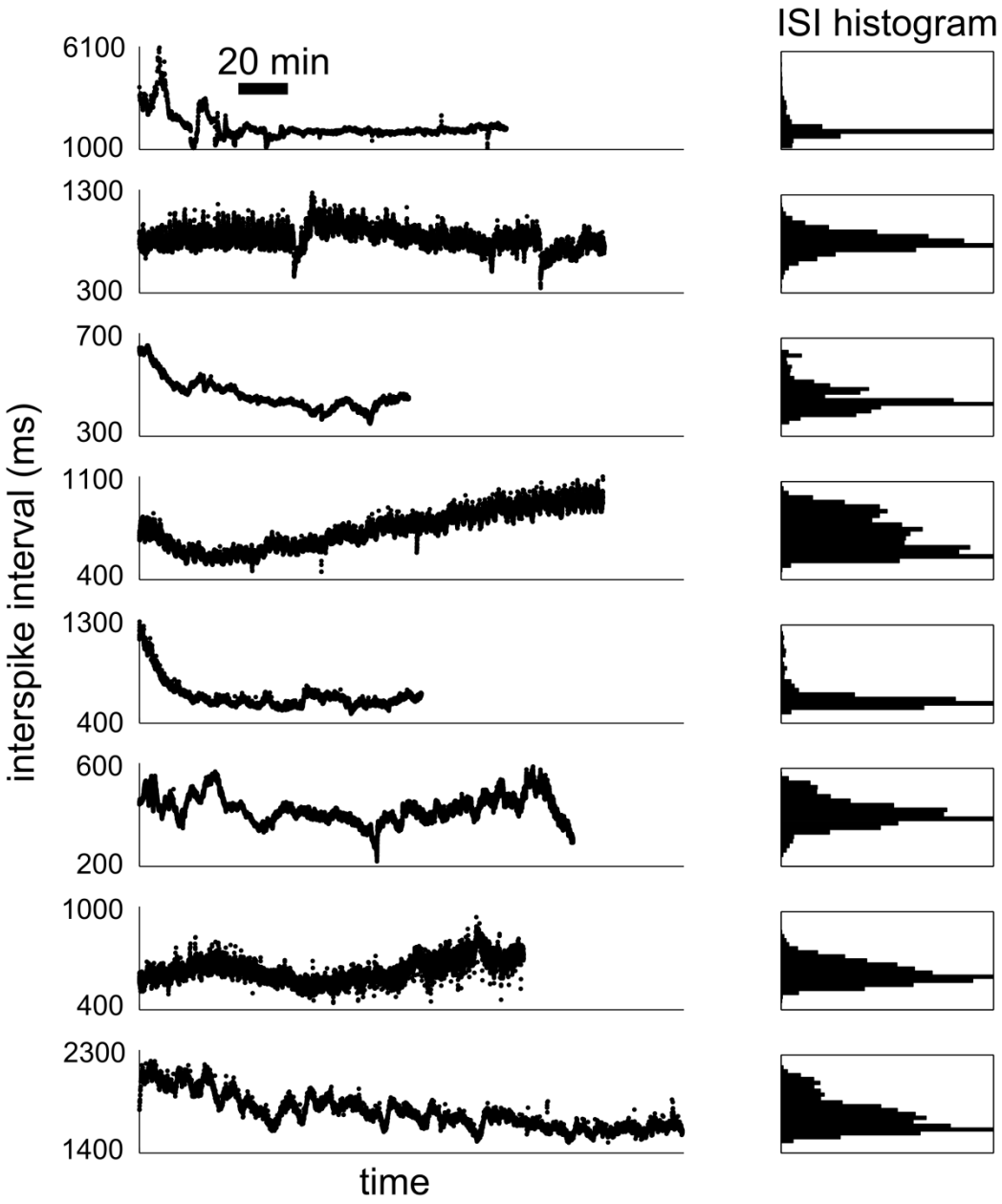


**Figure 16: Interspike interval over time in experimental preparations.** Black scale bar represents 20 minutes. Eight data sets from seven *Aplysia* ganglia are shown. Histograms of ISI are shown to the right of each time trace. Y axes for histograms and time traces have identical scales.

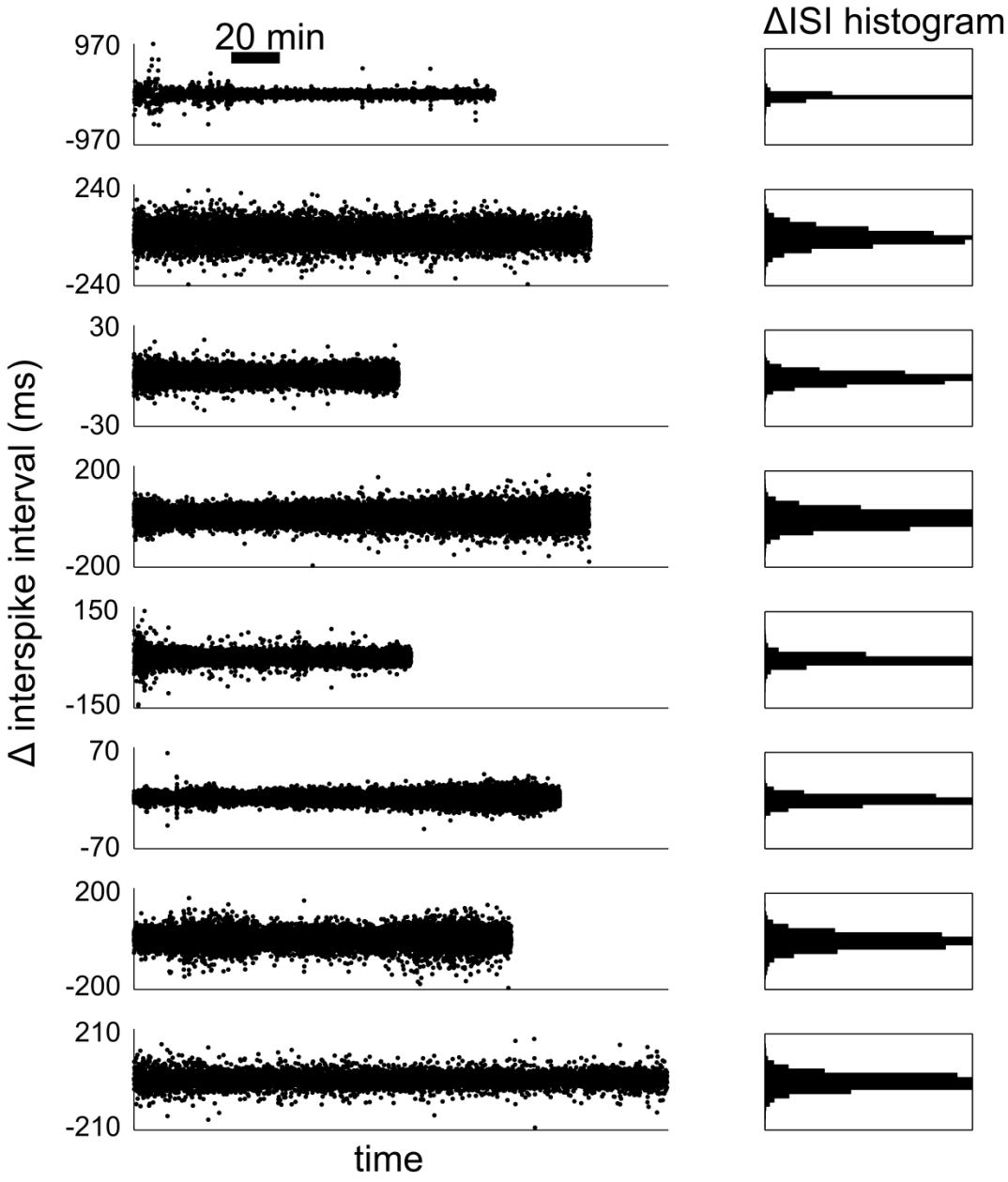


**Figure 17: Change in interspike interval (delta ISI) over time in experimental preparations.** Black scale bar represents 20 minutes. Eight data sets from seven *Aplysia* ganglia are shown. Histograms of delta ISI are shown to the right of each time trace. Y axes for histograms and time traces have identical scales.

In contrast to ISI, the change in sequential ISIs, also called delta ISI here, is more regular over time (Figure 17). Histograms of delta ISI (Figure 17, right side) appear more regular and symmetric than ISI histograms.

The conjecture that delta ISI has a more regular, symmetric distribution than ISI can be verified by observing the cumulative distribution function (CDF) and probability distribution function (PDF) of all data sets. The CDF of the ISI and delta ISI distributions are shown in the left and right panels of Figure 18, respectively. Each experimental data set is shown in grey. For comparison, the black traces represent eight sets of Gaussian random variables with mean 0, standard deviation 1, and a matched number of elements to each experimental ISI data set. Orange lines indicate a theoretical Gaussian CDF. The x-axis for the CDFs and PDFs is in standard deviations from the mean so that ISI distributions with very different average values can be compared. The ISI CDFs are more irregular than the delta ISI CDFs, and both have a steeper slope in the central region than Gaussian CDFs. ISI and delta ISI distributions both fail Kolmogorov-Smirnov tests for normality.

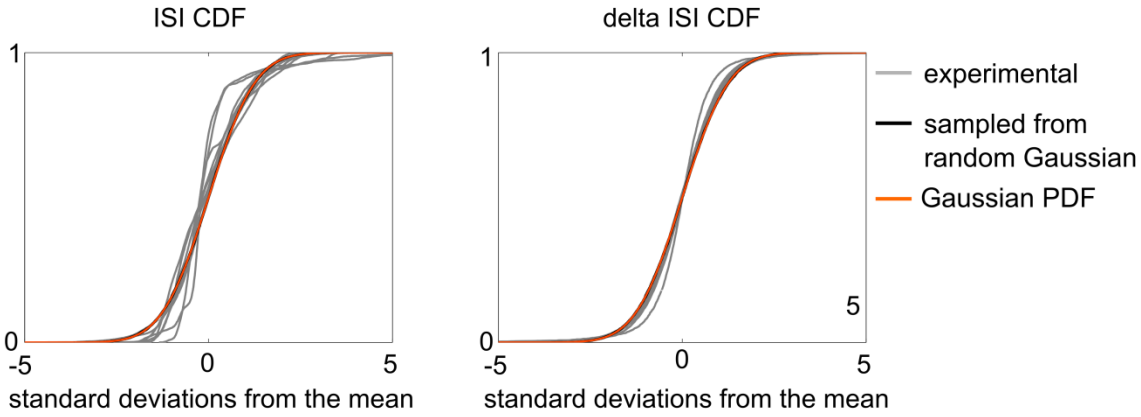


**Figure 18: Cumulative distribution function of ISI (left) and delta ISI (right).** Units on the x-axis represent standard deviations from the mean. Grey traces represent each experimental data set, black traces represent sequences of random numbers with mean zero and standard deviation 1 of identical length as each experimental data set. Theoretical Gaussian distribution is shown in orange.

The PDFs for ISI are more irregular than the PDFs for delta ISI (Figure 19, top left). Black, grey, and orange are the same as for Figure 18. ISI and delta ISI distributions are taller than Gaussian PDFs and have heavier tails. Tail weight, defined as the proportion of points in a data set greater than two or three standard deviations away from the mean, is shown on the bar graphs below the PDFs. Grey bars represent the average tail weight and triangles represent each individual data set. The average tail weight of ISI is asymmetric, while the tail weight of delta ISI is symmetric. In addition, at three standard deviations from the mean, delta ISI has heavier tails than would be expected for a Gaussian distribution. At two standard deviations from the mean, the relative proportion of points in the tail versus in the peak is the same as for a Gaussian. This indicates that delta ISI has more outliers that would be expected for a Gaussian distribution. This is true in all cases.

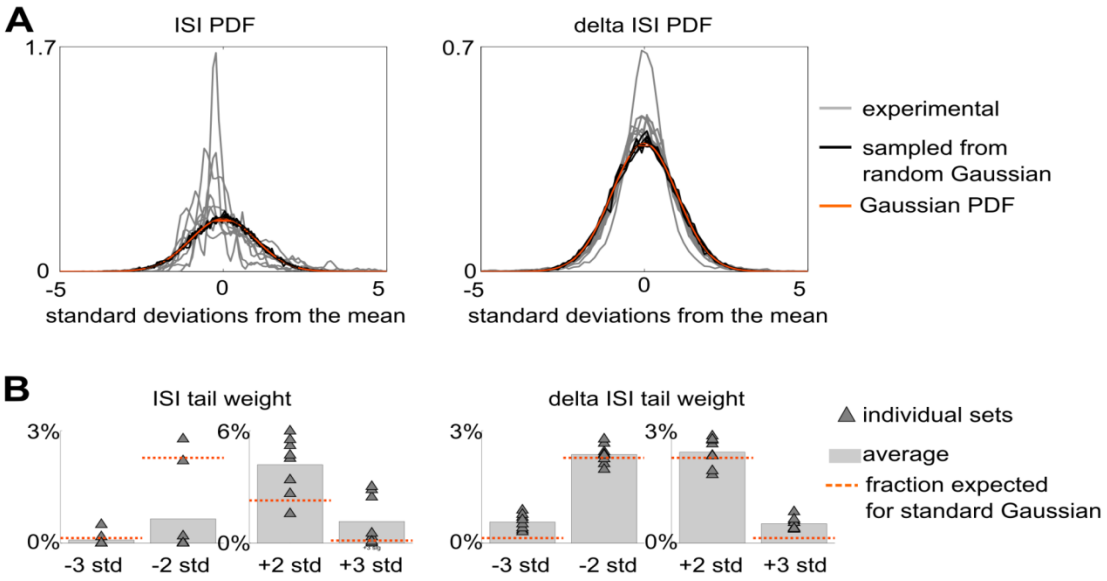


**Figure 19: Probability density function (PDF) for ISI (left) and delta ISI (right).** (A) experimental data sets shown in grey, a matched number (for ISI) of random Gaussian variables with mean zero and standard deviation 1 shown in black, theoretical Gaussian in orange. (B) fraction of points in distribution tails at 2 or 3 standard deviations from the mean. Grey bars represent the average of all experimental sets, grey triangles represent individual experimental data sets, orange lines represent the expected tail weight for Gaussian distributions.

3.3.1.2 cycle-to-cycle variability is not independent

The ISI over time shows more variability than delta ISI, which has a symmetric distribution that is Gaussian-like but with heavy tails. A random walk process in which a random Gaussian variable is added to a prior process value can produce traces similar to those in Figure 17. If ISI could be adequately described by this type of random walk, delta ISI should be an independent process.

Delta ISI outliers are defined as values of delta ISI equal to or greater than three standard deviations from the mean. Small values are within three standard

deviations from the mean. Return maps of delta ISI (Figure 20) indicate that some correlation exists between sequential delta ISI values, especially when sequential values are not outliers (region 1, Figure 20); correlations in region 1 are negative, indicating that a small positive delta ISI value is likely to be followed by s a small negative delta ISI value and vice versa. Certain patterns of delta ISI outliers are more common than others; points in region 2 of Figure 20 represent a positive delta ISI outlier followed by a positive delta ISI outlier. This kind of sustained change in ISI is not observed in the return maps. In contrast, cases where a large positive delta ISI outlier is followed by a large negative delta ISI outlier (Figure 20, region 3) are observed in the return maps. Transition probabilities from a given delta ISI state (positive outlier, negative outlier, or small delta ISI) to another delta ISI state confirm that delta ISI is not an independent random variable (Figure 21); if it were, these transitions would not be state-dependent. Transition probabilities are quantified in Table 4.

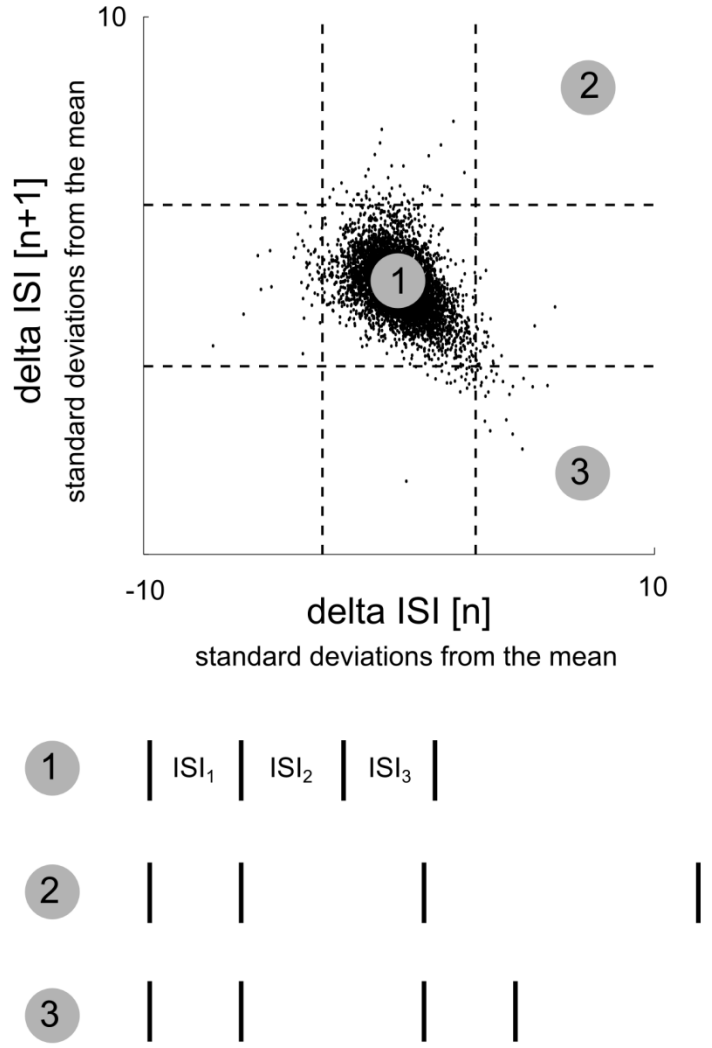


**Figure 20: Delta ISI return map.** Delta ISI [n+1] versus delta ISI [n]. Return map is in units of standard deviations from the mean, dotted lines indicate three standard deviations from mean. Most points cluster in region 1, which has a negative slope and could result from the slight changes in ISI shown in spike trace 1. Region 2, which could result from a sustained change in ISI as shown in spike train 2, is essentially empty. Region 3, which could be described by spike train 3, has a small population of points.

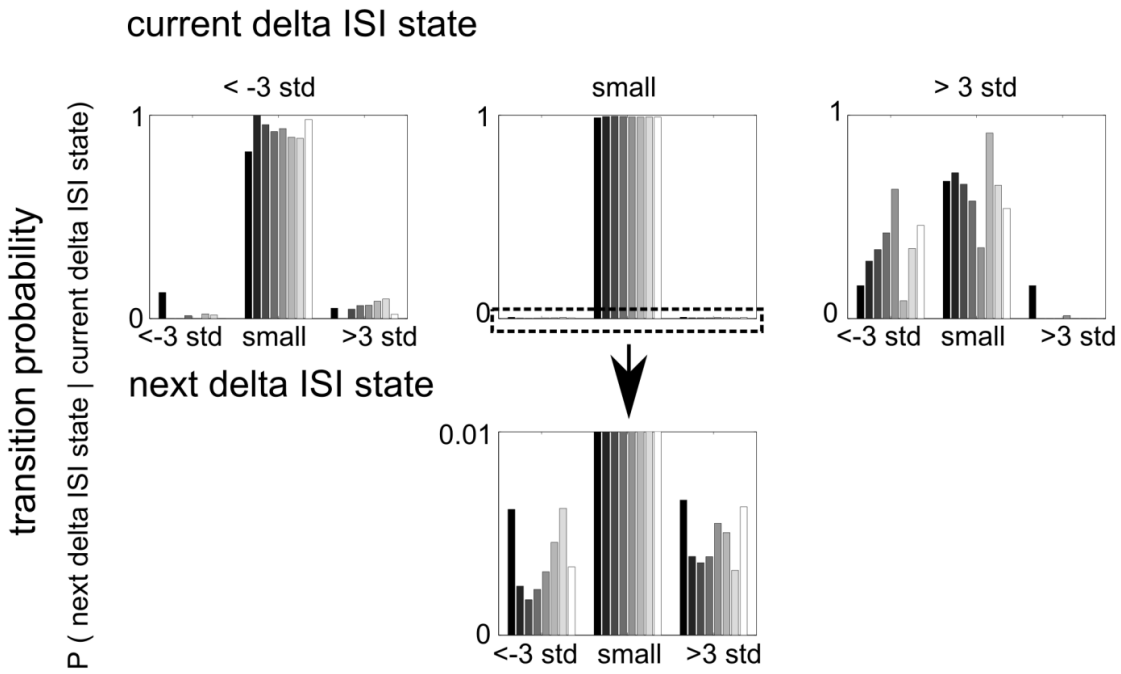


**Figure 21: Transition probabilities to delta ISI states from a specific delta ISI state.** Delta ISI outliers are defined as points three standard deviations or more from the mean. The four panels represent current delta ISI state; negative outliers on the left, positive outliers on the right, non-outlier delta ISI values in the middle. Within each panel there are three sets of eight bars: each bar represents a data set and each set of bars represents the probability that, given the current state, the next delta ISI state will be negative outlier (left set of bars), positive outlier (right set of bars), or a non-outlier (center set of bars). Because transition probabilities are state-dependent (Table 4), delta ISI is not an independent process.

**Table 4: Transition probabilities P(ΔISI [n+1] | ΔISI [n])**

| | | delta ISI [n] | | |
|---|---|---|---|---|
| | | negative outlier | small | positive outlier |
| delta ISI [n+1] | positive outlier | 0.0539 +/- 0.0318 | 0.0047 +/ 0.0013 | 0.0222 +/- 0.0568 |
| | small | 0.9230 +/- 0.0573 | 0.9915 +/- 0.0025 | 0.6361 +/- 0.1605 |
| | negative outlier | 0.0231 +/- 0.0435 | 0.0037 +/- 0.0017 | 0.3417 +/- 0.1720 |

3.3.1.3 ISI and delta ISI correlations reveal history

Correlational structure within the ISI and delta ISI sequences can be quantified using autocorrelation plots. Autocorrelation values for the first 25 lags of each data set are shown in grey, the average of the autocorrelation values at each lag is shown in black and the error bars at each lag represent one standard deviation in Figure 22. The ISI sequence displays high autocorrelation values for many lags (Figure 22, left). This is indicative of a process that has history, or dependence on previous values; such processes can appear nonstationary (like the ISIs in Figure 17). In contrast, delta ISI has, on average, only one prominent autocorrelation value at lag 1. This means that positive delta ISI values tend to be followed by negative delta ISI values and vice versa, indicating a "corrective" feature. It should be noted that not all individual data sets share features of the average, but many do.

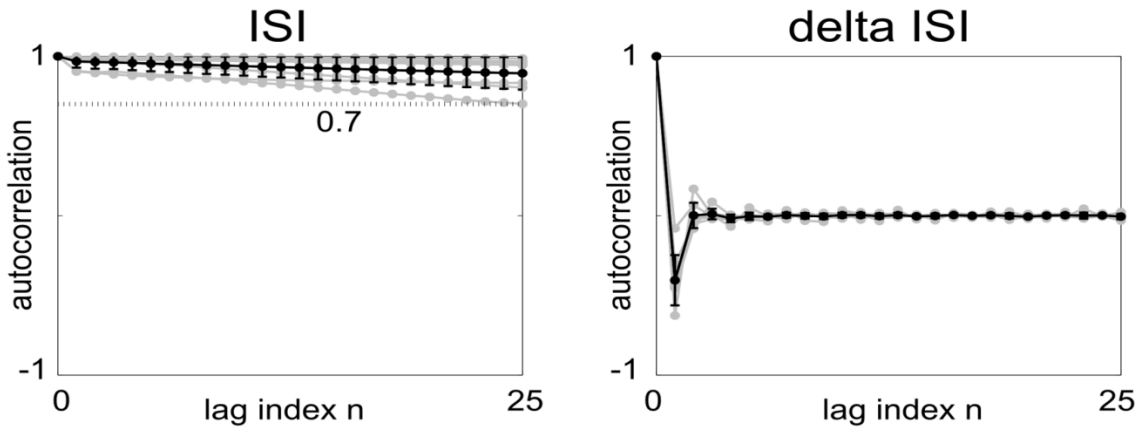


**Figure 22: Autocorrelation for ISI (left) and delta ISI (right).** Each experimental trace is shown in grey while the average autocorrelation coefficients are shown in black. Bars represent one standard deviation. The lowest ISI autocorrelation value shown, at lag 25, is 0.7.

### 3.3.2 Mathematical description of ISI over time

3.3.2.1 Correlational structure suggests an ARIMA model

As discussed in the methods, the autocorrelation plot can reveal an appropriate model for the experimental data (Box & Jenkins, 1970). The average autocorrelation sequences of ISI and delta ISI (Figure 22, black traces) suggest that an ARIMA (0, 1, 1) model may appropriately represent experimental data, on average. When the AIC for the estimated 1st or 0th order models of all data sets are ranked from lowest to highest (1-7), in seven out of eight sets the same three models perform best: (0, 1, 1), (1, 0, 1), and (1, 1, 1) (Figure 23).

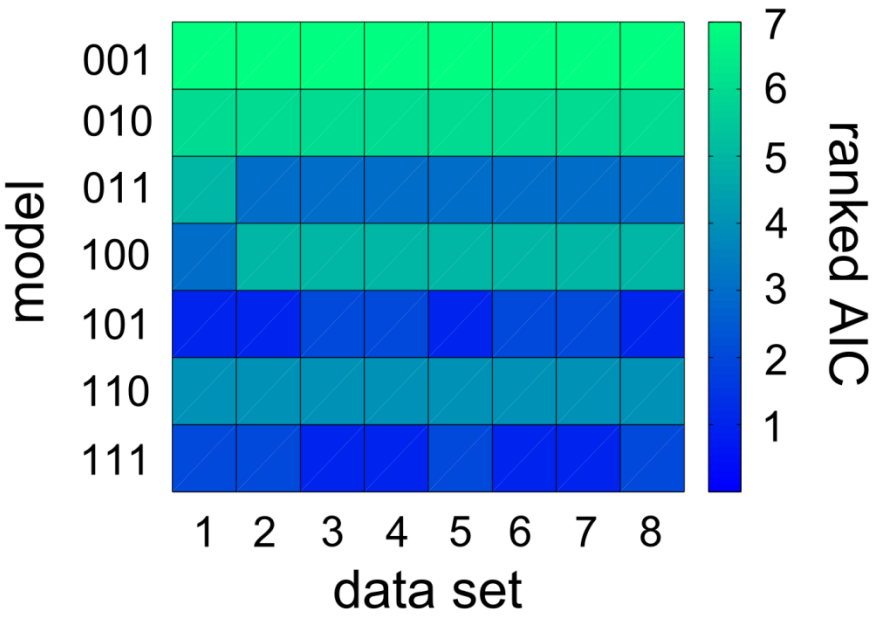


**Figure 23: Estimated Akaike Information Criterion for each ARIMA model with 0th or 1st order components, per data set.** AICs are ranked 1-7 from lowest to highest. Lower AIC indicates a better-performing model.

These models initially seem quite different, but the (1, 0, 1) and (1, 1, 1) models can reduce to the (0, 1, 1) model. The expanded versions of the ARIMA (0, 1, 1), (1, 0, 1) and (1, 1, 1) models, respectively, rewritten in terms of ISI, are

$$ISI\,[n] = \ ISI\,[n-1] + \ a[n] - \theta * a[n-1] + \theta_0$$

$$ISI\,[n] = \phi * \ ISI\,[n-1] + a[n] - \theta * a[n-1] + \theta_0$$

$$ISI\,[n] = (1+\phi) * \ ISI\,[n-1] - \phi * ISI[n-2] + \ a[n] - \theta * a[n-1] + \theta_0$$

where $\phi$ is the autoregressive coefficient, $\Theta$ is the moving average coefficient, and $\Theta_0$ is a constant. Note that estimated moving average coefficients are presented as - $\Theta$ in Figures 24, 25 b, and 28 A; this means if the estimated moving average coefficient is -0.7, the corresponding ARIMA (0, 1, 1) model would be represented $ISI\,[n] = \ ISI\,[n-1] + \ a[n] - 0.7 * a[n-1] + \theta_0$.

The estimated autoregressive coefficients, moving average coefficients, and constants for each of the three best-performing models are shown in Figure 24. Moving average coefficients are similar for all three models in data sets 2-8. The autoregressive coefficients for the (1, 0, 1) model and (1, 1, 1) model are close to 1 and 0 respectively, indicating that these models reduce to the (0, 1, 1) model. Constants vary depending on the model and data set.

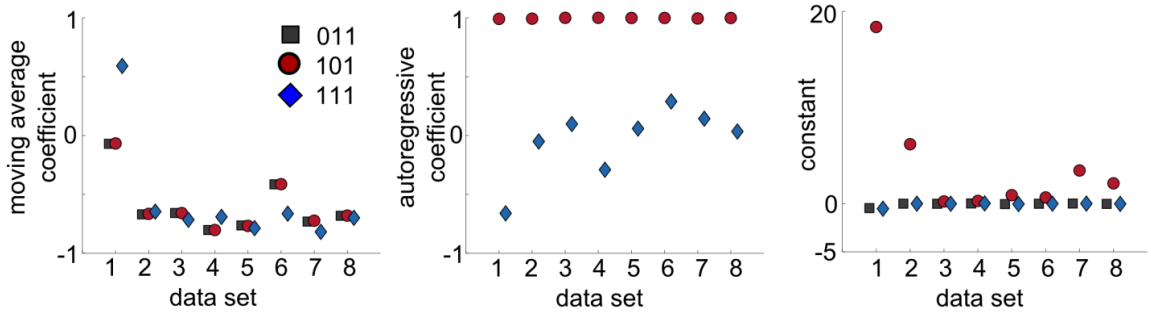


**Figure 24: Estimated ARIMA model parameters for each experimental data set.** Moving average coefficients (left), autoregressive coefficients (middle), and constants (right) estimated for each experimental data set using (0, 1, 1), (1, 0, 1), and (1, 1, 1) ARIMA models.

The Ljung-Box Q statistic determines if residuals from an estimated model are correlated; adequate models should have uncorrelated residuals. For the (0, 1, 1), (1, 0, 1), and (1, 1, 1) models estimated using the entire data set, all residuals test as correlated. This is not surprising; the models were constrained to have $0^{th}$ or $1^{st}$ order components but were estimated using data sets with thousands of points. If the data are divided into windows of 1000 ISIs (not shown) or 300 ISIs and model coefficients estimated for each of those windows, some of the residuals for those fits still test as correlated but most test as uncorrelated (white and grey, respectively, Figure 25 a), with the exception of data set 4. Estimated autoregressive coefficients, moving average coefficients and constants are not drastically different over time, or between windows where residuals test as correlated and uncorrelated (Figure 25, b-d).

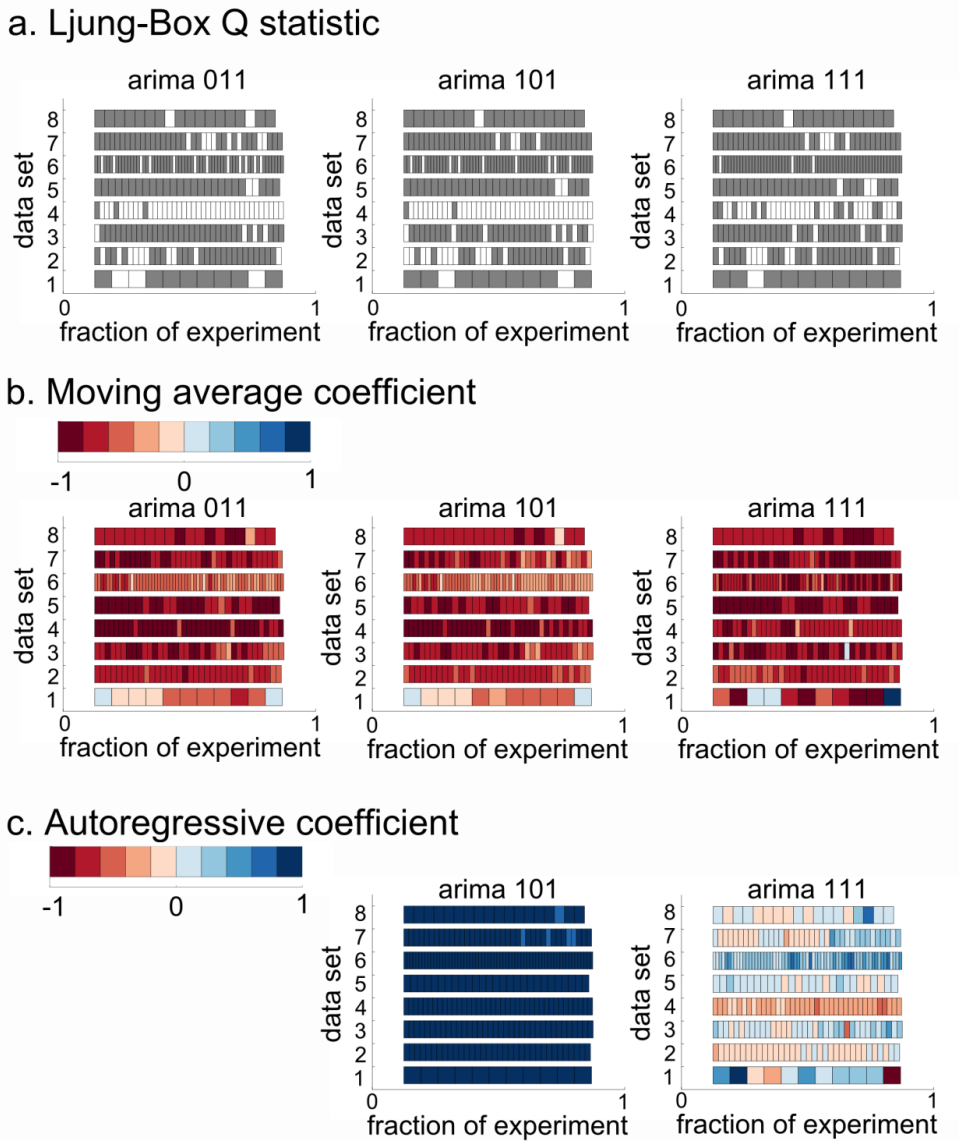


**Figure 25: Residual correlation and estimated ARIMA model coefficients for experimental data split into 300-point windows.** Each column represents an ARIMA model: ((0, 1, 1) left; (1, 0, 1) center; (1, 1, 1) right). Each panel shows all eight data sets as rows; the middle ¾ of each data set is split into sections of 300 ISIs. Coefficients are estimated per model using the ISI subset. The starting point of each subset, relative to the entire data set, is shown on the x-axis. (a) Ljung-Box Q statistic with 0.05 cutoff for estimated model residuals that are correlated (white) and uncorrelated (grey). (b) estimated moving average coefficient per 300-ISI window; scalebar shown at top. (c) estimated autoregressive coefficients ((1, 0, 1) and (1, 1, 1) models only) per window. (d) estimated constant per window, with corresponding scalebars shown above each plot.

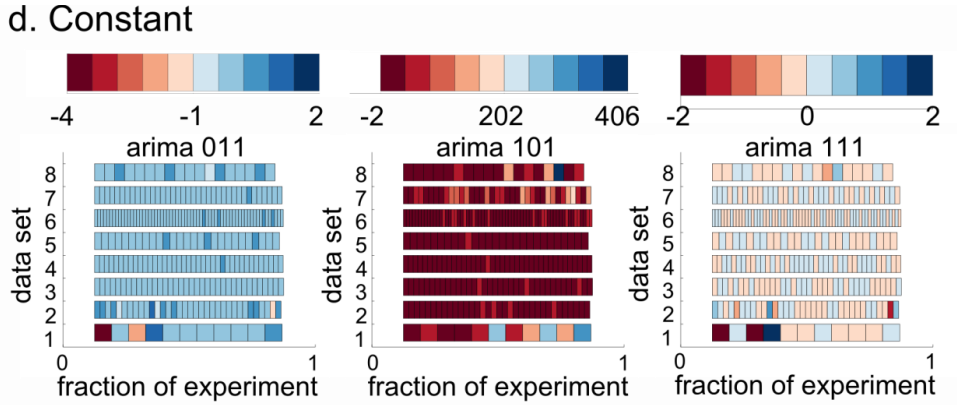


**(Figure 25 continued)**

3.3.2.2 Adaptation and stochastic channels could be responsible for the correlational structure

Noiseless integrate and fire models possess a specific firing frequency set by the applied current μ. When various types of noise are added to the model, this frequency can take range of values and shapes the ISI distribution. The addition of white noise current input to an integrate and fire model produces a skewed histogram with a long right tail (Gerstein & Mandelbrot, 1964). The addition of OU current noise creates a similar ISI distribution shape and a process with serial correlations present (Lindner, 2004). Schwalger et al showed that an integrate and fire model with "fast" white noise and a slower noise due to adaptation currents with stochastic channels could produce different types of ISI correlations and distribution shapes (Schwalger et al., 2010). In the presence of only fast noise and a deterministic adaptation component, they found that serial correlations in the ISI sequence were minimal. In the presence of only noise from adaptation currents with stochastic components, the amount of serial correlation could be

tuned according to the number of channels in the stochastic population and the time constant tau of the channels. Serial correlation of delta ISI was not a tested quantity in (Schwalger et al., 2010).

Using the model of Schwalger and colleagues, we can reproduce the correlational features seen in experimental data. The two extreme noise cases, in which only deterministic adaptation with white noise provided variability (Na set to infinity) or only stochastic channels of adaptation currents provided variability (D set to 0), could not produce an ISI autocorrelation that remained high for many lags and a delta ISI autocorrelation plot with one prominent component (Figure 26, right column and bottom row). However, the presence of both types of noise resulted in correlational structure similar to that observed in the experimental data, in particular the middle panel of Figure 26. It is entirely reasonable that both noise sources could exist in a biological system. To more formally assess a parameter space of integrate and fire models, five simulations were run per parameter set shown in Figure 27. The average ISI and delta ISI autocorrelation plot per parameter set were calculated and compared to the average ISI and delta ISI autocorrelation plots for experimental data, presented in Figure 22. The mean squared error (MSE) at lags 1-25 between the model averages and the experimental averages was calculated; normalized error values for ISI and delta ISI are shown in the left and middle panels of Figure 27. The sum of these normalized values is shown in the right panel of Figure 27 and indicates that minimization of differences in ISI and delta ISI autocorrelation plots requires both types of noise to be present. When the simulated data are used to

estimate ARIMA (0, 1, 1), (1, 0, 1), and (1, 1, 1) models, the estimated moving average and autoregressive coefficients are similar to those seen in experimental data (compare Figure 28 to Figure 24). Parameter sets for integrate and fire simulations presented in Figure 28 were selected because they had a low total error in Figure 27 (right panel).

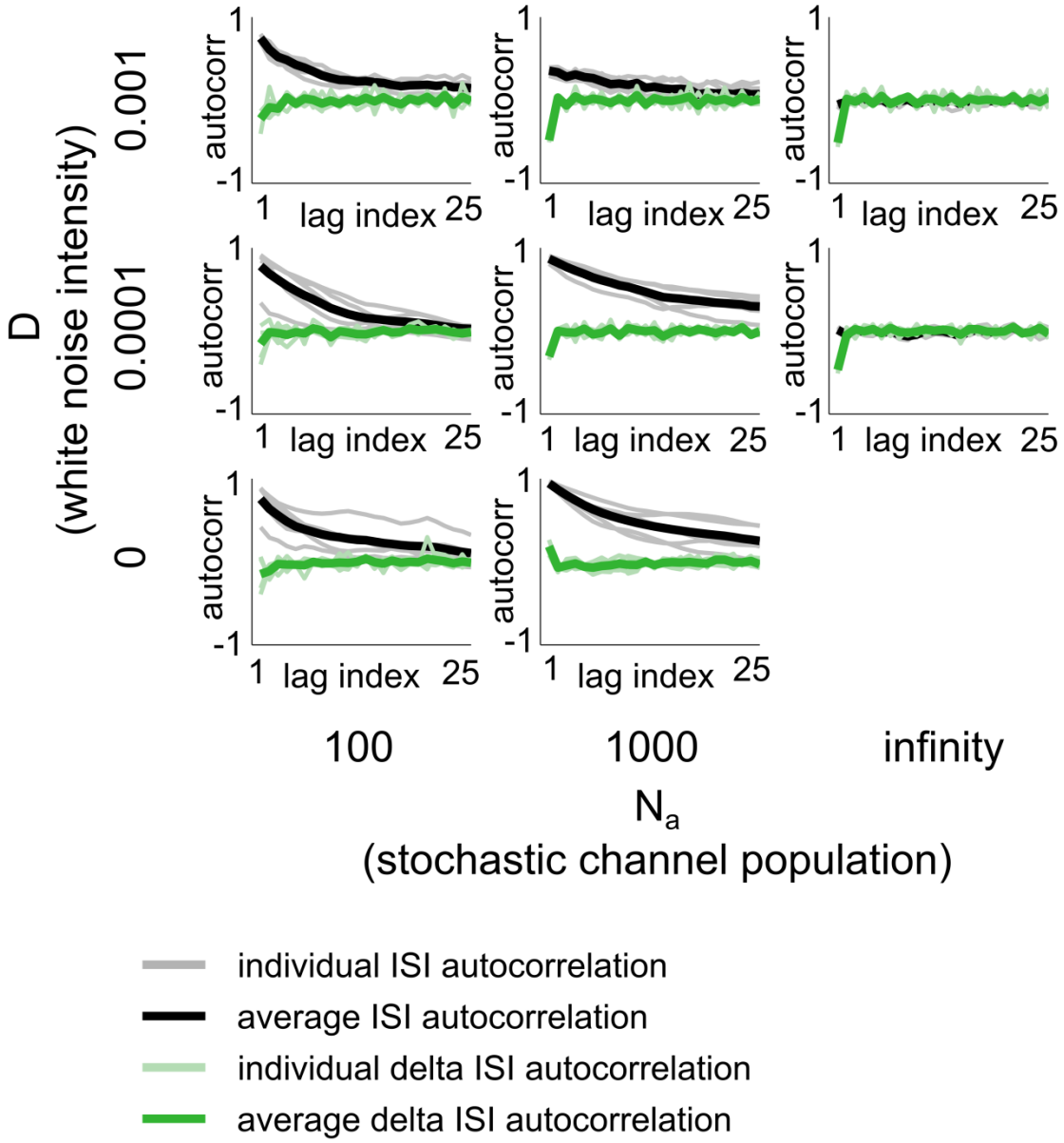


**Figure 26: Autocorrelation plots of ISI and delta ISI for the integrate and fire model.** tau = 1000 ms. Five simulations were run per model condition; ISI and delta ISI autocorrelation plots per simulation are shown in grey and light green. Average ISI and delta ISI autocorrelation plots are shown in black and dark green. Integrate and fire simulations shown here with ISI and delta ISI autocorrelation plots most similar to experimental data for tau = 1000 ms has (D = 0.0001, Na = 1000); this corresponds to the darkest square in Figure 26A, right panel.

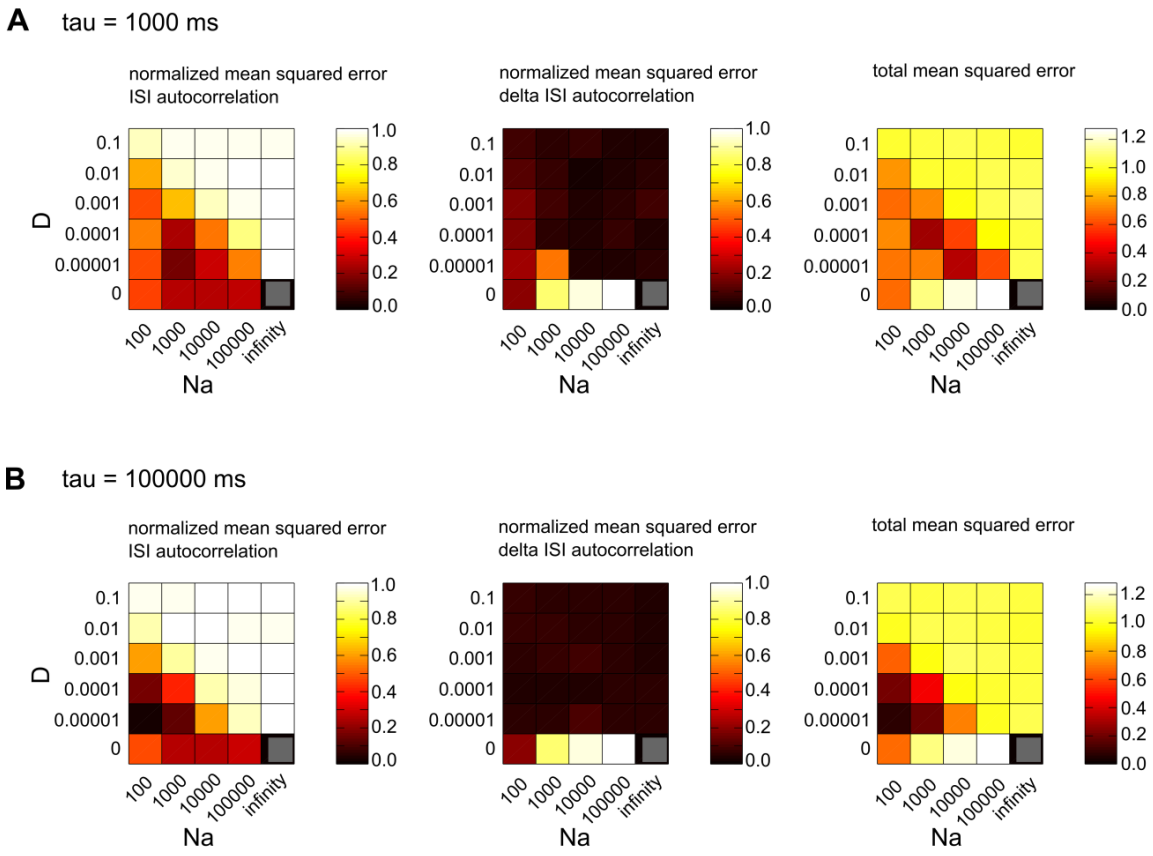


**Figure 27: Error between experimental autocorrelation plots and integrate and fire models.** (A) left panel, the mean squared error (MSE) between the average experimental data ISI autocorrelation trace (black line in Figure 22) and the average autocorrelation trace of five integrate and fire simulations with D and Na as indicated and tau as 1000 ms. This plots is normalized to the highest value. Middle, MSE between average experimental and average integrate and fire delta ISI autocorrelation trace, normalized to highest value. Right, the sum of the left and middle panels. (B) same as A, but tau for the integrate and fire model is set to 100 000 ms, The completely noiseless case (gray square, Na inifinity and D 0) is not computed in this figure.

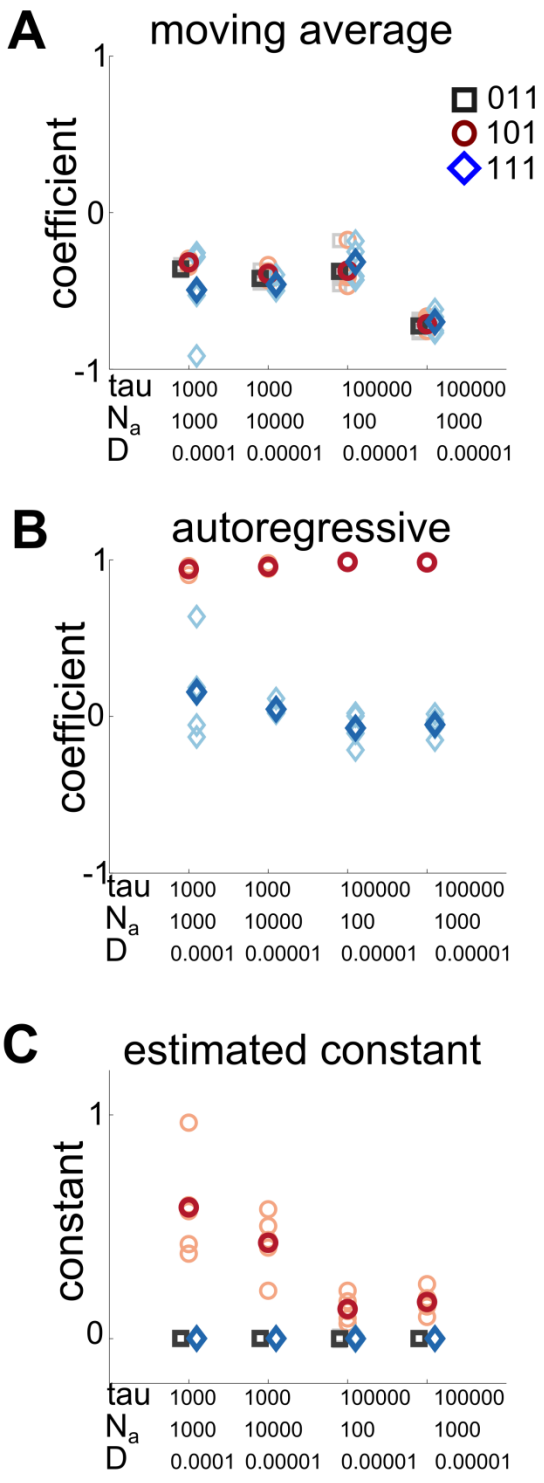


**Figure 28: Estimated ARIMA coefficients for select integrate and fire model simulations.** (A) estimated moving average coefficients. (B) estimated autoregressive coefficients. (C) estimated constants. The estimated coefficients for each of five simulations per parameter set are shown in pale colors; the average estimated coefficient is shown in dark colors.

### 3.3.3 Implications for biological systems and networks

3.3.3.1 Intrinsically active neuron ISIs are not independent

The evidence from these experimental studies indicates that endogenously active spiking neurons in the aplysia are not perfect oscillators but can be represented using an ARIMA (0, 1, 1) process, which is a type of random walk. The presence of correlation in the ISI sequence indicates that sequential ISIs are not independent and that ISI is therefore not a renewal process. This runs counter to a common model used to represent irregular neuron spiking, the Poisson process. In dynamical systems analysis of neurons and networks, neurons are often assumed to be regular oscillators and noise is not a standard feature of the analysis. It is reasonable to think that neurons are not perfect oscillators, but it is not necessarily obvious that there should be correlation present in sequential ISIs and that a white noise process is not sufficient to represent that variability.

3.3.3.2 ARIMA model suggests randomness and history are important to represent intrinsically active neuron ISIs

The ARIMA (0, 1, 1) model represents a random walk with history. This essentially means that adding a set of random values to the current ISI to get the next ISI can describe the system. Such a process can be wildly divergent – it is not mean-reverting and can take a large range of values. This is unsettling because we assume that networks of neurons accomplish their functions robustly and repeatably; representing the individual components of a network this way seems unideal for robust network function.

Variability arises in neural systems in a number of ways, but there are physiological constraints on spike time variability. A lower bound on ISI exists because the number of channels on a cell membrane is limited and because neurons experience a refractory period after spiking. Any use of the ARIMA process to describe neuron ISI, especially for extended periods of time, will likely need to incorporate these physiological features. Simulations of neurons with stochastic channels reveal that those channels can contribute to spike time variability (Chow & White, 1996) and that they can impart serial correlations to cells that are spiking (Schwalger et al., 2010).

The average autocorrelation traces in Figure 22 suggest that an ARIMA (0, 1, 1) model should represent experimental data, on average; this does not mean that the ARIMA (0, 1, 1) model is the ideal representation for each individual data set, or even for all data sets presented. The AIC plot in Figure 23 does indicate that certain features enhance the fit of ARIMA models to experimental data. In particular, models with moving average coefficients outperform models that do not have moving average coefficients. This indicates that a random process that itself has history can enhance fit. The second feature is that any model with history outperforms the model without history (the ARIMA (0, 0, 1)).

### 3.3.4 Limitations

#### 3.3.4.1 Neuron temperature sensitivity

Invertebrate neurons are known to be sensitive to temperature (Katz, 2004; L. S. Tang et al., 2012; Lamont S. Tang et al., 2010). Preparation temperatures were

controlled during experiments but variation did occur. Temperature and ISI over time, as well as fitted correlations for ISI versus temperature and ISI versus log(temperature) are presented in Appendix 1.

3.3.4.2 Endogenous spiking activity

The cells studied in these experiments are endogenously active. Properties of endogenously spiking neurons are not the same as those of non-endogenously spiking neurons. It is possible that the noise model presented and its potential mechanism are specific to neurons with intrinsic activity.

No command for external current was explicitly applied during long term recordings, other than to test cellular resistance. When no current was applied, current output measured from the Axoclamp 2B was small (pA range) but nonzero, indicating that a small amount of current may have been present during recording.

High Mg2+ low Ca2+ saline is used to silences synaptic activity (Nowotny et al., 2003). Voltage fluctuations that could result from inhibitory pulses could still be seen in some data sets, but in general their presence was minimal (see Appendix A).

3.3.4.3 Sampling artifacts

Sampled data is not sampled at perfectly regular intervals; jitter exists in the sampling time (Bettencourt, Lillis, Stupin, & White, 2008; Butera Jr, Wilson,

DelNegro, & Smith, 2001). Spike times, ISIs, and delta ISIs presented here are measured in cycles and converted to time assuming a regular 10 kHz sampling rate. Spike time jitter can introduce correlational features into delta ISI, but is not sufficient to replicate all the correlational structure seen in experimental data.

### 3.4 Conclusions

We have shown that interspike intervals (ISIs) of intrinsically active *Aplysia* neurons show variability over time, but that cycle-to-cycle changes in ISI (delta ISI) are more regular. Distributions of ISI are irregular but delta ISI distributions are symmetric. ISI and delta ISI are not independent processes and show correlation with past history.

The correlational features of experimental data suggest that ISI can be represented as an autoregressive integrated moving average (ARIMA) model of order (0, 1, 1). This model represents a type of random talk (Box & Jenkins, 1970). Of the simple ARIMA models estimated, the (0, 1, 1), (1, 0, 1) and (1, 1, 1) models fitted to each experimental data set performed best, as determined by the lowest AIC values; estimated autoregressive coefficients indicated that the (1, 0, 1) and (1, 1, 1) models could reduce to the (0, 1, 1) model.

An integrate-and-fire model with white noise and an adapting current with OU noise could replicate the correlational features of the experimental data. These findings indicate that intrinsically active neurons are not regular oscillators and are not independent processes. These conclusions suggest that more complex

models of noise may be necessary to replicate experimental variability in simulation.

### 3.5 Statement of effort

Long term experiments, data analysis, ARIMA model estimation, and integrate-and-fire model simulation were all performed by me. Intellectual enhancements of this work have been supplied by Rob Butera and Carmen Canavier.

# CHAPTER 4: A FRAMEWORK TO EVALUATE ETHICAL AND POLICY CONSIDERATIONS REGARDING NEURAL INTERFACE SYSTEMS FOR NATIONAL SECURITY USES

## 4.1 Introduction and objective

Neural interface systems are devices that connect with the nervous system. Enormous progress has been made on the refinement and implementation of such systems in the last several decades. Neural interfaces for national security uses are currently under development, but a concise framework to discern which technologies need assessment and how they should be regulated is lacking.

National security and neuroscience are a current topic. A 2012 publication (The Royal Society, 2012) by the Royal Society spelled out some of the neuroscience-related technologies of interest to governments around the world. The report describes two general categories for such technologies: technologies for enhancement and technologies for degradation. Performance degradation is addressed in some form by a number of existing treaties and conventions (The Royal Society, 2012), depending on whether is it achieved via pharmacological agents or other means, as well as conventions of war; as such, performance degradation will not be discussed here. In addition, the Royal Society report discusses a number of pharmacological agents for performance enhancement. We restrict our discussion to performance or occupational enhancement that is achieved via a neural interface because such devices exist in a novel domain of

national security and they raise a number of unique concerns that have strong ethical implications.

There is current military interest in neuroscience. In 2009, the National Academies press released a document which spelled out neuroscientific applications for Army investment and development (National Research Council, 2009). Neural interface technologies in various forms made the short lists of high-interest and very-high interest technologies for development (table S2 and S3 in (National Research Council, 2009)). The priority list of neural interfaces includes stress monitoring systems that would use a number of neurological (electroencephalogram) and physiological (galvanic skin response) markers and in-helmet systems to monitor and influence neural function.

The Defense Advanced Research Projects Agency (DARPA) is funding neuroscience research. As part of the Brain Research through Advancing Innovative Neurotechnologies (BRAIN) Initative, DARPA has announced two projects that intend to create closed-loop interfaces with the central and peripheral nervous systems. The goal of the Hand Proprioception and Touch Interfaces (HAPTIX) project is to create a prosthetic device that forms a closed-loop with the peripheral nervous system (Defense Advanced Projects Research Agency (DARPA) Biological Technologies Office, 2014). The target subject group is amputees, and the idea is to provide a prosthetic device that not only moves but also sends tactile sensory information to the user. The Systems-Based Neurotechnology for Emerging Therapies (SUBNETS) project is geared toward

rehabilitation from mental illness using neural interfaces; the ideal outcome of the project is an interface that can modulate brain activity and change subject behavior in a closed-loop manner (Defense Advanced Projects Research Agency (DARPA) Defense Sciences Office, 2013). Both devices have amazing rehabilitative potential but also lay the groundwork for general closed-loop interfaces with the human nervous system. The use of such interfaces may not be restricted to rehabilitation in the future.

In 2014, the National Academies press released a policy framework to evaluate ethical issues relevant to emerging technologies (National Research Council, 2014). Neuroscience and prosthetic devices, including neural interface systems, were among the applications discussed. The framework is expansive and encompassing, provides a general methodology to assess ethical implications at the funding agency level, and serves as an excellent guide to emerging technologies and the ethical implications they may pose. Two potential problems with the framework are: 1) the identification of a necessary comprehensive ethical review is the responsibility of a funding official, who must note the ethical implications of a proposal they are reviewing and initiate the process, and 2) the framework considers stakeholders and ethical concerns but does not focus attention on technologies that need more immediate action.

Motivated by the recent reports from distinguished bodies such as the National Academies and the Royal Society, and the influx of funding opportunities in neuroscience applications to national security, we sought to produce a

framework that incorporated facets of science, engineering, policy, and ethics. The initial screen portion of the framework is informed by the current state of scientific understanding and engineering accomplishment; the comprehensive review portion requires consideration of a unique set of ethical implications posed by neural interfaces. The framework is designed to be a real-time capable system for policy making that is reflective of scientific, ethical, and policy issues and applies them to generate meaningful resolutions.

## 4.2 Neuroscience and national security: what could possibly go wrong?

### 4.2.1 The issues

Science and engineering have an intimate relationship with war and conflict. The development of better tools, including weapons, accompanied humans through their biological and intellectual evolution. Because the possession of superior offensive or defensive resources can prove decisive during conflict, technological effort for defense purposes continues today.

One of the most conspicuous examples of modern science influencing the outcome of a war emerged from the deserts of New Mexico in the 1940s. The successful development and deployment of a nuclear weapon by scientists working at several government labs, including those at Los Alamos and Oakridge, profoundly brought the implications of science applied to war to the forefront of consciousness. During the development and after, some scientists were concerned about the implications of their current project on future conflicts; J. Robert Oppenheimer and Albert Einstein were among the ranks of

these concerned scientists (Wolk, 2009). There is precedent for the active role scientists and engineers should take in advocating the appropriate use guidelines of their craft.

The ethical and policy considerations posed by NIS are not necessarily unique to NIS systems; human enhancement in a civilian context raises some of the same concerns, including subtle (or not) coercion of an individual to become enhanced, access to and availability of enhancements, and the effect enhancements have on perception of self (M. J Farah et al., 2004; Martha J. Farah, 2012; Greely et al., 2008). What makes NIS for national security different is the context. Service members operate in a strictly hierarchal organization with strong deferral to chain-of-command and, correspondingly, compromised autonomy. The national security establishment, and the organizations and employees therein, are charged with protecting a country; this motivation is substantially different than that of a traditional commercial sector business.

The concerns about the use of neuroscience and neurotechnology in national security are varied. Neutoethicists have voiced concerns about coercion (Tennison & Moreno, 2012), premature deployment of technology (Canli et al., 2007), putting service members and employees at undue risk for unknown gain, military readiness (Forsythe & Giordano, 2011), and development in secret (Tennison & Moreno, 2012) or with obfuscating terminology and unclear capability (Marks, 2010).

Coercion is a primary concern related to human enhancement. In civilian applications, employees can feel coerced to take stimulant drugs such as Adderall if they feel they are not performing to standard in their occupations, especially if co-workers that are outperforming them are taking such substances (M. J Farah et al., 2004; Greely et al., 2008). The potential for this kind of "horizontal" coercion is present in national security contexts, but there is concern about "vertical" coercion from superior officers as well (Tennison & Moreno, 2012). Some precedent for coercion in the military exists; pilots concerned about their lack of rest time were encouraged to forget their claims and take stimulants instead (McGregor, 2002).

Premature deployment of neuroscience-based technologies into the national security arena is a worry articulated by some scholars (Canli et al., 2007; Marks, 2010; Tennison & Moreno, 2012). The primary concern is that some technologies are subject to hype and may be used in the field before they are completely understood. One strategy to counter this problem is to realistically assess the current scientific and technological state-of-the art. Scientists and engineers can be consulted for consensus on the principles behind such an interface and whether a device is really measuring or stimulating what it's supposed to.

### 4.2.2 Suggestions so far

Actionable suggestions regarding the appropriate use of neuroscience in national security are varied and exist at many levels. Some authors stress the

need for policy, some for researcher education, others for the creation of review committees and frameworks. We discuss some of these suggestions below.

#### 4.2.2.1 Researcher education

One topic that emerges from neuroethics papers is a call for neuroscientists to receive better training regarding the ethical and dual-use implications of their work (Tennison & Moreno, 2012). This call has recently been echoed by the Presidential Commission on Bioethical Issues in their latest report (Presidential Commission for the Study of Bioethical Issues, 2014). Sensible ethics training and knowledge of dual-use potential are valuable assets, however these do not lay out a clear chain of events that should occur if researchers suspect their work will be used in a national security setting. Defense of a nation is a legitimate enterprise, and DARPA funds a number of proposals in the area of neuroscience and neuroengineering; individuals funded by such grants know their projects have applications for defense. Knowledge of the ethical issues at hand is important, but appropriate actions to take to reduce those implications are unclear.

#### 4.2.2.2 Existing policy

At the policy level, existing codes address some of the issues relevant to neural interfaces. The 'Common Rule' pertains to human subjects involved in government-funded research studies ("Code of Federal Regulations Title 45," 2009). Some of the ideas central to the common rule are informed consent, voluntary participation, and the ability to withdraw from a study without

repercussions. These tenets exist to both protect and empower research subjects, but it is not clear if they can translate to those involved in the national security sphere because the objectives and environments of these two institutions are fundamentally different. For example, a service member using a neural interface may not be able to stop using it while engaged in a mission, where the roles and expectations of individuals in the operational unit have already been set. The refusal to use a neural interface may change the types of jobs an employee can perform. Obtaining Informed consent may not be feasible or possible.

The dual-use research of concern (DURC) framework is a policy that applies to individuals and institutes performing research that has the potential for civilian and military uses. In particular, scientific research involving 15 specific pathogens and toxins is subject to additional oversight by the funding agency and institution conducting the work ("United States Government Policy for Institutional Oversight of Life Sciences Dual Use Research of Concern," 2012). Several classes of work that change how, how well, and what hosts pathogens can infect or affect also involve extra layers of oversight. DURC policy is focused on pathogens, especially the variety that could be taken from a lab and used to harm public health. Pathogens and toxins can operate on populations, but neural interfaces are implemented on individuals. Pathogens degrade public health or resources, but the neural interfaces we discuss here are for enhancement. The types of concerns relevant to pathogens are not the same types of concerns relevant to neural interfaces.

4.2.2.3 Committees to review neuroscience in national security

One suggestion is to create an entity, somewhat like the National Science Advisory Board for Biosecurity (NSABB), to monitor the use of neural interfaces in national security (Moreno, 2012). The NSABB reviews research of interest and advises the National Institutes of Health (NIH) director on dual-use implications of NIH research ("National Science Advisory Board for Biosecurity Charter," 2014). In 2012, the NSABB attracted attention when it recommended that two influenza papers be published after it initially recommended they be published with incomplete information (Malakoff, 2012). The NSABB or a similar body could perform ethical reviews of proposals and publications regarding neurotechnology for national security.

The Presidential Commission for the Study of Bioethical Issues is a committee established by each president of the United States; each commission serves for two years, and their service can be renewed ("Presidential Commission for the Study of Bioethical Issues Charter," 2010). The commission is asked to create reports and provide input on various topics of ethical interest to the president and the country. In May 2014, the commission released their first of four volumes pertaining to ethical issues relevant to neuroscience research and the BRAIN Initiative. In it, they recommend that ethics education should be integrated with neuroscience research, and at more levels than just graduate training (Presidential Commission for the Study of Bioethical Issues, 2014). This body often reflects a diverse range of academic backgrounds and expertise, making it an

appropriate organization to review neuroscience applications to national security, but its existence is transient.

#### 4.2.2.4 The National Academies Framework

The National Academies released a comprehensive framework to address ethical, legal, and social issues pertaining to emerging technologies in February 2014 (National Research Council, 2014). This document was commissioned by DARPA in 2010 to consider legal and ethical issues pertaining to new technology. Cybersecurity, autonomous robotics, and synthetic biology were all topics of discussion. Two very relevant chapters are those on neuroscience and "prosthetics and human enhancement".

The framework consists of two parts. In the first, stakeholders of the technology in question are identified along with ethical and legal issues pertaining to them. Next, ethical issues that transcend stakeholders are considered, such as how this technology will influence society as a whole. It is suggested that ethical concerns be considered from a range of viewpoints, including consequentialist and deontological stances, ethical codes governing professions, and rules of war.

The suggested implementation of this framework is at the funding agency level. In the hypothetical example of its use, one person responsible for approving a research proposal notices that the work described may have downstream ethical implications. The approver solicits advice and makes a decision about whether to fund the program or not, along with what conditions should be

satisfied if the research does proceed. This requires that the approver 1) be familiar with what kinds of work have ethical issues, 2) have the time, resources, and authority to take action in such a way, and 3) be prescient enough to think about future implications of the work.

The framework is an excellent compendium of ethical issues pertaining to neural interfaces, as well as general ethical perspectives. Many of the issues we discuss in our framework have been reflected in the chapters on neuroscience and prosthetics. Likewise, implementation at the funding agency level is effective: oversight can happen before major development begins or during development, and securing funding can be a method to enforce proper conduct. However, the framework is cumbersome. A uniform set of specific concerns is not articulated, and technologies are not prioritized for review; they must all be fully evaluated. It is likely that some technologies have more potential than others for ethical violations, and those should be watched more critically. Placing the responsibility of detecting potential ethical issues is also a lot to ask of one person.

### 4.3 Our solution: A policy framework to evaluate neural interfaces for enhancement in the national security context

We present a streamlined policy framework that balances efficiency and efficacy when evaluating neural interface systems (NIS) for national security purposes. The framework is composed of two parts: an initial screen and a comprehensive review. The initial screen is designed to filter out technologies

that are not immediate, feasible, or impactful. It prioritizes what technologies policy makers should focus on. The comprehensive review considers how the NIS could affect individuals, operational norms, and multi-use applications.

### 4.3.1 Initial screen

In addition to prioritizing technologies that are immediate, feasible, and impactful, the initial screen can guard against premature deployment of unproven technologies by realistically assessing the state of the technology.

#### 4.3.1.1 Immediacy

We define a technology as immediate if the scientific concepts behind it are in place and well-accepted. The timeline for scientific advancement is often unpredictable, so technologies that are based on facts already established are more immediately useable than technologies based on theories in progress. One or more criteria that assess scientific consensus should be explicitly articulated, keeping in mind that there are levels of consensus within the scientific community. For example, most neuroscientists agree that neural activity measured at a high, whole-brain level is related to the activity of individual neurons, but the nature of this relationship is as yet unclear.

#### 4.3.1.2 Feasibility

Feasibility refers to the environmental and operational constraints pertaining to a technology. Colloquially, this asks the question "Can we build it?". Engineering constraints on portable devices include power consumption, serviceability,

ruggedness of operation, and ability to withstand the elements. Size and weight are also important. Examples of operational constraints are the amount of specialized training needed to use a device or interpret the signals from it and the number of people required to operate it.

#### 4.3.1.3 Impact

Impact refers to the strategic advantage conveyed by a technology. In military history, there are many examples of military paradigm shifts, from sword to firearm and single-shot firearm to those capable of repeating rounds. The promise of a technology capable of favorably tipping the scales during a conflict is a strong incentive for development.

#### 4.3.1.4 Initial screen in action, plus some examples

The initial screen is used to identify technologies that should undergo a more comprehensive ethical review. We envision that a technology that scores strongly on two of the three filter criteria should be reviewed further. An example of a technology that is immediate but not feasible would be an ambulatory functional magnetic resonance imaging (fMRI) device to monitor brain activity while a service member is in the field; fMRI machines exist, but they are large, heavy, expensive, and sensitive to subject movement. It is not feasible currently to develop an fMRI device that can be worn while a subject is walking around. A technology that is feasible but not immediate would be something that is possible to build but not scientifically justified; data could be measured but the meaning or efficacy would be unknown.

### 4.3.2 Comprehensive review

4.3.2.1 Concerns for the individual

The brain is an organ, and like most other organs in the body, it is necessary for the survival of humans. Unlike most other organs in the body, the brain cannot be surgically replaced. Each brain is unique to each individual, and each individual's sense of self originates in the brain. To interface with the brain is to interface with the organ most identified with sense of self, memories, capabilities, capacities, aspirations, emotion – in short, one of the most personal parts of an individual. Ethical issues raised by brain interfaces are fundamentally different from other types of prosthetics or interfaces. We discuss five ethical issues pertaining to concern for individuals. They are identity, privacy, autonomy, nonmaleficence, and beneficence.

Identity is the self-conception of an individual, or how they see themselves. It is possible that individuals will see or think of themselves differently with a neural interface for enhancement. What consequences this difference has, both for personal behavior and personal responsibility, are important considerations.

Privacy is the ability for an individual to keep certain information and activities unobservable. There has been discussion among ethicists about 'mind-reading', particularly in the fMRI for lie detection debates, and if such scans are an unlawful search of thoughts (Martha J. Farah, Hutchinson, Phelps, & Wagner, 2014). While we are not yet capable of mind-reading, things that can measured from brain activity are levels of attention and awareness, which are components

of an individual's cognitive state. The question 'is your neural activity private' likely depends on what precedent is used; cognitive state could be treated as a vital sign like pulse and respiratory rate, in which case individuals may not mind sharing it, or as a tool to identify what someone is looking at, which could be more problematic to privacy.

Autonomy, nonmaleficence, and beneficence are terms borrowed from medical ethics but are applicable here. Autonomy is the ability of someone to act on their own behalf as their own agent. If the addition of a neural interface changes an individual's conception of themselves, particularly their conception that they can act on their own behalf, that may compromise autonomy. Service members in particular already have a reduced state of autonomy; military culture stresses deference to the chain of command, so lower level members are required by code to follow their superior officers' orders. The security establishment as a whole, including contractors, is engaged in a unique industry that has different objectives than the rest of the commercial sector, that is, it monitors and ensures the safety of a nation. Employees of the security establishment face pressures not put upon employees in commercial or government spheres, and these pressures may compromise their ability to act as independent agents. These features of the military and national security environment make the concepts of autonomy and duty particularly hazy.

Nonmaleficence refers to the medical ethic of "do no harm". The use of a non-invasive technique to monitor brain activity, such as the electroencephalogram

(EEG), is probably harmless from a physical wellbeing point of view. However, the stimulation of brain activity has the potential to do more damage and the effects of prolonged exposure are unknown (Hamilton, Messing, & Chatterjee, 2011). Surgical interventions such as those used to place deep brain stimulation (DBS) electrodes into patients are major procedures and carry all the risks of major brain surgery. One of the priorities to consider should be the wellbeing of the individual to be enhanced, and whether any risks outweigh potential enhancement benefits.

Beneficence is the medical ethic of working in the patient's best interest. As well as potential problems and negative effects associated with neural interfaces, these should be balanced with potential positive outcomes. Survival is a positive outcome, and if some of these enhancements can enhance survival, this is a strong reason to recommend them. Likewise, if any interventions can alleviate suffering and distress that can come with exposure to conflict, these factors need to be considered.

#### 4.3.2.2 Operational norms

Operational norms refer to the day-to-day functioning of individuals and groups as well as the conduct of military and national security institutions. We have divided them into intra-unit engagement, inter-unit engagement, and conflict engagement.

Intra- and inter-unit engagement refer to how an individual functions as a member of an operational unit and how those operational units function with each other. If NIS for enhancement are not applied to all individuals involved in national security, then the criteria for selection, number of people selected, and the ability to opt in or opt out will strongly influence the enhanced population's characteristics. Whether populations of enhanced individuals occupy entire units or exist within units with non-enhanced individuals, and how those units interact, could also affect the dynamics between units. The potential for advancement, the types of missions undertaken, and the frequency of assignments for enhanced and unenhanced individuals are all subjects that should be considered and possibly codified before neural enhancements are used.

Norms of conflict engagement refer to the 'rules of war'. The development of new technologies, particularly weapons, can profoundly change the way wars are conducted. Improvements in firearms put a stop to the convention of marching an army in plain sight and ushered in an age of trenches. The use of drones has moved boots off the ground and changed the way operations can be conducted. Norms change. Units of or with neurally-enhanced individuals could be another catalyst for changing how conflict is conducted.

#### 4.3.2.3 Multi-use applications

A dual-use technology is one that has both military and civilian uses. Information and devices with dual-use potential are regulated and monitored in a variety of ways, including with oversight committees (as discussed in the DURC policy

framework section) and through export control. Technologies developed for military use do find their way back into civilian society.

Neural interfaces developed for military use could very well end up in civilian life. As has been discussed, neural interfaces raise a number of ethical concerns not typical for other devices. Guidelines for appropriate use of these technologies may depend on where they end up. Possible sectors include consumer products, commercial applications, medical/clinical interventions, other military uses, and academic research. The appropriate use of neural interfaces will be different in each of these domains, but some of the general issues articulated here may be useful in framing those discussions.

### 4.3.3 Implementing the framework

To be effectively implemented, the framework needs to be incorporated at a level where enough details are known about a potential neural interface to effectively evaluate it. This could be at the funding agency level, which can leverage a strong incentive for compliance and voluntary cooperation. One disadvantage of implementation at the time of funding is that technologies may only undergo evaluation when proposals are reviewed.

It is possible that technologies may need to be evaluated while the work is in progress, because new ethical issues are uncovered (National Research Council, 2014). Likewise, a deployed technology may possess ethical issues not considered initially but apparent once implemented. Periodic and systematic

review of NIS by a standing agency such as the NSABB or a new organization may be a prudent precaution to take, especially if neural interfaces are adopted to national security settings at a large scale.

The framework we have presented is designed to operate efficiently and effectively; it should not cause undue burden on existing organizations and resources. It is designed to protect the rights of the enhanced individual and provide guidance about the types of technologies that should be developed and funded, paying particular attention to ethical and technological concerns. Such a framework deserves congressional support and backing. We anticipate that the framework can be flexibly implemented within agencies that fund relevant work, such as the NIH and DARPA, or within an advisory council such as the NSABB.

### 4.4 Concluding remarks

We have presented a framework to evaluate neural interface systems for national security applications. This framework is designed to be efficient and effective. The initial screen prioritizes attention to technologies needing the most immediate action. The comprehensive review evaluates potential ethical implications regarding individuals, the units those individuals belong to, and society. It is likely that this framework will require re-evaluation as technologies and societal norms change. We intend it to function as a useful scaffold on which collaborative scientists, ethicists, engineers, policy makers, and the public can remodel and build.

### 4.5 Statement of effort

This work has been an ongoing collaboration between Roberta Berry, Robert Butera, and myself. It has benefitted immensely from this diverse set of perspectives.

# CHAPTER 5: CONCLUSIONS AND FUTURE WORK

## 5.1 General conclusions and philosophy of the work

Synchronized, coordinated neural activity is a feature common to many functions mediated by the brain, from respiration (Koshiya & Smith, 1999), to cognition (Juergen Fell & Axmacher, 2011; Jutras & Buffalo, 2010; Siegel et al., 2012). The conditions that establish persistent synchrony and the dynamics observed in those networks are critical to how circuits function. Understanding synchrony dynamics and how to manipulate them may yield insights into both synchrony functions and disorders of synchrony, such as schizophrenia (Grützner et al., 2013; Uhlhaas & Singer, 2006, 2012) and epilepsy (Dominguez et al., 2005).

Hybrid circuits are a reduced model for studying synchronization; many properties of the circuit can be adjusted, but a biological component with relevant biological noise is still present. Small circuits are of interest because synchronization in small circuits and synchronization in large neuron populations are probably related. The work described in this dissertation builds upon prior hybrid circuit experiments, which revealed that network activity, in the form of phase-locking or phase slipping, did not always persist even though parameters were held constant (Thounaojam et al., 2014). The biological portion of the hybrid circuit was responsible for modulating the network activity. In simulation, the addition of Gaussian noise to the PRC or modeling neuron period as a Gaussian process were both insufficient to cause transitions in network activity. Transitions could be replicated when an Ornstein-Uhlenbeck (OU)-type process,

which has a history-dependent term and a random Gaussian term (Uhlenbeck & Ornstein, 1930), was used to simulate the period of one neuron in the circuit.

Two questions emerged from that previous work. First, what is the best model to describe variability observed in a "regularly" spiking biological neuron? Second, if the biological neuron properties change over time, how can we capture those dynamic changes and still predict if synchrony or phase-locking will occur? The answer to the first question is in chapter 3, where I demonstrate that an autoregressive integrative moving average (ARIMA) model of order (0,1,1) captures, on average, the correlational features seen in the data; such a process could be the result of both white noise fluctuations and stochastic channels of adaptation currents. A solution to the second question is presented in chapter 2, where I consider the time series of a coupled neural system and use the movements of that coupled system on the ts-tr plane to infer underlying dynamics of the system.

### 5.2 Main take-home points

Project 1: System dynamics dictate the robustness and presence of synchronized or phase-locked network activity. Vectors based on the time series trace of a coupled neuron system can be used to infer features of the underlying system dynamics, such as the presence and location of stable fixed points or ghost attractors. This method quantifies movement along the PRC-based map and extends the technique to cases where the PRCs cannot be measured, where

noise intrinsic to the system precludes the use of the map, or where system dynamics change over time.

Project 2: Neurons possess intrinsic variability that can cause changes in network activity patterns (Thounaojam et al., 2014). Interspike interval variability over the course of hours can be described, on average, by an ARIMA(0, 1, 1) model. Correlational features characteristic of the ARIMA (0, 1, 1) process are replicated in an integrate-and-fire model used by (Schwalger et al., 2010) that incorporates white noise current fluctuations and adaptation currents with finite numbers of stochastic channels. This work demonstrates that the ISI of intrinsically active neurons is not an independent process, adaptation currents may contribute to these features, and that adequate models to represent this type of variability may require multiple types of noise sources. In addition, ISI over time may not be a stationary process, but is likely bounded by physiological constraints.

Project 3: The use of neuroscience and neurotechnology for national security purposes is a current topic of discussion. Which technologies should be developed, from strategic, realistic, and ethical points of view, is not clear. We propose a framework that incorporates the current state of scientific knowledge, engineering feasibility, and potential strategic impact as an initial screen to prioritize technologies for further ethical review. Our comprehensive ethical review assesses concerns for the enhanced individual, operational implications, and multi-use applications.

### 5.3 Neural system dynamics: navigating without a map

In chapter 2, we described how a time series trace from a two-neuron circuit could be used to infer system dynamics. Properties of the time-series vectors could be used to distinguish cases with stable fixed points and ghost attractors that were ambiguous when observing the network phase only. The vector properties could also capture dynamic changes that occurred in the location of fixed points or ghost attractors during hybrid circuit experiments.

The dynamics underlying biological activity are important. In our two-neuron systems, stable fixed points corresponded to stable phase relationships between the two cells. In contrast, no stable attractor means that the phase relationship is not stable, though a preferred phase can still be observed if a ghost attractor is present. Both of these cases can be sensitive to noise, but the stable attractor case is likely to have a larger range of stability and tolerate more intrinsic variability than the ghost attractor case (Thounaojam et al., 2014).

The time-series vector method describes interactions between neurons; in contrast, the PRC of each neuron describes the properties of that neuron. The vector method is extendable to other types of systems besides those with reciprocal coupling. It can be used, unmodified, for feedforward, non-reciprocally coupled circuits. If the activity of two neural populations can each be described as an oscillator with well-defined pulsatile events, the PRC-based map could be used to capture the stability of interactions between those two

populations (Thounaojam et al., 2014); the same may be true of the vector method. More speculatively, if vector maps can be used to describe individual interactions within a population, the connections that show more stable properties may be more critical for network function. In networks where connectivity is inferred instead of known via physical connections, evidence for stable fixed points may be a way to distinguish randomly coincident activity from functionally connected synchrony.

### 5.4 Neuron variability: the need for more articulate description

Neurons are sometimes represented as oscillators, especially in the dynamical systems perspective (Izhikevich, 2010; Rinzel & Huguet, 2013). In neural circuits that have continually spiking or bursting components, this representation is appropriate. Because biological systems are dynamic and have components with probabilistic properties, it is unsurprising that biological oscillators are not perfectly regular. It is more surprising that oscillator cycles show correlation with past history.

The ARIMA (0, 1, 1) process model represents a type of random walk (Box & Jenkins, 1970). Describing interspike interval (ISI) with this type of model creates an explicit dependence on history in multiple places, which is one feature that makes this process different from an OU process. The next ISI depends on the previous ISI, a stochastic component, and one prior stochastic component. It is interesting and somewhat unsettling that the activity of single neurons can be described as a random process. The ARIMA model is flexible and places no

restrictions on the ISI histogram shape or stationarity; in real biological systems, physiological constraints exist, such as the refractory period and a finite number of ion channels. These physiological constraints would need to be incorporated into the ARIMA model if it were used to describe spiking in network simulations.

The ARIMA process is a linear model familiar to some categories of engineers. I opted to use the ARIMA framework for two reasons. First, the experimental data seemed well represented by ARIMA models. These models are not common in the neuroscience literature, but they are a useful addition to the ways neurons and neural variability are currently modeled. Second, linear models are conceptually simple. They can be used for forecasting, though a lot of variability may make the forecasted range so large it is not useful. It is possible that other types of analysis, such as deterministic chaos, could satisfactorily represent the data in chapter 3.

History in neural circuits has been described before. In studies of the *Aplysia* feeding circuit, features of the motor program are different depending on where the program is in a sequence of activity (Horn et al., 2004). The authors postulate that cycle-to-cycle variability may be advantageous because it makes the circuit activity flexible and there is a low cost associated with individual trial failures (the failure to find food during one bite). I think another reason variability may be present is because precision is expensive. When machining an object or constructing an electrical circuit, more precision and tighter tolerances require more money, time, and/or planning. Biologically, the maintenance of precise

spike timing may be metabolically expensive. If there is no strong evolutionary need for precision timing in a spiking neuron, the energy will be expended elsewhere.

One of the most interesting parts of studying neuron variability is, counterintuitively, how much it may not matter in a biological context. In biological systems, functions such as respiration, ingestion of nutrition, and escape from predators must be achieved for survival. If all neurons are variable, and all neural circuits are composed of these variable neurons, the survival-promoting functions must still be robust and function in a variety of contexts. Biological systems must have evolved ways to compensate for neural variability (Faisal, Selen, & Wolpert, 2008).

Circuit composition, topology, and neuromodulation are plausible ways to ensure that survival-level functions occur even in the presence of neuron spike variability. In networks, the percentage of pacemaking components, and their intrinsic properties, can make a difference in observed network activity (Butera, Rinzel, & Smith, 1999; Kam, Worrell, Ventalon, Emiliani, & Feldman, 2013). Small biological circuits can maintain stable rhythms even when network frequency is varied (Katz, 2004; Soofi et al., 2012; Lamont S. Tang et al., 2010), but our hybrid circuit could not (Thounaojam et al., 2014), suggesting that the composition of the biological circuits and the way they are wired together may make them more robust. Neuromodulators can modify properties of neural firing (Marder,

2012), so the presence of modulators could change the level of intrinsic neural variability and the resulting network activity.

## 5.5 Future work

### 5.5.1 Neuron variability and dynamics

Neurons are variable, and this variability could affect biological function by affecting network activity responsible for that function. Robust systems must continue to operate even in the presence of variability. Four obvious questions emerge: 1) what strategies exist to compensate for neural variability, both biologically and experimentally? 2) how variable are neural systems? 3) how should this variability be represented? 4) What effect does this variability have?

#### 5.5.1.1 Catalog how different systems manage neuron variability

I have suggested that composition, topology, and modulation of networks may be viable ways to compensate for system irregularity. There may be others. Conserved characteristics among robust networks may inform us of how those circuits maintain their activity. Conserved characteristics of flexible networks may illustrate how neural systems exploit the presence of noise or variability. It is possible that some of these strategies may be extendable to engineered biomimetic systems to increase robust function in the presence of variable components.

5.5.1.2 Expand the vector based method to examine population dynamics

The PRC-based map describes interactions between two neurons. The time-series vector method presented describes the same interactions, but can capture changes that occur while the system is coupled and does not require measurement of the PRC. The vector method is general and may be used to describe interactions between more than one neuron. It would be interesting to see if characteristics of stable fixed points and ghost attractors appear in larger, population level measures of electrical synchrony, as measured using EEG. Because the map yields a description of the stability of an interaction, a catalog of the interactions in a network may reveal a hierarchy about which connections are more important, or maintained more tightly, than others. This information could suggest function in networks whose purpose is unknown; in systems where function is known, information about the importance of certain connections may indicate targets for intervention that are easier to manipulate or have greater effects than others.

5.5.1.3 Measure variability in other systems with descriptive processes

Variability of neuron spiking is measured in a variety of ways, many of which do not capture cycle-to-cycle changes. Common metrics of variability are coefficient of variation (CV, the ratio of the ISI standard deviation to the ISI mean) and the Fano factor (FF, variance to mean ratio of spikes that occur in a time window of specified duration) (Dayan & Abbott, 2001). Both CV and FF are sensitive to the window size they are calculated for. As shown in Chapter 3, the ISI of an isolated neuron is not constant; the average ISI depends on the window

in time used to calculate it, which can change the resulting CV and FF. Unfortunately, these are sometimes the only measures of spike time variability provided in scientific papers. To be able to describe variability and its effects accurately, we need more detailed measures of it. The ARIMA model used in project 1 is one example of how to describe neuron variability over time. How noise manifests in neural systems can indicate its origin (Fisch, Schwalger, Lindner, Herz, & Benda, 2012).

5.5.1.4 Use appropriate models of variability in simulation

Finally, appropriate models of variability should be incorporated into neural simulations. From our previous work (Thounaojam et al., 2014), we know that variability can change network activity from synchronized to phase-slipping and back. Because understanding synchronous activity is important, especially how it is established and maintained in circuits, including appropriate noise in simulation is critical. In (Thounaojam et al., 2014), appropriate noise was not white noise but instead noise with history and randomness. It is possible that in other circuits, white noise is adequately descriptive. Noiseless simulations are a great foundation to test theories and observe dynamical interactions, but they represent a simplification of biology and a boundary for the types of activity observed. The range of possible biological outputs, particularly in the presence of appropriate noise, should also be of interest.

### 5.5.2 Neuroethics

The development of neural applications for national security is likely to continue in the near future. Our framework is a start but will need amended and refined as technologies are developed, tested, and deployed, and as more individuals take place in the conversation about these technologies. DARPA is a prominent funder in the BRAIN Initiative (White House Office of Science and Technology Policy, 2014); it is likely more neuroscientists will accept defense funding for their work in the future. These investigators should be cognizant of the ethical implications of their science and involved in the discussion on its development, both to realistically assess what is accomplishable and to voice their opinions and concerns about proper use. Formal partnerships between ethicists, scientists, and engineers are likely to be mutually beneficial, particularly for investigators developing neuroscience applications for national security.

## APPENDIX A

## ADDITIONAL INFORMATION ABOUT LONG DURATION EXPERIMENTS

**Table 5: Temperature range and record length per data set**

| Data set | Min temp (C) | Max temp (C) | Utilized record length (min) |
|---|---|---|---|
| 1 | 13.2 | 14.1 | 148 |
| 2 | 12.3 | 13.1 | 188 |
| 3 | 12.8 | 15.0 | 109 |
| 4 | 13.5 | 14.7 | 187 |
| 5 | 12.1 | 12.6 | 114 |
| 6 | 14.2 | 15.2 | 175 |
| 7 | 14.4 | 15.0 | 155 |
| 8 | 10.7 | 12.3 | 219 |

**Table 6: ISI descriptive statistics**

| Data set | Min ISI (ms) | Max ISI (ms) | Mean ISI (ms) | Median ISI (ms) | Number of ISIs in the set |
|---|---|---|---|---|---|
| 1 | 1070 | 6042 | 2003 | 1905 | 4442 |
| 2 | 347 | 1269 | 817 | 813 | 13797 |
| 3 | 348 | 651 | 453 | 440 | 14410 |
| 4 | 453 | 1099 | 718 | 703 | 15661 |
| 5 | 480 | 1284 | 619 | 596 | 11050 |
| 6 | 219 | 586 | 416 | 411 | 25255 |
| 7 | 440 | 938 | 624 | 613 | 14925 |
| 8 | 1491 | 2204 | 1742 | 1715 | 7548 |

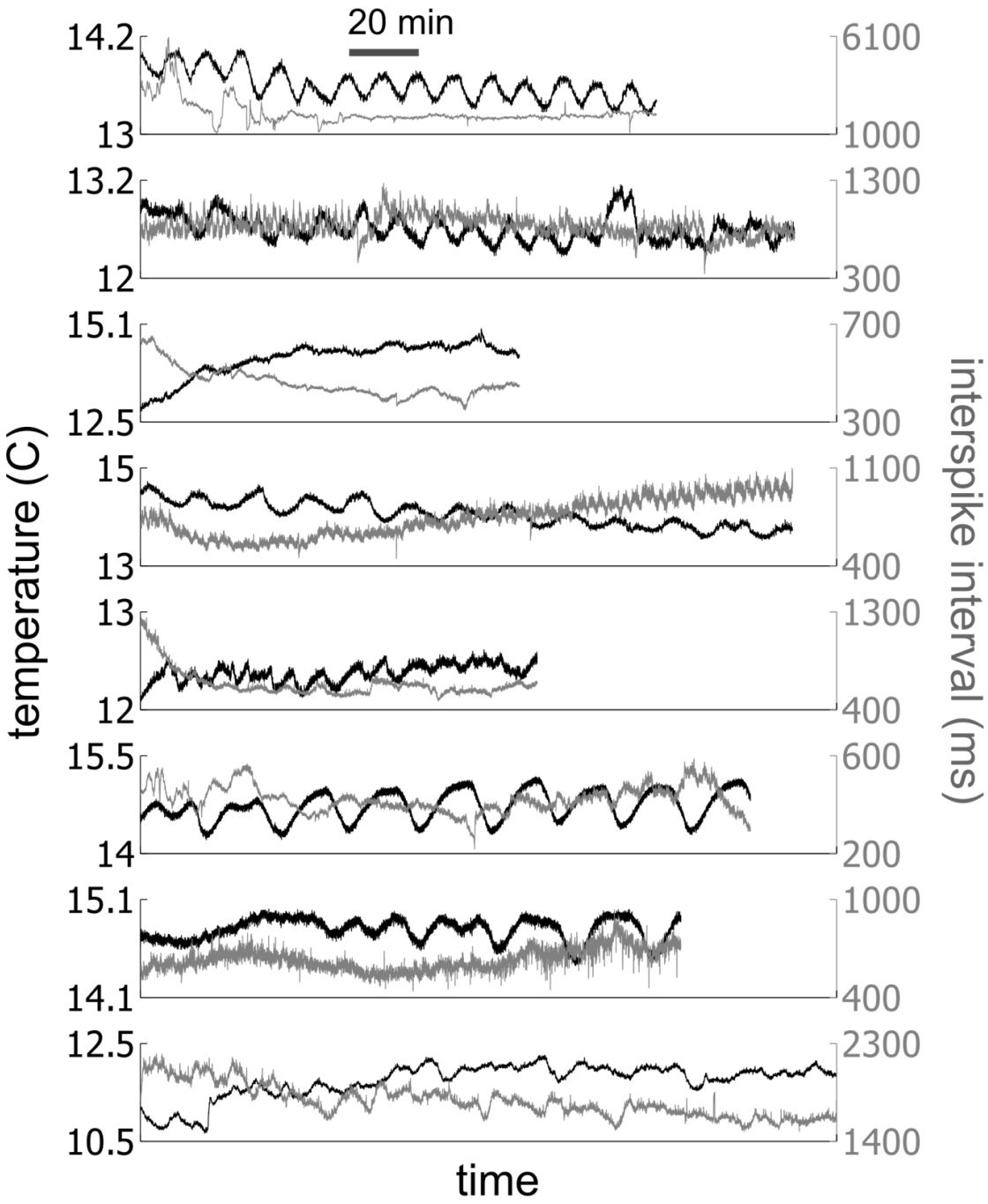


**Figure 29: Interspike interval and temperature over time during long experiments.** Gray traces represent ISI, axis labels are shown on the right. Black traces represent temperature, axis labels are shown on the left.

**Table 7: Linear fitting of ISI and temperature**

| | ISI vs temp | | | Log(ISI) vs temp | | |
|---|---|---|---|---|---|---|
| Data set | Slope | R2 | Rho (corr) | Slope | R2 | Rho (corr) |
| 1 | 993 | 0.12 | 0.35 | 0.34 | 0.08 | 0.29 |
| 2 | -117 | 0.03 | -0.18 | -0.14 | 0.03 | -0.17 |
| 3 | -118 | 0.83 | -0.91 | -0.24 | 0.80 | -0.90 |
| 4 | -407 | 0.59 | -0.77 | -0.56 | 0.58 | -0.76 |
| 5 | -201 | 0.03 | -0.18 | -0.23 | 0.02 | -0.15 |
| 6 | -72 | 0.10 | -0.31 | -0.18 | 0.10 | -0.32 |
| 7 | 65 | 0.01 | 0.11 | 0.10 | 0.01 | 0.11 |
| 8 | -310 | 0.47 | -0.69 | -0.17 | 0.45 | -0.67 |

**Table 8: Incidence of suspected inhibitory inputs**. Sections of 200 spikes were observed with starting times of T/4, 3T/8, T/2, 5T/8, and 3T/4, where T is the total length of used experimental data. Perturbations within an interspike interval strongly suspected to be inhibitory input were counted as definite (D), while obvious perturbations of questionable origin were marked (M). The fraction of interspike intervals with D or D+M perturbations is indicated by data set.

| | interval 1 | | interval 2 | | interval 3 | | interval 4 | | interval 5 | |
|---|---|---|---|---|---|---|---|---|---|---|
| | M | D | M | D | M | D | M | D | M | D |
| data set 1 | 0 | 0 | 0 | 0 | 0 | 0 | 0 | 0 | 1 | 0 |
| data set 2 | 16 | 14 | 25 | 11 | 8 | 12 | 6 | 14 | - | - |
| data set 3 | 0 | 0 | 0 | 0 | 0 | 0 | 0 | 0 | 0 | 0 |
| data set 4 | 4 | 2 | 9 | 2 | 2 | 1 | 1 | 1 | 4 | 4 |
| data set 5 | 1 | 0 | 1 | 0 | 0 | 0 | 0 | 0 | 1 | 0 |
| data set 6 | 0 | 0 | 0 | 0 | 0 | 0 | 0 | 0 | 0 | 0 |
| data set 7 | 2 | 1 | 5 | 3 | 1 | 0 | 1 | 1 | 0 | 0 |
| data set 8 | 0 | 1 | 0 | 0 | 1 | 0 | 1 | 0 | 0 | 0 |

**Table 9: Percent of sampled intervals with inhibitory perturbations.** Fraction out of 995 total intervals.

| | D (%) | M+D (%) |
|---|---|---|
| data set 1 | 0.0 | 0.1 |
| data set 2 | 6.4 | 13.3 |
| data set 3 | 0.0 | 0.0 |
| data set 4 | 1.0 | 3.0 |
| data set 5 | 0.0 | 0.3 |
| data set 6 | 0.0 | 0.0 |
| data set 7 | 0.5 | 1.4 |
| data set 8 | 0.1 | 0.3 |

## REFERENCES


Achuthan, S., & Canavier, C. C. (2009). Phase-resetting curves determine synchronization, phase locking, and clustering in networks of neural oscillators. *The Journal of Neuroscience*, *29*(16), 5218–5233.

Baschelet, E. (1981). *Circular Statistics in Biology*. London: Academic Press.

Bettencourt, J. C., Lillis, K. P., Stupin, L. R., & White, J. A. (2008). Effects of imperfect dynamic clamp: Computational and experimental results. *Journal of Neuroscience Methods*, *169*(2), 282–289. doi:10.1016/j.jneumeth.2007.10.009

Bi, G., & Poo, M. (1998). Synaptic modifications in cultured hippocampal neurons: dependence on spike timing, synaptic strength, and postsynaptic cell type. *The Journal of Neuroscience*, *18*(24), 10464–10472.

Bleeker, W. K., Mackaay, A. J., Masson-Pevet, M., Bouman, L. N., & Becker, A. E. (1980). Functional and morphological organization of the rabbit sinus node. *Circulation Research*, *46*(1), 11–22. doi:10.1161/01.RES.46.1.11

Börgers, C., & Kopell, N. (2005). Effects of noisy drive on rhythms in networks of excitatory and inhibitory neurons. *Neural Computation*, *17*(3), 557–608.

Box, G. E. P., & Jenkins, G. M. (1970). *Time series analysis: forecasting and control*. San Francisco: Holden-Day.

Butera Jr, R. J., Wilson, C. G., DelNegro, C. A., & Smith, J. C. (2001). A methodology for achieving high-speed rates for artificial conductance injection in electrically excitable biological cells. *Biomedical Engineering, IEEE Transactions on*, *48*(12), 1460–1470.

Butera, R. J., Rinzel, J., & Smith, J. C. (1999). Models of respiratory rhythm generation in the pre-Bötzinger complex. II. Populations of coupled pacemaker neurons. *Journal of Neurophysiology*, *82*(1), 398–415.

Cagnan, H., Kuhn, A. A., & Brown, P. (2014). Co-modulation of finely tuned high-gamma band activity across hemispheres in Parkinson's disease. *Clinical Neurophysiology*, *125*(4), 777–785. doi:10.1016/j.clinph.2013.10.001

Canavier, C. C., & Achuthan, S. (2010). Pulse coupled oscillators and the phase resetting curve. *Mathematical Biosciences*, *226*(2), 77–96.

Canli, T., Brandon, S., Casebeer, W., Crowley, P. J., DuRousseau, D., Greely, H. T., & Pascual-Leone, A. (2007). Neuroethics and National Security. *The American Journal of Bioethics*, *7*(5), 3–13. doi:10.1080/15265160701290249

Chacron, M. J., Longtin, A., & Maler, L. (2001). Negative interspike interval correlations increase the neuronal capacity for encoding time-dependent stimuli. *The Journal of Neuroscience*, *21*(14), 5328–5343.

Chow, C. C., & White, J. A. (1996). Spontaneous action potentials due to channel fluctuations. *Biophysical Journal*, *71*, 3013–3021.

Code of Federal Regulations Title 45: Public Welfare Part 46: Protection of Human Subjects. (2009). Retrieved from http://www.ncbi.nlm.nih.gov/books/NBK19891/

Cohen, M. X., & Gulbinaite, R. (2014). Five methodological challenges in cognitive electrophysiology. *NeuroImage*, *85*, 702–710. doi:10.1016/j.neuroimage.2013.08.010

Colgin, L. L., & Moser, E. I. (2010). Gamma Oscillations in the Hippocampus. *Physiology*, *25*(5), 319–329. doi:10.1152/physiol.00021.2010

Cui, J., Canavier, C. C., & Butera, R. J. (2009). Functional Phase Response Curves: A Method for Understanding Synchronization of Adapting Neurons. *Journal of Neurophysiology*, *102*, 387–398. doi:10.1152/jn.00037.2009

Dayan, P., & Abbott, L. F. (2001). *Theoretical Neuroscience*. Cambridge, MA: MIT Press.

Defense Advanced Projects Research Agency (DARPA) Biological Technologies Office. (2014, April 24). Hand Proprioception & Touch Interfaces (HAPTIX) Broad Agency Announcement, DARPA-BAA-14-30.

Defense Advanced Projects Research Agency (DARPA) Defense Sciences Office. (2013, October 24). Systems-Based Neurotechnology for Emerging Therapies (SUBNETS) Broad Agency Announcement, DARPA-BAA-14-09.

Dominguez, L. G., Wennberg, R. A., Gaetz, W., Cheyne, D., Snead, O. C., & Velazquez, J. L. P. (2005). Enhanced synchrony in epileptiform activity? Local versus distant phase synchronization in generalized seizures. *The Journal of Neuroscience*, *25*(35), 8077.

Faisal, A. A., Selen, L. P. J., & Wolpert, D. M. (2008). Noise in the nervous system. *Nature Reviews Neuroscience*, *9*(4), 292–303. doi:10.1038/nrn2258

Farah, M. J. (2012). Neuroethics: The Ethical, Legal, and Societal Impact of Neuroscience. *Annual Review of Psychology*, *63*(1), 571–591. doi:10.1146/annurev.psych.093008.100438

Farah, M. J., Hutchinson, J. B., Phelps, E. A., & Wagner, A. D. (2014). Functional MRI-based lie detection: scientific and societal challenges. *Nature Reviews Neuroscience*, *15*(2), 123–131.

Farah, M. J., Illes, J., Cook-Deegan, R., Gardner, H., Kandel, E., King, P., … Wolpe, P. R. (2004). Neurocognitive enhancement: what can we do and what should we do? *Nature Reviews Neuroscience*, *5*(5), 421–425.

Fell, J., & Axmacher, N. (2011). The role of phase synchronization in memory processes. *Nature Reviews Neuroscience*, *12*, 105–118.

Fell, J., Klaver, P., Lehnertz, K., Grunwald, T., Schaller, C., Elger, C. E., & Fernández, G. (2001). Human memory formation is accompanied by rhinal-hippocampal coupling and decoupling. *Nature Neuroscience*, *4*, 1259–1264.

Fisch, K., Schwalger, T., Lindner, B., Herz, A. V. M., & Benda, J. (2012). Channel Noise from Both Slow Adaptation Currents and Fast Currents Is Required to Explain Spike-Response Variability in a Sensory Neuron. *Journal of Neuroscience*, *32*(48), 17332–17344. doi:10.1523/JNEUROSCI.6231-11.2012

Forsythe, C., & Giordano, J. (2011). Introduction-On the need for neurotechnology in the national intelligence and defense agenda: Scope and trajectory. *Synesis: A Journal of Science, Technology, Ethics, and Policy*, *2*(2), T5–T8.

Frazier, W. T., Kandel, E. R., Kupfermann, I., Waziri, R., & Coggeshall, R. E. (1967). Morphological and functional properties of identified neurons in the abdominal ganglion of Aplysia californica. *Journal of Neurophysiology*, *30*, 1288–1351.

Funk, G. D., & Greer, J. J. (2013). The rhythmic, transverse medullary slice preparation in respiratory neurobiology: Contributions and caveats. *Respiratory Physiology & Neurobiology*, *186*(2), 236–253. doi:10.1016/j.resp.2013.01.011

Gerstein, G. L., & Mandelbrot, B. (1964). Random walk models for the spike activity of a single neuron. *Biophysical Journal*, *4*(1), 41–68.

Glass, L., & Mackey, M. C. (1988). *From Clocks to Chaos: The Rhythms of Life*. Princeton, NJ: Princeton University Press.

Gollo, L. L., Mirasso, C., Sporns, O., & Breakspear, M. (2014). Mechanisms of Zero-Lag Synchronization in Cortical Motifs. *PLoS Computational Biology*, *10*(4), e1003548. doi:10.1371/journal.pcbi.1003548

Greely, H., Sahakian, B., Harris, J., Kessler, R. C., Gazzaniga, M., Campbell, P., & Farah, M. J. (2008). Towards responsible use of cognitive-enhancing drugs by the healthy. *Nature*, *456*(7223), 702–705.

Grützner, C., Wibral, M., Sun, L., Rivolta, D., Singer, W., Maurer, K., & Uhlhaas, P. J. (2013). Deficits in high- (> 60 Hz) gamma-band oscillations during visual processing in schizophrenia. *Frontiers in Human Neuroscience*, *7*. doi:10.3389/fnhum.2013.00088

Hagglund, M., Dougherty, K. J., Borgius, L., Itohara, S., Iwasato, T., & Kiehn, O. (2013). Optogenetic dissection reveals multiple rhythmogenic modules underlying locomotion. *Proceedings of the National Academy of Sciences*, *110*(28), 11589–11594. doi:10.1073/pnas.1304365110

Hamilton, R., Messing, S., & Chatterjee, A. (2011). Rethinking the thinking cap Ethics of neural enhancement using noninvasive brain stimulation. *Neurology*, *76*(2), 187–193.

Horn, C. C., Zhurov, Y., Orekhova, I. V., Proekt, A., Kupfermann, I., Weiss, K. R., & Brezina, V. (2004). Cycle-to-Cycle Variability of Neuromuscular Activity in Aplysia Feeding Behavior. *Journal of Neurophysiology*, *92*(1), 157–180. doi:10.1152/jn.01190.2003

Izhikevich, E. M. (2010). *Dynamical Systems in Neuroscience*. Cambridge, MA: MIT Press.

Jhala, S., Tamvacakis, A. N., & Katz, P. S. (2011). Toward locating the source of serotonergic axons in the tail nerve of Aplysia. *Invertebrate Neuroscience*, *11*(2), 91–96. doi:10.1007/s10158-011-0121-6

Jutras, M. J., & Buffalo, E. A. (2010). Synchronous neural activity and memory formation. *Current Opinion in Neurobiology*, *20*, 150–155. doi:10.1016/j.conb.2010.02.006

Kam, K., Worrell, J. W., Ventalon, C., Emiliani, V., & Feldman, J. L. (2013). Emergence of Population Bursts from Simultaneous Activation of Small Subsets of preBotzinger Complex Inspiratory Neurons. *Journal of Neuroscience*, *33*(8), 3332–3338. doi:10.1523/JNEUROSCI.4574-12.2013

Katz, P. S. (2004). Cycle Period of a Network Oscillator Is Independent of Membrane Potential and Spiking Activity in Individual Central Pattern Generator Neurons. *Journal of Neurophysiology*, *92*(3), 1904–1917. doi:10.1152/jn.00864.2003

Koshiya, N., & Smith, J. C. (1999). Neuronal pacemaker for breathing visualized in vitro. *Nature*, *400*(6742), 360–363.

Lin, R. J., Bettencourt, J., White, J. A., Christini, D. J., & Butera, R. J. (2010). Real-time experiment interface for biological control applications. In *Engineering in Medicine and Biology Society (EMBC), 2010 Annual International Conference of the IEEE* (pp. 4160–4163).

Lindner, B. (2004). Interspike interval statistics of neurons driven by colored noise. *Physical Review E*, *69*(2). doi:10.1103/PhysRevE.69.022901

Ljung, G. M., & Box, G. E. P. (1978). On a measure of lack of fit in time series models. *Biometrika*, *65*(2), 297–303.

Ly, C., & Ermentrout, G. B. (2010). Coupling regularizes individual units in noisy populations. *Physical Review E*, *81*(1). doi:10.1103/PhysRevE.81.011911

Malakoff, D. (2012, April 20). U. S. accepts NSABB recommendation to publish H5N1 flu papers. *Science*, pp. 1–4.

Maran, S. K., & Canavier, C. C. (2008). Using phase resetting to predict 1:1 and 2:2 locking in two neuron networks in which firing order is not always preserved. *Journal of Computational Neuroscience*, *24*(1), 37–55. doi:10.1007/s10827-007-0040-z

Marder, E. (2012). Neuromodulation of neuronal circuits: back to the future. *Neuron*, *76*, 1–11.

Marder, E., & Calabrese, R. L. (1996). Principles of rhythmic motor pattern generation. *Physiological Reviews*, *76*(3), 687–717.

Marks, J. H. (2010). A Neuroskeptic's Guide to Neuroethics and National Security. *AJOB Neuroscience*, *1*(2), 4–12. doi:10.1080/21507741003699256

McDonnell, M. D., & Abbott, D. (2009). What Is Stochastic Resonance? Definitions, Misconceptions, Debates, and Its Relevance to Biology. *PLoS Computational Biology*, *5*(5), e1000348. doi:10.1371/journal.pcbi.1000348

McGregor, G. (2002, June 3). Fatigue dogged U.S. figuter squadron: Pilots urged to use amphetamines days before Canadian troops killed. *The Vancourver Sun*. British Columbia.

Middleton, J., Chacron, M., Lindner, B., & Longtin, A. (2003). Firing statistics of a neuron model driven by long-range correlated noise. *Physical Review E*, *68*(2). doi:10.1103/PhysRevE.68.021920

Mirollo, R. E., & Strogatz, S. H. (1990). Synchronization of pulse-coupled biological oscillators. *SIAM Journal on Applied Mathematics*, 1645–1662.

Moreno, J. D. (2012). *Mind Wars: Brain science and the military in the 21st century*. New York: Bellevue Literary Press.

National Research Council. (2009). *Opportunities in Neuroscience for Future Army Applications*. The National Academies Press.

National Research Council. (2014). *Emerging and Readily Available Technologies and National Security: a Framework for Addressing Ethical, Legal, and Societal issues*. The National Academies Press.

National Science Advisory Board for Biosecurity Charter. (2014, March 21).

Nowotny, T., Zhigulin, V. P., Selverston, A. I., Abarbanel, H. D. I., & Rabinovich, M. I. (2003). Enhancement of synchronization in a hybrid neural circuit by spike-timing dependent plasticity. *The Journal of Neuroscience*, *23*(30), 9776–9785.

Oprisan, S.A., P., A.A. (2004). Phase resetting and phase locking in hybrid circuits of one model and one biological neuron. *Biophysical Journal*, *87*, 2283–2298.

Ozaki, T. (1977). On the Order Determination of ARIMA Models. *Applied Statistics*, *26*(3), 290. doi:10.2307/2346970

Presidential Commission for the Study of Bioethical Issues. (2014). *Grey Matters: Integrative Approaches for Neuroscience, Ethics, and Society*.

Presidential Commission for the Study of Bioethical Issues Charter. (2010, March 10).

Prinz, A. A., Abbott, L. ., & Marder, E. (2004). The dynamic clamp comes of age. *Trends in Neurosciences*, *27*, 218–224. doi:10.1016/j.tins.2004.02.004

Rinberg, A., Taylor, A. L., & Marder, E. (2013). The Effects of Temperature on the Stability of a Neuronal Oscillator. *PLoS Computational Biology*, *9*(1), e1002857. doi:10.1371/journal.pcbi.1002857

Rinzel, J., & Huguet, G. (2013). Nonlinear Dynamics of Neuronal Excitability, Oscillations, and Coincidence Detection. *Communications on Pure and Applied Mathematics*, *66*(9), 1464–1494.

Schulthesis, N. W., Prinz, A. A., & Butera, R. J. (Eds.). (2012). *Phase response curves in neuroscience: theory, experiment, and analysis*. Springer.

Schwalger, T., Fisch, K., Benda, J., & Lindner, B. (2010). How Noisy Adaptation of Neurons Shapes Interspike Interval Histograms and Correlations. *PLoS Computational Biology*, *6*(12), e1001026. doi:10.1371/journal.pcbi.1001026

Schwemmer, M. A., & Lewis, T. J. (2012). The Theory of Weakly Coupled Oscillators. In *Phase response curves in neuroscience: Theory, experiment, and analysis* (pp. 3–31).

Selverston, A. I. (2010). Invertebrate central pattern generator circuits. *Philosophical Transactions of the Royal Society B: Biological Sciences*, *365*(1551), 2329–2345. doi:10.1098/rstb.2009.0270

Shao, J., Tsao, T.-H., & Butera, R. (2006). Bursting without slow kinetics: a role for a small world? *Neural Computation*, *18*(9), 2029–2035.

Sharp, A. A., O'Neil, M. B., Abbott, L., & Marder, E. (1993). The dynamic clamp: artificial conductances in biological neurons. *Trends in Neurosciences*, *16*(10), 389–394.

Siegel, M., Donner, T. H., & Engel, A. K. (2012). Spectral fingerprints of large-scale neuronal interactions. *Nature Reviews Neuroscience*. doi:10.1038/nrn3137

Sieling, F. H., Canavier, C. C., & Prinz, A. A. (2009). Predictions of Phase-Locking in Excitatory Hybrid Networks: Excitation Does Not Promote Phase-Locking in Pattern-Generating Networks as Reliably as Inhibition. *Journal of Neurophysiology*, *102*(1), 69–84. doi:10.1152/jn.00091.2009

Soofi, W., Archila, S., & Prinz, A. A. (2012). Co-variation of ionic conductances supports phase maintenance in stomatogastric neurons. *Journal of Computational Neuroscience*, *33*(1), 77–95. doi:10.1007/s10827-011-0375-3

Spencer, K. M., Nestor, P. G., Niznikiewicz, M. A., Salisbury, D. F., Shenton, M. E., & McCarley, R. W. (2003). Abnormal neural synchrony in schizophrenia. *The Journal of Neuroscience*, *23*(19), 7407–7411.

Tang, L. S., Goeritz, M. L., Caplan, J. S., Taylor, A. L., Fisek, M., & Marder, E. (2010). Precise Temperature Compensation of Phase in a Rhythmic Motor Pattern. *PLoS Biology*, *8*(8), e1000469. doi:10.1371/journal.pbio.1000469

Tang, L. S., Taylor, A. L., Rinberg, A., & Marder, E. (2012). Robustness of a Rhythmic Circuit to Short- and Long-Term Temperature Changes. *Journal of Neuroscience*, *32*(29), 10075–10085. doi:10.1523/JNEUROSCI.1443-12.2012

Tennison, M. N., & Moreno, J. D. (2012). Neuroscience, Ethics, and National Security: The State of the Art. *PLOS Biology*, *10*(3), e1001289. doi:10.1371/journal.pbio.1001289

The Royal Society. (2012). *Brain Waves Module 3: Neuroscience, conflict, and security*. The Royal Society.

Thounaojam, U. S., Cui, J., Norman, S. E., Butera, R. J., & Canavier, C. C. (2014). Slow Noise in the Period of a Biological Oscillator Underlies Gradual Trends

and Abrupt Transitions in Phasic Relationships in Hybrid Neural Networks. *PLoS Computational Biology*, *10*(5), e1003622. doi:10.1371/journal.pcbi.1003622

Uhlenbeck, G. E., & Ornstein, L. S. (1930). On the theory of the Brownian motion. *Physical Review*, *36*(5), 823–841.

Uhlhaas, P. J., & Singer, W. (2006). Neural synchrony in brain disorders: relevance for cognitive dysfunctions and pathophysiology. *Neuron*, *52*(1), 155–168.

Uhlhaas, P. J., & Singer, W. (2012). Neuronal Dynamics and Neuropsychiatric Disorders: Toward a Translational Paradigm for Dysfunctional Large-Scale Networks. *Neuron*, *75*(6), 963–980. doi:10.1016/j.neuron.2012.09.004

United States Government Policy for Institutional Oversight of Life Sciences Dual Use Research of Concern. (2012).

Wang, X.-J., & Buzsaki, G. (1996). Gamma oscillation by synaptic inhibition in a hippocampal interneuronal network model. *The Journal of Neuroscience*, *16*(20), 6402–6413.

Watts, D. J., & Strogatz, S. H. (1998). Collective dynamics of "small-world" networks. *Nature*, *393*(6684), 440–442.

White House Office of Science and Technology Policy. (2014, March). Obama administration proposes doubling support for the BRAIN initiative.

Winfree, A. T. (2001). *The Geometry of Biological Time* (Second Edition.). New York: Springer.

Wolk, H. S. (2009, March). Making the H-bomb. *Air Force Magazine*, 66–69.

Zhu, W., Zeng, N., & Wang, N. (2010). Sensitivity, specificity, accuracy, associated confidence interval and ROC analysis with practical SAS implementations. *NESUG Proceedings: Health Care and Life Sciences, Baltimore, Maryland*.